NOTICE

The quality of this microform is heavily dependent upon the quality of the original thesis submitted for microfilming. Every effort has been made to ensure the highest quality of reproduction possible.

If pages are missing, contact the university which granted the degree.

Some pages may have indistinct print especially if the original pages were typed with a poor typewriter ribbon or if the university sent us an inferior photocopy.

Previously copyrighted materials (journal articles, published tests, etc.) are not filmed.

Reproduction in full or in part of this microform is governed by the Canadian Copyright Act, R.S.C. 1970, c. C-30.

AVIS

La qualité de cette microforme dépend grandement de la qualité de la thèse soumise au microfilmage. Nous avons tout fait pour assurer une qualité supérieure de reproduction.

S'il manque des pages, veuillez communiquer avec l'université qui a conféré le grade.

La qualité d'impression de certaines pages peut laisser à désirer, surtout si les pages originales ont été dactylographiées à l'aide d'un ruban usé ou si l'université nous a fait parvenir une photocopie de qualité inférieure.

Les documents qui font déjà l'objet d'un droit d'auteur (articles de revue, tests publiés, etc.) ne sont pas microfilmés.

La reproduction, même partielle, de cette microforme est soumise à la Loi canadienne sur le droit d'auteur, SRC 1970, c. C-30.

Canada

Analysis of Mutual Coupling Effects In a Finite Planar Circular Waveguide Array

Duy Ngoc Nguyen

A Thesis

in

The Department

of

Electrical Engineering

Presented in Partial Fulfillment of the Requirements
for the Degree of Master of Engineering at
Concordia University
Montréal, Québec, Canada

December 1987

ISBN 0-315-41651-3

ABSTRACT

Analysis of Mutual Coupling Effects In a Finite Planar Circular Waveguide Array

Duy Ngoc Nguyen

Array feeds are widely used in spacecraft antennas for generating either multiple beams or shaped beams. Flexibility in the design of array feeds is readily available; however, the design can be complicated by the effects of multiple interactions between the radiating elements. These interactions give rise to distortion of the co-polarized radiation pattern and an increase in the level of cross-polarization, a feature which is crucial in dual-polarization or in frequency re-use satellite systems.

This thesis presents a mathematical model to analyze the mutual coupling effects in a finite planar array of open-ended circular waveguides and terminated in an infinite ground plane. The problem is formulated as an integral equation by requiring that the transverse electric and magnetic fields be continuous across the apertures. The integral equation is then solved by the moment method leading to a complete description of the aperture field, including all the reflected modes, in each element of the array. The radiation pattern of the antenna array is obtained by Fourier transforming the aperture field which has included all the mutual coupling effects. By deforming the contour integrals in the mode coupling expressions, the coupling coefficient can be computed efficiently.

Computed results compare favorably with experimental and published data, thus establishing the validity of the analysis and the computer program.

ACKNOWLEDGEMENTS

I wish to extend my sincere thanks to my thesis Supervisors, Dr. S. J. Kubina of Concordia University and Dr. G. S. Gupta of SPAR Aerospace Ltd., for their continuous encouragement and support throughout the course of this study. The wonderful attitude and the expertise of Dr. G. S. Gupta have provided me with unfailing confidence at critical paths of the study. The warm and caring atmosphere given by Dr. S. J. Kubina during the last stage of the thesis preparation is most remembered.

Thanks are also due to the Management of SPAR Aerospace Ltd., Satellite and Aerospace Systems Division, for their financial support and permission to publish the results. Acknowledgements are extended to my colleague, Dr. K. S. Rao for his valuable suggestions and discussions toward the manuscript; and for his permission to use some of the measured data.

The thesis would not be completed without the encouragement, caring and patience of my family. I am indebted to this paramount support and would like to dedicate this work to my family.

To my Mother and Father

TABLE OF CONTENTS

NOMEMCLATURE

∇_t	Transverse gradient operator
$\bar{J}_s, \bar{M}_s$	Surface electric and magnetic currents
$\bar{E}_t, \bar{H}_t$	Tangential electric and magnetic fields to the x-y plane
$\bar{e}_m, \bar{h}_m$	Transverse field components of the m-th mode in a circular waveguide
Z_m	Mode impedance
λ_m	Transverse wavenumber of the m-th mode
γ_m	Propagation constant of the m-th mode
$a_m^{(i)}$	Complex amplitude of the incident m-th mode in the i-th waveguide
$b_m^{(i)}$	Complex amplitude of the reflected m-th mode in the i-th waveguide
$C_{mn}^{(ij)}$	Coupling coefficient between the m-th mode in the i-th and the n-th mode in the j-th waveguide.
$G(\lvert\bar{r}-\bar{r}'\rvert)$	Free-space Green's function
J_p	Bessel function of order p
Q_p	Lommel's integral of order p

LIST OF TABLES

LIST OF FIGURES

CHAPTER 1

INTRODUCTION

1.1 Purpose of the work

Current and future trends in both global and regional satellite communication systems require high gain spacecraft antennas of complex designs which radiate either a contoured beam or a number of narrow spot beams over high density traffic areas. The objective of a contoured beam antenna is to concentrate a high portion of the radiated power as uniformly as possible within a desired geographic coverage area and to minimize the radiation to adjacent service areas. The shaping of the radiated beams can be achieved by the superposition of individual constituent beams from an array of primary feed elements illuminating either a single or dual reflector system. The multiple beam antenna can be realized in a similar manner but in this case the elemental beam is considered independently and it is necessary to maximize the isolation between beams employing either the same polarization or the same frequency. For either application, the requirements demand that the co-polar sidelobes and the cross-polar field components are kept to minimum.

Quite often contoured beam patterns or a number of closely-spaced spot beams are formed by weighting the amplitude and phase of each element in the feed cluster. Such an exercise gives a better shaping of the radiated footprint while maintaining low sidelobe levels. The selection of primary feed elements constitutes a major step in the design of contoured or multi-

beam reflector antennas. The optimum horn geometry is dependent upon the reflector to be illuminated and the overall RF performance objectives, e.g. gain coverage, gain ripple over the coverage area, sidelobes, polarization purities, etc. The aperture antennas such as pyramidal and dominant or dual mode conical horns, in general, offer many desirable features. The radiation properties of these antennas are usually well represented and the computations are in good accord with measurements. Clearly, a primary feed array comprising of one of these types can be considered as a good candidate for the antenna system.

To avoid excessive spill-over losses due to grating lobes[†], the elements in a feed cluster must be small – in the order 1.0 to 1.6 wavelength – and tightly packed. The inclusion of mutual coupling effects in the computation of radiated fields from the antenna, in that case, cannot be ignored. For horns with relatively small aperture, a number of higher order modes are generated at the aperture due to an impedance mismatch at the waveguide-to-air junction. These higher order modes are then reflected back into the horn, coupled to the dominant mode and alter the aperture distribution. In addition, since the horn is placed in close proximity to scattering objects, i.e. the remaining horns of the feed cluster, both the modal content of the aperture field and the radiation patterns will be changed. These interactions are denoted as mutual coupling. The mutual coupling causes the element factor to change with element spacing, leading to the asymmetry of the co-polarized and significant deterioration in the cross-polarized patterns. The

[†] "A lobe, other than the main lobe, produced by an array antenna when the inter-element spacing is sufficiently large to permit the in-phase addition of radiated field in more than one direction" (IEEE Standard Definitions of Terms for Antennas, New York, 1983, p.15).

degree to which the mutual coupling affects the performance of the array will depend upon the element type, the polarization and excitation of each element and the geometry of the array. Marked effects in the radiation patterns of an embedded conical horn (surrounding elements are terminated with matched loads) has been reported by Clarricoats *et al* [1]. The effect of mutual coupling on the cross-polarized field of three different types of active array was also investigated by Rao in his recent experimental study [2]. It is noted that the deterioration of the cross-polar pattern can be as high as 7.5 dB for linear polarization (LP) and 4.0 dB for circular polarization (CP) when a dominant mode circular horn of size 1.135 wavelengths is placed in an array configuration.

A knowledge of mutual coupling characteristics associated with a finite primary-feed array is a clear advantage to antenna designers. Appropriate corrections can be incorporated into the overall antenna design for any modifications to the radiation patterns of immersed elements. Saving in fabrication of the feed hardware could be substantial. An analytical approach to determine the mutual coupling effects in a given primary-feed array is therefore considered important.

1.2 Review of Earlier Works

The problem of calculating the mutual coupling between apertures in an array has been a topic of interest for quite some time. Analytical treatments of the problem have been reported by a number of authors, some of these will be briefly discussed in this section.

In general, the mutual coupling effects in an array are analyzed by

using the integral equation method. The scattered field in the exterior of an array is represented by an integral over the plane of the horn apertures, having the tangential component of the electric field in the integrand. If an approximation is made that the planar array is terminated in an infinite ground plane, then the tangential electric field will vanish everywhere on the aperture plane except on the horn openings themselves. The original integration is thus reduced to only that over the physical apertures of the horns. In the interior region, which is the ensemble of all the horn waveguide regions, the field can be expanded as a summation of modal fields which satisfy the boundary condition at the horn apertures, i.e. continuity of the tangential electric ($\bar{E}$) and magnetic ($\bar{H}$) fields.

As the observation point approaches the aperture plane, the imposition of a boundary continuity condition as well as the limit of the integral representation of the scattered field and of the modal fields leads to an integral equation for the unknown tangential electric field. An approximate solution of such an equation can be obtained by the Method of Moments (MoM) [3].

Although the above procedure is common in most of the recent works, the particular formulations are quite different among authors [4-12]. Mailloux [10], in his first paper, found the near field coupling between two collinear open-ended rectangular waveguides by formulating the problem as a set of simultaneous integral equations and solving the resulting equations approximately by expanding the aperture field in a Fourier series. In a second paper, Mailloux [11] found the near field coupling between two closely-spaced open-ended waveguides by a first-order analysis which is based on the method of moments using a single mode approximation to the aperture field.

An improved first order analysis is also presented using a higher order mode solution to the self admittances.

The works of Wu [9], Cha and Hsiao [6] and Steyskal [7] are quite similar in nature. The integral equation is set up by imposing the continuity condition of the tangential field components across the apertures. Again, the method of moments was used by these authors to arrive at a solution for the unknown tangential electric (E) field. The formulation of Wu originated from a problem of finite parallel-plate waveguide arrays, i.e. the fields are independent of one of the coordinate variables. When applied to an array of rectangular waveguides, this condition is satisfied only at two major cardinal planes. The solution is, thus, a limited one. Such a limitation is overcome in the analysis of Cha and Hsiao, where the modal fields are the TE and TM waveguide modes. Cha and Hsiao also emphasize the computational efficiency. The elements of the interaction matrix have a translational symmetry relation similar to that of elements in a block-Toeplitz matrix. Unlike other presentations, Steyskal's paper concerns itself with the mutual coupling in a finite array of circular waveguides. The unknown aperture field is again expressed as a combination of waveguide modal fields. The author also selects the set of basis functions equal to the weighting functions (i.e. waveguide modal fields) for the reason that the lower order solution usually is dependent on the particular location of the matching points.

For another particular formulation, Harrington [4] and Fenn [5] obtained the integral equation through the use of the equivalence principle and image theory, whereby the tangential electric field is replaced with a magnetic surface current density backed by a perfectly conducting plane. Both authors employ Galerkin's version of the method of moments, but Fenn [5]

carries it much further by considering several basis functions within each radiating aperture, and by allowing for coupling of cross-polarized fields as well (because orthogonally polarized basis functions are used). Computational efficiency is of prime interest in these works, and use is made of a very fast algorithm to solve a system of linear equations, which is only valid if the matrix of the system has block-Toeplitz symmetry. The array is, thus, constrained to a rectangular-grid and equal radiating elements. Any other general case will require considerably more computer time and storage. With the generation of higher order modes at relative large apertures, a sufficient number of basis functions must be considered to adequately describe the aperture field distribution. Each basis function at each aperture corresponds to one line or one row of the admittance matrix, and it is therefore clear that the order of the matrix may quickly become too large to be handled [5]. For the internal region, Fenn [5] uses the method of images to obtain the field due to each basis function. This method is found less elegant than the modal expansion introduced by Harrington [4].

A slightly different integral equation is the starting point of formulations by Fernez [8] and Bird [12]. Galerkin's version of the method of moments is again employed, but the basis functions now considered are the tangential electric fields corresponding to the various waveguide modes of propagation. The mutual coupling effect in a finite rectangular waveguide array is dealt with by Fernez [8] whilst that in a finite circular waveguide array is dealt with by Bird [12]. Therefore, the basis functions are different, but the method is basically the same in the two formulations. In Bird's work [12], the mode coupling expressions are reduced to forms that are computationally quite efficient. The numerous mode cross coupling between apertures is

handled through the use of an asymptotic formula to speed up the computation time.

In summary, the analytical treatment to the problem depends mainly on the particular formulation used by each author. The formulation generally commences with an integral equation which will then be solved by the method of moments. The complexity of the resultant matrix equation, as well as the generality of the solution, depend on the selection of the set of basis and testing functions. This, again, varies between the authors. However, for the waveguide-type problems, the natural choice for the basis (and testing) functions is often the modal fields of the associated waveguides, since the integration required to be performed for reducing the integral equation into a matrix equation can then be carried out in closed form. This consideration is shared by Mittra [13]. Finally, it is noted that investigations are generally carried out for planar arrays of identical size to ease the analysis and computation.

1.3 Outline of the Present Work

The increasing demand of "clean beams" (low sidelobes, low cross polarization) from a satellite antenna has prompted efforts to be concentrated in formulating and computing efficiently the mutual coupling effects in a finite array. Such efforts have been initially directed to circular waveguide arrays. The treatment of these will be presented in this thesis. The present analysis will be more general than earlier investigations [7,12,14] in the sense that it considers the mutual coupling between possible modes in the waveguides whether propagating or evanescent. This is rather important, since in a practical situation there are a number of higher-order modes being

generated locally at the aperture due to the boundary condition. Both Bailey *et al* [14] and Steyskal [7] included only a brief description of the effect of modes of higher order than the dominant TE_{11} in the solution. The two analyses are essentially extensions of methods employed earlier to derive the self-admittance of the TE_{11} mode in a flanged circular waveguide [15,16]. Ease of numerical implementation is not discussed in these works. Bird [12], on the other hand, has supplemented higher-order modes in the self-admittance analysis but has considered only TE_{11} to TE_{11} mode coupling in a seven-element cluster of circular waveguides. The inter-element mode cross-coupling coefficients were handled differently by these authors; Bailey *et al* evaluated them directly while Steyskal and Bird utilized an asymptotic formula. Although the use of an asymptotic formula provides considerable saving in computing time, it does lead to inaccuracies when an array of closely-packed large diameter feeds is considered. In this thesis, the formulation for all possible couplings and the cross-coupling coefficients in separate apertures are put in exact expressions and then reduced to forms that are suitable for numerical calculation.

Formulation of the mutual coupling problem is discussed in Chapter 2. The integral equation is first constructed through an identity that relates the scattered magnetic field to the tangential electric field at the apertures. The method of moments is then employed to obtain an approximate solution for the unknown tangential electric field. To facilitate the analysis, the waveguide modal fields are used as basis functions to expand the unknown field in terms of a series. By applying Galerkin's procedure, the functional equation is reduced to a matrix equation, in which the coupling coefficients can be explicitly defined. Initial analysis of mode coupling in a single

aperture is presented in Chapter 3. The coupling coefficients have terms depending upon contour integrals. These integrals can be evaluated efficiently by deforming the integration path in the complex plane. The deformation process is also discussed in Chapter 3.

The mutual coupling between modes in separate waveguides is dealt with in Chapter 4. The resultant coupling coefficients contain contour integrals involving triple products of Bessel functions, or their derivatives, whose argument is not expressed explicitly in terms of the integration variables. Graf's addition theorem is used to separate the variables associated with one of the apertures. Contour integration, as is used in Chapter 3, can again be applied to transform the oscillatory integrands to monotonic ones. Fast-convergent numerical integration is thus obtained. Once the coupling coefficients have been derived, the radiation characteristics of the array are readily developed using the E-field mathematical model. Chapter 5 presents the analysis and expressions of the radiation fields.

Validation of the analysis and the computer program is made through comparison of numerical results to measured data and to those in the open literature. These comparisons are detailed in Chapter 6.

CHAPTER 2

PROBLEM FORMULATION

2.1 Introduction

The investigation of waveguide arrays has shown that such problems can be most effectively solved by regarding them as interface problems. In this approach, the whole space is viewed as consisting of two separate, uniform regions; one of them is composed of the aggregate of the waveguides while the other is a half space. The two regions meet at a common interface, i.e. the array face. Since a knowledge of either the tangential electric or magnetic field at the interface will suffice to characterize the fields everywhere, it is desirable to formulate the problem so as to solve for one of the quantities. The integral equation formulation is found to be particularly suitable for this purpose.

2.2 Formulation of Waveguide Scattering

A combination of the equivalence principle and image theorem can be used to obtain solutions to boundary-value problem for which the field in half-space is to be determined from its tangential components over the bounding plane. A brief discussion in the light of these concepts is given herein, whereas detailed treatment can be found in Harrington [17] and Collin and Zucker [18]. With reference to Figure 2.1a, let the original problem consist of sources in $z < 0$ and free space in $z > 0$. An application of the equivalence theorem leads to an equivalent problem in Figure 2.1b. This

consists of the magnetic current $\overline{M}_s = \overline{E} \times \overline{n}$ adjacent to an infinite ground plane. One may now image the magnetic current in the ground plane as shown in Figure 2.1c. The image is equal in magnitude to, and essentially coincident with, the $\overline{M}_s$ of Figure 2.1b. Therefore, as pictured in Figure 2.1d, the magnetic current $2\overline{M}_s$ radiating into unbounded space produces the same field in $z > 0$ as do the original sources. The image field in $z < 0$ region is of no interest.

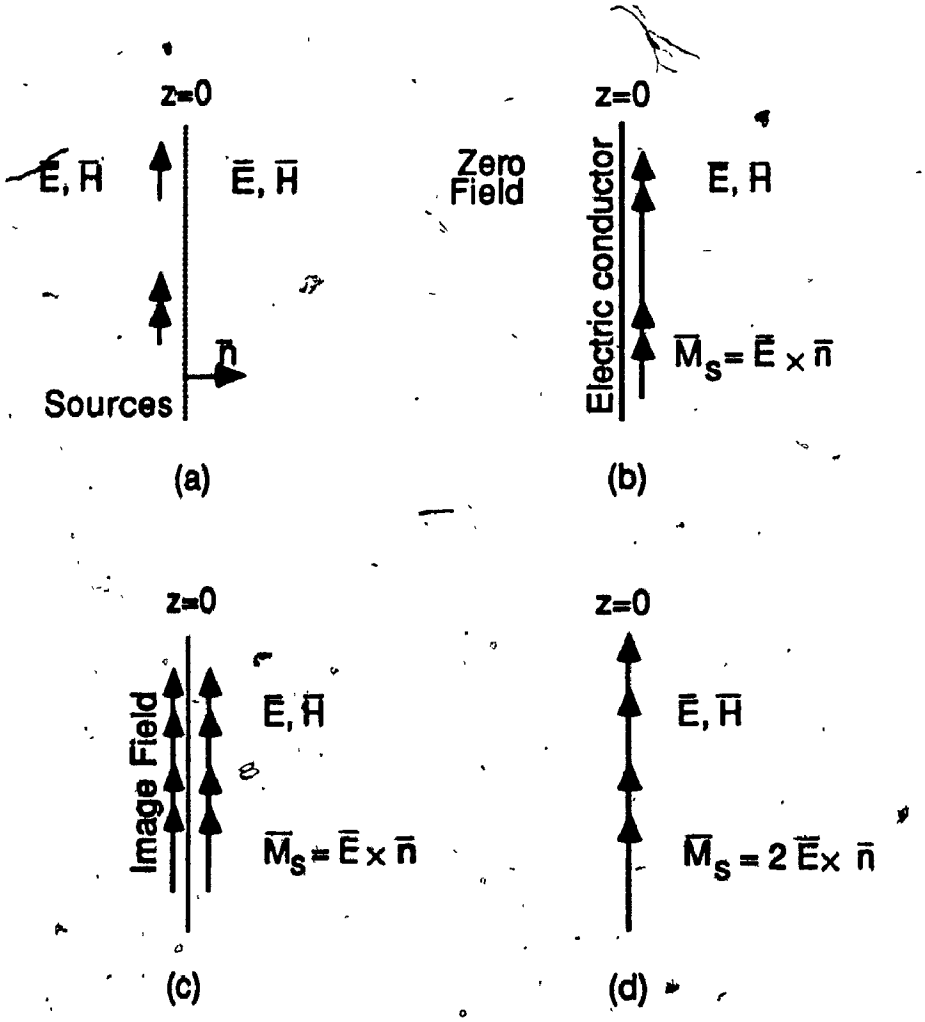

Figure 2.1 Illustration of the equivalence principle and image theory

The duality of the above problem is to replace the z = 0 plane by a perfect magnetic conductor, i.e. a fictitious surface on which the tangential magnetic field must vanish. In this case the magnetic current $\bar{M}_s$ is short circuited and the field in the z > 0 region may be found from the electric current $\bar{J}_s = 2\,\bar{n}\times\bar{H}$ on the z = 0 plane alone.

The scattered field in the unbounded free space can be determined from the following identities,

$$\bar{E}_s = -\nabla\times\bar{F} + \frac{1}{j\omega\varepsilon_0}\nabla\times\nabla\times\bar{A} \tag{2.1}$$

$$\bar{H}_s = -\nabla\times\bar{A} + \frac{1}{j\omega\mu_0}\nabla\times\nabla\times\bar{F} \tag{2.2}$$

where $\bar{A}$ is the magnetic vector potential and $\bar{F}$ is the electric vector potential. The two quantities are defined by

$$\bar{A} = \frac{1}{4\pi}\iint_S \bar{J}_s \frac{e^{-jkR}}{R}\,dS \tag{2.3a}$$

$$\bar{F} = \frac{1}{4\pi}\iint_S \bar{M}_s \frac{e^{-jkR}}{R}\,dS \tag{2.3b}$$

The surface S and vector notations are shown in Figure 2.2. k is the free-space wave number.

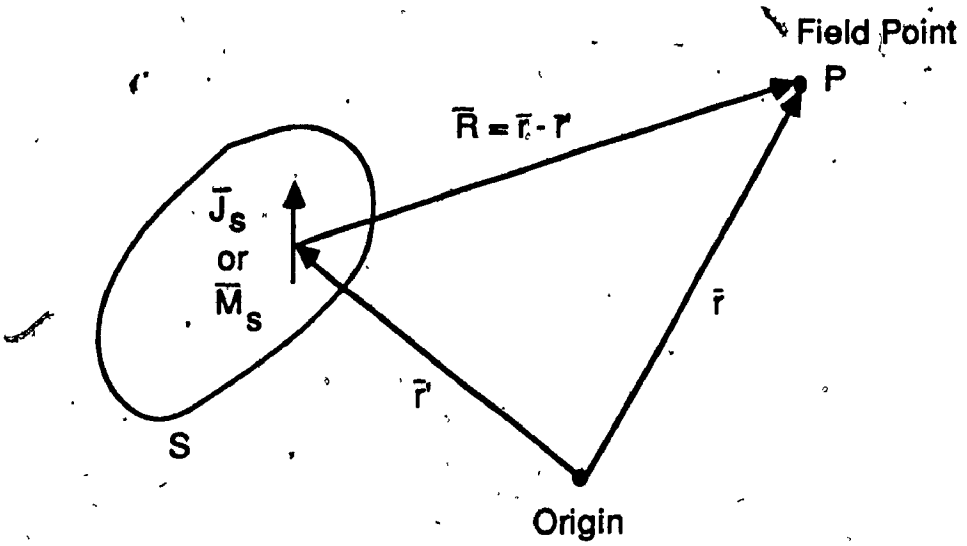

Figure 2.2 Vector nomenclature

According to the field equivalence principle and the image theory discussed earlier, it is apparent that the scattered field in the half space ($z > 0$) can be determined in terms of electric and magnetic currents $\bar{J}_s = \hat{n}\times\bar{H}$, $\bar{M}_s = -\hat{n}\times\bar{E}$ located on the aperture or in terms of electric current $\bar{J}_s = 2\hat{n}\times\bar{H}$ or magnetic current $\bar{M}_s = -2\hat{n}\times\bar{E}$. In the latter two cases a perfect magnetic or perfect electric conducting surface is postulated to be placed just inside the $z = 0$ plane. The present analysis assumes a perfect electric conducting surface over the horn aperture, thus short circuiting the current $\bar{J}_s$.

It is now appropriate to consider the integral equation for the scattered field from an array. For simplicity, the following assumptions have been made prior to the analysis :

(a) all apertures are openings of waveguides (this is to provide a simplified description of the modal fields),

(b) all apertures are identical and may be loaded with dielectric, and

(c) apertures are located arbitrarily in an infinite electric ground plane.

The planar array under considerations, Figure 2.3, consists of N circular apertures terminated in a ground plane. From (2.2), the magnetic field at points on a plane perpendicular to the ground plane, at a distance R from the origin is

$$\bar{H}_s = \frac{j}{2\pi\omega\mu_0}\iint (\nabla_t\nabla_t + k^2)\,.\,\bar{z}\times\bar{E}_t\, G(|\bar{r}-\bar{r}'|)\,dS \qquad (2.4)$$

The tangential electric field is denoted as $\bar{E}_t$ and is assumed to have the form $\bar{E}_t = \bar{E}_0\, e^{-j(\omega t + kz)}$. The unit vector $\bar{z}$ is normal to the aperture plane, ∇_t is the transverse gradient operator. The kernel $G(|\bar{r}-\bar{r}'|)$ is given by

$$G(|\bar{r}-\bar{r}'|) = \exp(-jk|\bar{r}-\bar{r}'|)/(|\bar{r}-\bar{r}'|)$$

where r is the position vector of the field point and r' is the position vector of the source point on the aperture.

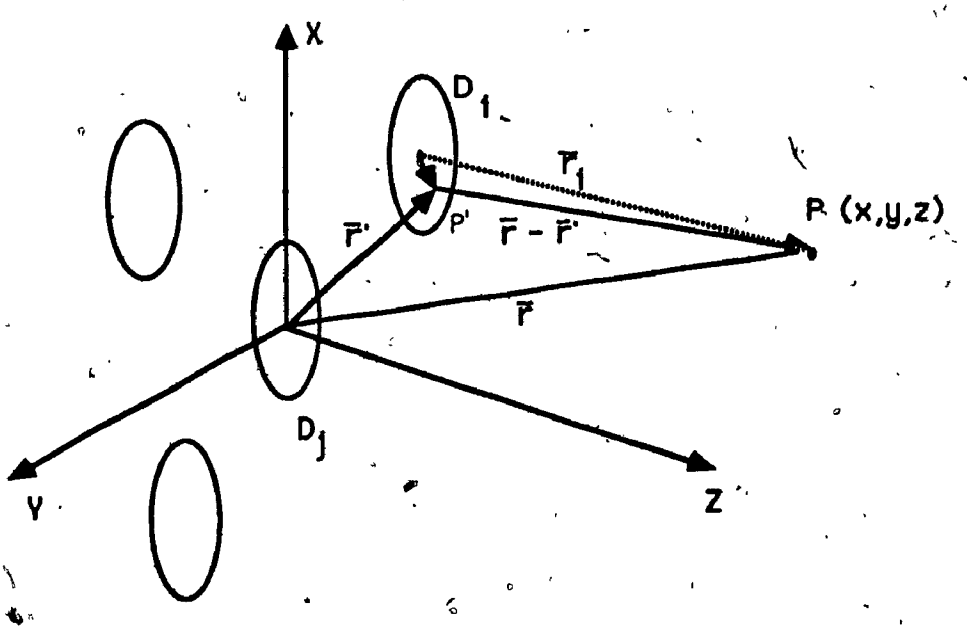

Figure 2.3 Planar array with the observation field point P and the source point P' on the waveguide aperture

When the observation point P lies on the plane z = 0, equation (2.4) becomes an integral equation in the fields components tangential to the array aperture. This equation is constrained upon all possible trial solutions to the aperture fields. One possible set of trial solutions is the modal fields of the waveguides. Furthermore, for the assumption that all apertures are terminated on a ground plane, the tangential electric field $\bar{E}_t$ vanishes everywhere except on the openings, the surface integral in equation (2.4) then becomes a sum of integrals over the N waveguide apertures. The total aperture field is now composed of N discontinous field "patches" as

$$\bar{E}_t = \sum_{i=1}^{N} \bar{E}_t^{(i)} \tag{2.5}$$

The continuity of the tangential electric and magnetic fields permits equation (2.4) to be rewritten as

$$\sum_{i=1}^{N} \bar{H}_t^{(i)} = \frac{j}{2\pi\omega\mu_0} \sum_{i=1}^{N} \iint_{D_i} (\nabla_t \nabla_t + k^2) . \bar{z} \times \bar{E}_t^{(i)} G(|\bar{r} - \bar{r}'|) \, dS \tag{2.6}$$

This equation expresses the unknown coupled field $\bar{E}^{(i)}_t$ in all waveguide apertures in terms of the known incident fields $\bar{H}^{(i)}_t$. The method of moments can be used to obtain an approximate solution for the above coupled equation. In the next Section, steps in transforming equation (2.6) into a system of linear algebraic equations will be presented.

2.3 The Method of Moments Solution

The unified concept in the numerical treatment of radiation problems

is the method of moments [3]. This method applies the concept of linear spaces and linear operators to the problem. The solution proceeds by expanding the unknown electric field as a linear combination of a set of expansion functions or basis functions, with complex coefficients, defines a suitable inner product over the operating domain of the operator and a set of weighting functions or testing functions. The next step in the solution is to take the inner product to form a matrix equation and solve this matrix for the unknown complex coefficients of the electric field expansion. For the present scattering problem, the linear operator in the deterministic L(f) = g can be identified as

$$L(\bar{E}) = \frac{j}{2\pi\omega\mu_0} \iint_{D_i} (\nabla_t \nabla_t' + k^2) \cdot \bar{z} \times \bar{E}\, G(|\bar{r} - \bar{r}'|)\, dS \qquad (2.7)$$

$\bar{E}$ is the unknown tangential electric field, g is the known incident magnetic field at the waveguide apertures. The unknown electric field can be expanded in a series of basis functions $\{\bar{e}_n\}$,

$$\bar{E} = \sum_n \alpha_n \bar{e}_n \qquad (2.8)$$

where α_n are complex coefficients to be defined. For exact solutions, equation (2.8) is usually an infinite summation and the e_n's form a complete set of basis functions. For approximate solutions, this summation is usually finite. Substituting equation (2.8) into equation (2.7) and using the linearity of L to get

$$\sum_n \alpha_n L(\bar{e}_n) = g \qquad (2.9)$$

A set of equations for the coefficients α_n is then obtained by taking an inner product of equation (2.9) with a set of weighting functions $\{\bar{w}_n\}$,

$$\sum_n \alpha_n < \bar{w}_m , L(\bar{e}_n) > = < \bar{w}_m , g > \qquad (2.10)$$

$m = 1,2,3,...$

This set of equations can be rewritten in a matrix form as

$$[C_{mn}][\alpha_n] = [g_{mn}] \qquad (2.11)$$

In explicit form,

$$[C_{mn}] = \begin{bmatrix} <\bar{w}_1 , L(\bar{e}_1)> & <\bar{w}_2 , L(\bar{e}_2)> & ..... \\ <\bar{w}_2 , L(\bar{e}_1)> & <\bar{w}_2 , L(\bar{e}_2)> & ..... \\ & & \end{bmatrix}$$

$$[\alpha_n] = \begin{bmatrix} \alpha_1 \\ \alpha_2 \\ \alpha_3 \\ . \\ . \end{bmatrix} \qquad [g_{mn}] = \begin{bmatrix} <\bar{w}_1 , g> \\ <\bar{w}_2 , g> \\ <\bar{w}_3 , g> \\ . \\ . \end{bmatrix} \qquad (2.12)$$

If the matrix $[C_{mn}]$ is nonsingular, then its inverse $[C]^{-1}$ exists. The coefficients α_n are readily obtained by

$$[\alpha_n] = [C_{mn}]^{-1} [g_{mn}]$$

The particular choice $\{\bar{e}_n\}$ equals to $\{\bar{w}_n\}$ is known as Galerkin's method. The choice of the sets of basis and weighting functions has significant impact on the convergence rate of the solution and the complexity of the elements $\langle \bar{w}_m , L(\bar{e}_n) \rangle$ that must be evaluated. Fast convergence is of prime interest in this particular problem. The number of unknown $\bar{e}_n$ and thus the number of equations to be solved must be kept at a minimum. The mode functions are considered suitable basis functions since a small number of modes usually suffices to give an accurate field representation at the waveguide apertures. For the weighting functions it is believed worthwhile to sacrifice ease of evaluation and to employ a more sensitive function than the common delta function, since a low order solution usually is dependent on the particular location of the matching point.

In view of the above discussion, the tangential electric field in the i-th horn is approximated by an M-mode expansion,

$$\bar{E}_t^{(i)} = \sum_{m=1}^{M} (a_m^{(i)} e^{-j\gamma_m z} + b_m^{(i)} e^{j\gamma_m z}) \bar{e}_m \qquad (2.13a)$$

$$\bar{H}_t^{(i)} = \sum_{m=1}^{M} (a_m^{(i)} e^{-j\gamma_m z} - b_m^{(i)} e^{j\gamma_m z}) \bar{h}_m \qquad (2.13b)$$

where $a^{(i)}_m$ and $b^{(i)}_m$ are the unknown modal coefficients of the m-th mode propagating in the positive and negative z-direction, respectively. $\bar{e}_m$ and $\bar{h}_m$ are the transverse electric and magnetic fields of mode m, and are related to each other by

$$\bar{h}_m = \frac{1}{Z_m} (\bar{z} \times \bar{e}_m)$$

Z_m is the transverse mode impedance which is given by

$$Z_m = \begin{cases} \dfrac{kZ_0}{\gamma_m} & ; \text{ for TE modes} \\ \dfrac{\gamma_m Z_0}{k\varepsilon_r} & ; \text{ for TM modes} \end{cases}$$

Z_0 is the intrinsic wave impedance of free space, ε_r is the relative dielectric constant of the waveguide medium and γ_m is the propagation constant of mode m. The field characteristics of a circular waveguide are given in Appendix A. It is noted that a single subscript notation m (or n) is chosen to refer to the double subscript notation lk (or pq), for the sake of convenience.

Substitution of (2.13a) and (2.13b) into (2.6) leads to

$$\sum_{i=1}^{N}\sum_{m=1}^{M}(a_m^{(i)} - b_m^{(i)})\,\bar{h}_m = \frac{j}{2\pi\omega\mu_0}(\nabla_t\nabla_t + k^2)\cdot\bar{z}\times \sum_{j=1}^{N}\sum_{n=1}^{M}\iint_{D_j}(a_n^{(j)} + b_n^{(j)})\,\bar{e}_n\,G(|\bar{r}-\bar{r}'|)\,dS' \qquad (2.14)$$

Additional indices i and j are used to identify the apertures under consideration. It is convenient to define

$$A_n^{(j)} = a_n^{(j)} + b_n^{(j)} \qquad (2.15)$$

$$B_m^{(i)} = a_m^{(i)} - b_m^{(i)}$$

and rewrite (2.14) as

$$\sum_{i=1}^{N}\sum_{m=1}^{M} B_m^{(i)}\,\bar{h}_m = \frac{j}{2\pi\omega\mu_0}(\nabla_t\nabla_t + k^2)\cdot\bar{z}\times\sum_{j=1}^{N}\sum_{n=1}^{M} A_n^{(j)}\,\bar{e}'_n\,G(|\bar{r}-\bar{r}'|)dS' \tag{2.16}$$

Following Galerkin's method to perform an inner product of (2.16) with a set of weighting functions $\bar{h}_m$ (m=1,2,3,...,M) over the apertures D_i's to arrive at

$$N_m B_m^{(i)} = \frac{j}{2\pi\omega\mu_0}\sum_{j=1}^{N}\sum_{n=1}^{M} A_n^{(j)}\iint_{D_i}\Big\{\bar{h}_m^{(i)}(\nabla_t\nabla_t + k^2)\cdot\bar{z}\times \iint_{D_j}\bar{e}'_n\,G(|\bar{r}-\bar{r}'|)\,dS'\Big\}\,dS \tag{2.17}$$

Notice that the modal fields $\bar{h}_m$ are identically zero outside the appropriate waveguide region. In addition, they are orthogonal to each other and that results in non-vanishing inner product of two similar modes.

The constant N_m in equation (2.17) is identified as normalization factor and is given by

$$N_m = \iint_{D_i}\bar{h}_m^{(i)}\cdot\bar{h}_m^{(i)}dS = -\frac{\pi a^4}{\varepsilon_{0p}}\begin{cases}\left(\dfrac{\gamma_m Y_m}{X_m}\right)^2\left(1-\dfrac{p^2}{X_m^2}\right) & ;\ \text{for TE modes}\\[2ex] \left(\dfrac{k_0\varepsilon_r}{Z_0 X'_m}Y'_m\right)^2 & ;\ \text{for TM modes}\end{cases} \tag{2.18}$$

with

$$\varepsilon_{0p} = \begin{cases} 1 & ; \text{ when } p = 0 \\ 2 & ; \text{ when } p > 0 \end{cases}$$

p denotes the azimuthal variation of the mode

$X_m = \lambda_m a$, $Y_m = J_p(\lambda_m a)$ and $Y'_m = J'_p(\lambda_m a)$. J_p is the Bessel function of the first kind, order p and J'_p is its first derivative.

After dividing both sides by N_m, a matrix equation for the unknown coefficients is obtained as

$$B_m^{(i)} = C^{(ij)}_{mn} A_n^{(j)}$$

The mutual coupling coefficient $C^{(ij)}_{mn}$ relates the interaction between mode m in the i-th waveguide and mode n in the j-th waveguide. The following general expression of the element $C^{(ij)}_{mn}$ has been extracted from equation (2.17) as

$$C_{mn}^{(ij)} = \frac{j}{2\pi\omega\mu_0} \frac{Z_n}{N_m} \iint_{D_i} \left\{ \bar{h}_m^{(i)} (\nabla_t \nabla_t + k^2) \cdot \iint_{D_j} \bar{h}_n^{(j)} G(|\bar{r} - \bar{r}'|)\, dS' \right\} dS \tag{2.19}$$

The coupling matrix [C] deserves additional discussion. This is a complex square matrix of size N×M by N×M, where N represents the number of waveguides in the array and M represents the number of modes assumed to be present in each waveguide. The elements of matrix [C] are arranged in the following manner,

$$\begin{bmatrix} C_{11}^{(11)} & \cdots & C_{1M}^{(11)} & C_{11}^{(12)} & \cdots & C_{1M}^{(12)} & \cdots & C_{1M}^{(1N)} \\ C_{21}^{(11)} & \cdots & C_{2M}^{(11)} & C_{21}^{(12)} & \cdots & C_{2M}^{(12)} & \cdots & C_{2M}^{(1N)} \\ \cdot & \cdot & \cdot & \cdot & \cdot & \cdot & \cdot & \cdot \\ C_{M1}^{(N1)} & \cdots & C_{M2}^{(N1)} & \cdot & \cdot & \cdot & \cdot & C_{MM}^{(NN)} \end{bmatrix}$$

In the above illustration, apertures are identified by superscript whereas modes are identified by subscript.

One may characterize the array as a microwave multi-port network, represented by a scattering matrix [S]. The elements of the [S] matrix carry the same meaning as those used in the network theory, i.e. S_{ii} is the reflection coefficient seen at port i when all other ports are match terminated. S_{ij} is the transmission coefficient into port i from port j. Using the values obtained from equation (2.19) as the coefficients of matrix [C], the scattering matrix [S] for a finite array can be deduced from the relation

$$[S] = [I+C]^{-1}\,[I-C]$$

where [I] is a unitary diagonal matrix and $[.]^{-1}$ denotes matrix inversion. The scattering matrix [S] can be used to study the impedance properties of each element (self and mutual) for any amplitude and phase excitation of the array, i.e.

$$[b] = [S][a]$$

where [a] and [b] are column matrices for the complex amplitudes of the incident and reflected waveguide fields, respectively.

It should be noted that the coefficients $C^{(ij)}_{mn}$ are independent of the amplitudes of the individual modal fields assumed in the waveguides. However, the complex amplitude [a] of various waveguide modes incident upon the apertures must be previously known. The amplitudes of the incident waveguide modes are determined by a method in which the waveguides are excited. Usually, the apertures are fed by long straight sections of waveguide in which all but one mode are well below cut off and therefore the incident amplitude of higher order evanescent modes may be neglected. However, the assumption of reflected evanescent modes (due to the aperture discontinuity) can have some effects on the calculation of elements in the scattering matrix and hence the reflection coefficients of the propagating mode.

Our main interest is now focused on the evaluation of the coupling coefficient $C^{(ij)}_{mn}$. From equation (2.19), one realizes that further efforts are required to simplify this expression to a programmable form.

Let us expand equation (2.19) as

$$C^{(ij)}_{mn} = \frac{j}{2\pi\omega\mu_0}\frac{Z_n}{N_m}\Big\{k^2\iint_{D_i}\bar{h}^{(i)}_m\cdot\Big[\iint_{D_j}\bar{h}'^{(j)}_n\,G(|\bar{r}-\bar{r}'|)\,dS'\Big]dS + \iint_{D_i}dS\,\bar{h}^{(i)}_m\cdot\nabla_t\nabla_t\cdot\iint_{D_j}\bar{h}'^{(j)}_n\,G(|\bar{r}-\bar{r}'|)\,dS'\Big\} \qquad (2.20)$$

The operator ∇_t acts upon the unprimed (field) coordinates inside the integral over the aperture D_j. By means of Green's theorem, and properties of the modal functions h'_n, this operator can be eliminated from equation (2.20). A detailed discussion of such process can be found in Appendix B. Equation

(2.20) can now be written in a more convenient form,

$$C_{mn}^{(ij)} = \frac{j}{2\pi\omega\mu_0}\frac{Z_n}{N_m}\left\{k^2\iint_{D_i}\bar{h}_m^{(i)}\cdot\left[\iint_{D_j}\bar{h}_n'^{(j)}G(|\bar{r}-\bar{r}'|)\,dS'\right]dS + \right.$$

$$\left.\gamma_m\gamma_n\iint_{D_i}h_{zm}^{(i)}\cdot\left[\iint_{D_j}h_{zn}'^{(j)}G(|\bar{r}-\bar{r}'|)\,dS'\right]dS\right\} \qquad (2.21)$$

Alternatively,

$$C_{mn}^{(ij)} = \frac{jk^2}{2\pi\omega\mu_0}\frac{Z_n}{N_m}\iint_{D_i}dS\,\bar{h}_m^{(i)}\cdot\iint_{D_j}\bar{h}_m'^{(j)}G(|\bar{r}-\bar{r}'|)\,dS' +$$

$$\frac{j\gamma_m\gamma_n}{2\pi\omega\mu_0}\frac{Z_n}{N_m}\iint_{D_i}dS\,h_{zm}^{(i)}\cdot\iint_{D_j}h_{zn}^{(j)}\,G(|\bar{r}-\bar{r}'|)\,dS' \qquad (2.22)$$

For TM modes, the second term in equation (2.22) vanishes.

It is convenient to introduce

$$\bar{\Psi}_m^{TE} = \bar{h}_m + \frac{\gamma_m}{k}h_{zm}\bar{z} \qquad (2.23a)$$

$$\bar{\Psi}_m^{TM} = \frac{1}{Z_m}\bar{z}\times[\bar{\Psi}_m]^{TE} \qquad (2.23b)$$

so that $C^{(ij)}_{mn}$ can be further simplified to

$$C_{mn}^{(ij)} = \frac{j\omega\varepsilon_0}{2\pi}\frac{Z_n}{N_m}\iint_{D_i}dS\,\bar{\Psi}_m\cdot\iint_{D_j}\bar{\Psi}'_n\,G(|\bar{r}-\bar{r}'|)\,dS' \qquad (2.24)$$

With reference to Figure 2.4, for any point on the z = 0 plane, the Green's function can be represented by a contour integral in the eigenvalue

plane [19], i.e.

$$G(|\bar{r}-\bar{r}'|) = G(|\bar{\rho}-\bar{\rho}_j|) = \int_0^{\infty} \frac{\xi J_0(|\bar{\rho}-\bar{\rho}_j|\xi)}{\sqrt{\xi^2-k^2}} d\xi \qquad (2.25)$$

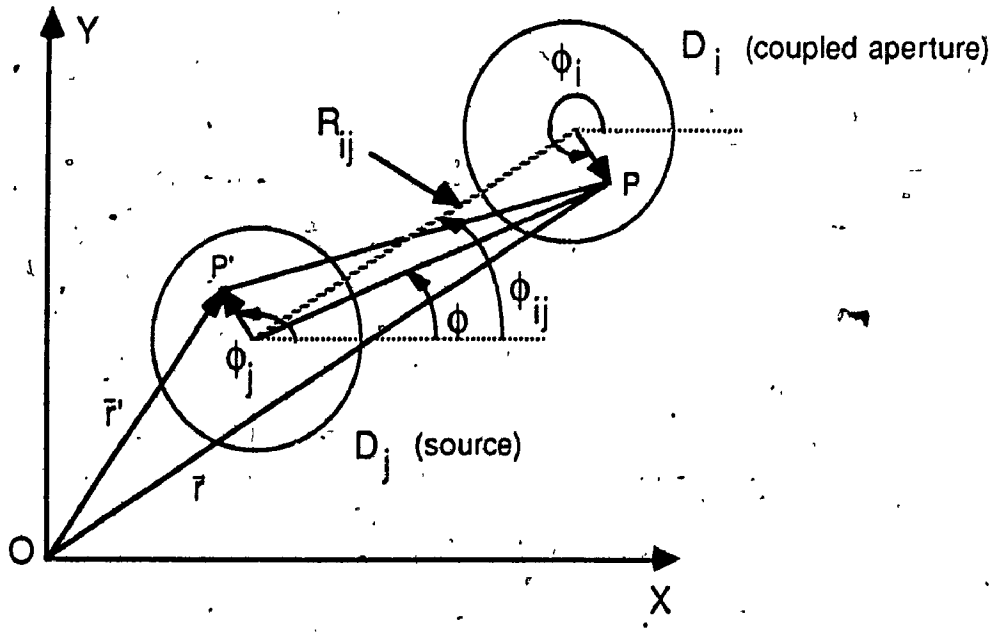

Figure 2.4 Geometry for determining the coupling between aperture point P and P'

By means of the addition theorem for Bessel functions of the first kind [17],

$$J_0(|\bar{\rho}-\bar{\rho}_j|\xi) = \sum_{s=-\infty}^{\infty} J_p(\rho\xi) J_s(\rho_j\xi) e^{js(\phi-\phi_j)} \qquad (2.26)$$

or equivalently

$$J_0(|\bar{\rho}-\bar{\rho}_j|\xi) = \sum_{s=0}^{\infty} \varepsilon_s J_s(\rho\xi)\, J_s(\rho_j\xi) \cos(s(\phi-\phi_j)) \qquad (2.27)$$

$$\text{with} \qquad \varepsilon_s = \begin{cases} 1 & \text{when } s = 0 \\ 2 & \text{when } s > 0 \end{cases}$$

The modification of the kernel $G(|\bar{r}-\bar{r}'|)$ enables the expression of the coupling coefficient $C^{(ij)}_{mn}$ in equation (2.24) to be rewritten as,

$$C^{(ij)}_{mn} = \frac{j\omega\varepsilon_0}{2\pi}\frac{Z_n}{N_m}\left\{\iint_{D_i} dS\, \bar{\Psi}_m \cdot \int_0^{\infty} \frac{\xi\, d\xi}{\sqrt{\xi^2-k^2}} \iint_{D_j} \bar{\Psi}'_n \sum_{s=0}^{\infty} \varepsilon_s J_s(\rho\xi)\, J_s(\rho_j\xi) \cos(s(\phi-\phi_j))\, dS' \right\} \qquad (2.28)$$

For compactness, let us define a vector $\bar{F}^{(j)}_n$ as

$$\bar{F}^{(j)}_n = \sum_{s=0}^{\infty} \varepsilon_s J_s(\rho\xi) \iint_{D_j} J_s(\rho_j\xi) \cos(s(\phi-\phi_j))\, \bar{\Psi}'_n\, dS'$$

Equation (2.28) then becomes

$$C^{(ij)}_{mn} = \frac{j\omega\varepsilon_0}{2\pi}\frac{Z_n}{N_m}\left\{\int_0^{\infty} \frac{\xi\, d\xi}{\sqrt{\xi^2-k^2}} \iint_{D_i} \bar{\Psi}_m \cdot \bar{F}^{(j)}_n\, dS \right\} \qquad (2.29)$$

The vector $\bar{F}^{(j)}_n$ needs be expanded before evaluating the coefficients $C^{(ij)}_{mn}$. One may observe that there will be two different vectors $\bar{F}^{(j)}_n$ corresponding to the TE and TM modes (this is due to $\bar{\Psi}_n$ defined earlier). The derivation of $\bar{F}^{(j)}_n$ is straightforward but quite lengthy to be presented here. The final expressions of $\bar{F}^{(j)}_n$ for TE and TM modes are summarized below.

a. TE modes

$$F_{nx}^{(j)} = \frac{j\pi\gamma_n}{\lambda_n}\left\{-J_{p-1}(\xi\rho)\int_0^a J_{p-1}(\xi\rho_j)J_{p-1}(\lambda_n\rho_j)\cos((p-1)\Phi-\psi_n)\rho_j d\rho_j + J_{p+1}(\xi\rho)\int_0^a J_{p+1}(\xi\rho_j)J_{p+1}(\lambda_n\rho_j)\cos((p-1)\Phi-\psi_n)\rho_j d\rho_j\right\} \quad (2.30a)$$

$$F_{ny}^{(j)} = \frac{j\pi\gamma_n}{\lambda_n}\left\{J_{p-1}(\xi\rho)\int_0^a J_{p-1}(\xi\rho_j)J_{p-1}(\lambda_n\rho_j)\sin((p-1)\Phi-\psi_n)\rho_j d\rho_j + J_{p+1}(\xi\rho)\int_0^a J_{p+1}(\xi\rho_j)J_{p+1}(\lambda_n\rho_j)\sin((p+1)\Phi-\psi_n)\rho_j d\rho_j\right\} \quad (2.30b)$$

$$F_{nz}^{(j)} = \frac{2\pi}{k}\gamma_n J_p(\xi\rho)\int_0^a J_p(\xi\rho_j)J_p(\lambda_n\rho_j)\cos(p\Phi-\psi_n)\rho_j d\rho_j \quad (2.30c)$$

In equation (2.30) above, "a" denotes the aperture radius and λ_m (λ_n) is the cut-off wave number of the m-th (n-th) mode.

b. TM modes

The vector $\bar{F}^{(j)}_n$ for TM modes can be obtained from that of the TE modes using

$$\bar{F}_n^{(j)} = \frac{1}{Z_n}\bar{z}\times[\bar{F}_n^{(j)}]^{TE} \quad (2.31)$$

To this end, a matrix solution for the integral equation in the unknown tangential electric field at apertures has been presented. The matrix

elements are expressed in terms of intermodal and interelement coupling coefficients. This set of linear equations may be solved by either matrix inversion or elimination, leading to the transmission and reflection coefficients of various modes. A knowledge of those coefficients will readily define the apertures' electric field.

Having defined and explicitly expressed all relevant terms, the computation of the coupling coefficients can now be undertaken. Two separate intermodal couplings will be examined in the following Sections. The first of the two kinds is the self coupling which results when apertures D_i's and D_j's are common (or coincident with each other). The self-coupling coefficients $C^{(ii)}_{mn}$, which form diagonal blocks in the [C] matrix, are evaluated in Chapter 3. The other possible coupling is between modes in different apertures, i.e. when apertures D_i's and D_j's are separated. The resultant coefficients are termed as cross-coupling coefficients, and they form the main discussion of Chapter 4.

CHAPTER 3

ANALYSIS OF MODE COUPLING IN A SINGLE WAVEGUIDE

3.1 Introduction

As mentioned earlier, apart from the dominant mode that propagates in a waveguide, additional modes will be generated at the aperture and will travel back toward the throat. These higher order modes are, however, cut off before reaching the throat, but they do couple to the propagating mode to alter the input impedance of the waveguide. Single waveguide mode couplings will be dealt with in this Chapter.

One may easily see that there are four possible mode couplings in a waveguide, they are TE_{lk} to TE_{pq}, TE_{lk} to TM_{pq}, TM_{lk} to TE_{pq}, TM_{lk} to TM_{pq}. Nevertheless, not all modes can freely interact with one another. By the existence of sinusoidal functions in the analytical expression of $C^{(ij)}_{mn}$, coupling between two modes occurs only when they have similar azimuthal variation and polarization, i.e. $p = 1$ and $\psi_m = \psi_n$. Presentation of the detailed analysis is deemed impractical, thus only essential steps in the derivation and final expressions are included herein.

3.2 The TE to TE Mode Coupling

From equation (2.29), the mode coupling coefficient is given by

$$C_{mn}^{(ii)} = \frac{j\omega\epsilon_0}{2\pi}\frac{Z_n}{N_m}\left[\int_0^{\infty}\frac{\xi\, d\xi}{\sqrt{\xi^2-k^2}}\iint_{D_i}\bar{\Psi}_m^{(i)}\cdot\bar{F}_n^{(i)}\, dS\right] \qquad (3.1)$$

For TE mode, the Cartesian components of vector $\bar{\Psi}^{(i)}_m$ are given by

$$\Psi_{mx}^{TE} = \frac{j\gamma_m}{2\lambda_m}\left[-J_{l-1}(\lambda_m\rho)\cos((l-1)\phi-\psi_m) + J_{l+1}(\lambda_m\rho)\cos((l+1)\phi-\psi_m)\right]$$

$$\Psi_{my}^{TE} = \frac{j\gamma_m}{2\lambda_m}\left[J_{l-1}(\lambda_m\rho)\sin((l-1)\phi-\psi_m) + J_{l+1}(\lambda_m\rho)\sin((l+1)\phi-\psi_m)\right]$$

$$\Psi_{mz}^{TE} = \frac{\gamma_m}{k}J_l(\lambda_m\rho)\cos(l\phi-\psi_m) \qquad (3.2)$$

The components of vector $\bar{F}^{(j)TE}_n$ have been derived previously in equation (2.30). A generalized picture of the self coupling in a waveguide between modes TE_{lk} to TE_{lq} is given Figure 3.1.

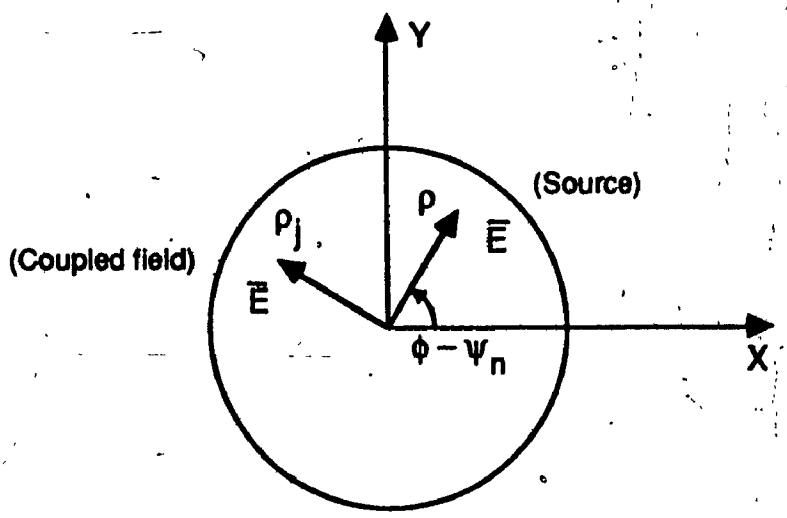

Figure 3.1 Electric fields of mode m and n in a waveguide

In considering the TE to TE mode coupling, it is realized that the TE_{01} modes are circularly symmetric, the polarization angles ψ_m and ψ_n can arbirarily be set to zero.

Let us further define

$$\kappa(\xi) = \int_0^a \int_0^{2\pi} \bar{\Psi}_m \cdot \bar{F}_n \rho d\rho \, d\phi \qquad (3.3)$$

The superscript is dropped since only one waveguide is presently considered.

Substitution of appropriate expressions and expansion of (3.3) lead to

$$\kappa(\xi) = \frac{4\pi^2 \gamma_m \gamma_n}{\lambda_m \lambda_n} \left[\frac{\lambda_m \lambda_n}{k^2} Q_0 Q_0' - Q_1 Q_1' \right] ; \text{ for } p = 0 \qquad (3.4a)$$

$$= \frac{\pi^2 \gamma_m \gamma_n}{\lambda_m \lambda_n} \left[\frac{2\lambda_m \lambda_n}{k^2} Q_p Q_p' - Q_{p-1} Q_{p-1}' - Q_{p+1} Q_{p+1}' \right] \cos(\psi_m - \psi_n) ; \text{ for } p > 0 \qquad (3.4b)$$

In equation (3.4) above, Q_p and Q'_p are Lommel's integrals of order p, defined as

$$Q_p = \int_0^a J_p(\xi\rho) J_p(\lambda_m \rho) \rho d\rho \quad \text{and} \quad Q_p' = \int_0^a J_p(\xi\rho_j) J_p(\lambda_n \rho_j) \rho_j d\rho_j$$

The evaluation of terms that involve Lommel's integral is simplified

by using the TE mode boundary condition at the edge of the horn aperture, i.e. $J'_p(\lambda_m a) = 0$ and $J'_p(\lambda_n a) = 0$. The final expressions of Q_p, Q_{p-1} and Q_{p+1} are listed below. Those of Q'_p, Q'_{p-1} and Q'_{p+1} can be derived by replacing λ_m by λ_n wherever applicable.

$$Q_p = \frac{-\xi a}{\xi^2 - \lambda_m^2} J_p(\lambda_m a)\, J_p'(\xi a) \qquad (3.5)$$

$$Q_{p-1} = \frac{p}{\xi \lambda_m} J_p(\lambda_m a)\, J_p(\xi a) - \frac{\lambda_m a}{(\xi^2 - \lambda_m^2)} J_p(\lambda_m a)\, J'_p(\xi a) \qquad (3.6)$$

$$Q_{p+1} = -\frac{p}{\xi \lambda_m} J_p(\lambda_m a)\, J_p(\xi a) - \frac{\lambda_m a}{(\xi^2 - \lambda_m^2)} J_p(\lambda_m a)\, J'_p(\xi a) \qquad (3.7)$$

By introducing the following new variables

$\zeta = \xi a$, $X_m = \lambda_m a$, $X_n = \lambda_n a$, $Y_m = J_p(\lambda_m a)$, $Y_n = J_p(\lambda_n a)$ and $K = ka$

equation (3.4) can be rearranged to

$$\kappa(\xi) = \frac{4\pi^2 a^6 \gamma_m \gamma_n Y_m Y_n}{(\zeta^2 - X_m^2)(\zeta^2 - X_n^2)} \left(\frac{\zeta^2}{K^2} - 1\right) (J'_0(\zeta))^2 \quad ; \text{ for } p = 0 \qquad (3.8)$$

$$= 2\pi^2 a^6 \gamma_m \gamma_n Y_m Y_n \left[\left(\frac{\zeta^2}{K^2} - 1\right) \frac{(J'_p(\zeta))^2}{(\zeta^2 - X_m^2)(\zeta^2 - X_n^2)} - \left(\frac{p\, J_p(\zeta)}{\zeta X_m X_n}\right)^2\right] \cdot \cos(\psi_m - \psi_n) \quad ; \text{ for } p > 0 \qquad (3.9)$$

The TE to TE self-coupling coefficient is readily obtained from (2.29) as

$$C^{(ii)}_{mn} = -\frac{2}{N_m K}\pi a^3 \gamma_m Y_m Y_n \int_0^\infty \frac{w\sqrt{1-w^2}}{(w^2-u_m^2)(w^2-u_n^2)} (J_0'(Kw))^2 \, dw \; ; \text{ for } p = 0 \tag{3.10}$$

$$= -\frac{1}{N_m K}\pi a^3 \gamma_m Y_m Y_n \left[\int_0^\infty \frac{w\sqrt{1-w^2}}{(w^2-u_m^2)(w^2-u_n^2)} (J_p'(Kw))^2 \, dw + \left(\frac{p}{X_m X_n}\right)^2 K \int_0^\infty \frac{(J_p(Kw))^2}{w\sqrt{1-w^2}} dw\right] \cos(\psi_m - \psi_n) \; ; \quad \text{for } p > 0 \tag{3.11}$$

In the above equations, $w = \zeta/K$, $u_m = X_m/K$ and $u_n = X_n/K$.

Similarity in equations (3.10) and (3.11) permits $C^{(ii)}_{mn}$ to be combined into one generalized form:

$$C^{(ii)}_{mn} = -\frac{1}{N_m}\pi a^3 \gamma_m Y_m Y_n \begin{cases} \frac{2}{K} G_{mn} \; ; \text{ for } p = 0 \\ \left[\frac{1}{K} G_{mn} + \left(\frac{p}{X_m X_n}\right)^2 K F_p\right] \cos(\psi_m - \psi_n) \; ; \\ \qquad \text{for } p > 0 \end{cases} \tag{3.12}$$

Two new terms have been introduced in equation (3.12), and given as

$$G_{mn} = \int_0^\infty \frac{w\sqrt{1-w^2}}{(w^2-u_m^2)(w^2-u_n^2)} (J_p'(Kw))^2 \, dw \tag{3.13}$$

$$F_p = \int_0^\infty \frac{(J_p(Kw))^2}{w\sqrt{1-w^2}} dw$$

When m = n, the coupling coefficient $C^{(ii)}_{mm}$ is understood as the

input admittance of mode m. In this case, the expression of $C^{(ij)}_{mn}$ is simplified to

$$C^{(ii)}_{mm} = -\frac{1}{N_m}\pi a^3 \gamma_m Y_m^2 \begin{cases} \frac{2}{K} G_{mn} & ; \text{ for } p = 0 \\ [\frac{1}{K} G_{mm} + (\frac{p}{X_m^2})^2 K F_p] & ; \text{ for } p > 0 \end{cases}$$

3.2 The TE to TM or TM to TE Mode Coupling

The following discussion focuses on the possible TE to TM or TM to TE mode coupling in a waveguide. A similar argument holds for the condition of mode interaction, that is two modes can couple to each other only when they have the same azimuthal variation. In the following derivation, subscript m (pq) stands for a TE mode and subscript n (pk) stands for a TM mode.

The components of vector $\bar{F}^{(j)}_n$ are derived from equation (2.31). They are

$$F^{TM(i)}_{nx} = -\frac{j\pi\gamma_n}{Z_n\lambda_n}\Big[J_{p-1}(\xi\rho)\int_0^a J_{p-1}(\xi\rho_j)\, J_{p-1}(\lambda_n\rho_j)\sin((p-1)\phi - \psi_n)\,\rho_j\, d\rho_j + J_{p+1}(\xi\rho)\int_0^a J_{p+1}(\xi\rho_j)\, J_{p+1}(\lambda_n\rho_j)\sin((p+1)\phi - \psi_n)\,\rho_j\, d\rho_j\Big] \quad (3.14a)$$

$$F_{ny}^{TM(i)} = \frac{j\pi\gamma_n}{Z_n\lambda_n}\Big[-J_{p-1}(\xi\rho)\int_0^a J_{p-1}(\xi\rho_j)\,J_{p-1}(\lambda_n\rho_j)\cos((p-1)\phi-\psi_n)\,\rho_j\,d\rho_j \;+$$

$$J_{p+1}(\xi\rho)\int_0^a J_{p+1}(\xi\rho_j)\,J_{p+1}(\lambda_n\rho_j)\cos((p+1)\phi-\psi_n)\,\rho_j\,d\rho_j\Big] \qquad (3.14b)$$

$$F_{nz}^{TM(i)} = 0 \qquad (3.14c)$$

For TM mode, the polarization angle ψ_n is referenced to the x axis.

The function $\kappa(\xi)$, as has been proposed in equation (3.3), is

$$\kappa(\xi) = \int_0^a\int_0^{2\pi} \bar{\Psi}_m^{TE}\cdot\bar{F}_n^{TM}\,\rho d\rho d\phi$$

$$= \frac{\pi^2\gamma_m\gamma_n}{Z_n\lambda_m\lambda_n}\left(-Q_{p-1}\,Q'_{p-1} + Q_{p+1}\,Q'_{p+1}\right)\sin(\psi_m-\psi_n) \qquad (3.15)$$

where

$$Q_{p-1} = \int_0^a J_{p-1}(\lambda_m\rho)\,J_{p-1}(\xi\rho)\,\rho d\rho \quad \text{and} \quad Q'_{p-1} = \int_0^a J_{p-1}(\lambda_n\rho)\,J_{p-1}(\xi\rho)\,\rho d\rho$$

The prime is used to distinguish the cut-off frequencies between the TE_{pq} and TM_{pk} modes.

The expansion of Lommel's integral, with the use of the boundary conditions of both TE and TM modes, reduces equation (3.15) to

$$\kappa(\xi) = -2\frac{\pi^2\,a\,\gamma_m\gamma_n}{Z_n\lambda_m^2\,\lambda_n(\xi^2-\lambda_n^2)}\,p\,J_p(\lambda_m a)\,J_p'(\lambda_n a)\,(J_p(\xi a))^2\sin(\psi_m-\psi_n) \qquad (3.16)$$

Substituting (3.16) into equation (2.29) and grouping all constants, the final expression of TE to TM coupling coefficient can be expressed as

$$C_{mn}^{(ii)} = -\frac{\pi \gamma_m \gamma_n a^4}{Z_0 N_m X_m^2 X_n} Y_m Y_n' p K_{mn} \sin(\psi_m - \psi_n) \qquad (3.17)$$

where

$$K_{mn} = \int_0^{\infty} \frac{w J_p^2(Kw)}{\sqrt{1-w^2}\,(w^2 - u_n^2)} dw \qquad (3.18)$$

A sine function exists in equation (3.16) since the initial electric field vectors of TE and TM modes have a 90 degree phase separation.

In general, the coupling matrix is not symmetric. Consequently, when the order of the indices m and n is reversed, equation (3.18) becomes

$$C_{nm}^{(ii)} = \frac{Z_n}{Z_m} \frac{N_m}{N_n} C_{mn}^{(ii)} \qquad (3.19)$$

3.4 The TM to TM Mode Coupling

The remaining self coupling is between two TM modes. The derivation is similar to those in earlier cases, it commences with the evaluation of function $\kappa(\xi)$

$$\kappa(\xi) = \int_0^a \int_0^{2\pi} \bar{\Psi}_m \cdot \bar{F}_n \, \rho d\rho d\phi$$

The dot product of two vectors $\bar{\Psi}_m$ and $\bar{F}_n$ can be performed relatively

simply since all components have already been defined. Making use of the separation of variables in the surface integral, the function $\kappa(\xi)$ can easily be evaluated as

$$\kappa(\xi) = -\frac{2}{(2-\delta_{0p})}\frac{\pi^2\gamma_m\gamma_n}{Z_m Z_n \lambda_m \lambda_n}\left(Q_{p-1}Q'_{p-1} + Q_{p+1}Q'_{p+1}\right)\cos(\psi_m - \psi_n) \tag{3.20}$$

As before, Lommel's integrals are expanded and then simplified. The TM boundary condition is once again applied in the simplification process. Equation (3.20) is now

$$\kappa(\xi) = -\frac{2\pi^2\gamma_m\gamma_n}{(2-\delta_{0p})Z_m Z_n \lambda_m \lambda_n}\frac{(\xi a J_p(\xi a))^2}{(\xi^2-\lambda_m^2)(\xi^2-\lambda_n^2)} J'_p(\lambda_m a)\, J'_p(\lambda_n a)\cdot \cos(\psi_m - \psi_n) \tag{3.21}$$

δ_{0p} is the Kronecker delta function given as

$$\delta_{0p} = \begin{cases} 1 & \text{if } p = 0 \\ 0 & \text{if } p \neq 0 \end{cases}$$

From equation (2.29), the coupling coefficient between two TM modes in a waveguide is,

$$C_{mn}^{(ii)} = -\frac{2\pi\gamma_n a^3 \varepsilon_r}{(2-\delta_{0p})N_m Z_0^2 X_m X_n} K\, Y'_m\, Y'_n\, L_{mn}\cos(\psi_m - \psi_n) \tag{3.22}$$

where

$$L_{mn} = \int_0^{\infty} \frac{w^3 J_p^2(Kw)}{(w^2 - u_m^2)(w^2 - u_n^2)\sqrt{1 - w^2}} dw \qquad (3.23)$$

When m = n, equation (3.22) becomes the input admittance (or self-coupling coefficient) of the TM modes;

$$C_{mm}^{(ii)} = -\frac{2\pi \gamma_m a \varepsilon_r}{(2 - \delta_{0p}) N_m} K \left[\frac{a J'_p(\lambda_m a)}{Z_0 X_m} \right]^2 L_{mm}$$

For convenience, Table 3.1 summarizes expressions of the coupling coefficients between TE modes, TE to TM or TM to TE modes, and TM modes, in a waveguide. Definition of constants can be found in Section 3.2.

Table 3.1

COUPLING COEFFICIENTS BETWEEN MODES IN A WAVEGUIDE

a. TE to TE Mode Coupling

$$C_{mn}^{(ii)} = -\frac{1}{N_m}\pi a^3 \gamma_m Y_m Y_n \begin{cases} \frac{2}{K} G_{mn} \; ; \text{for } p = 0 \\ [\frac{1}{K} G_{mn} + (\frac{p}{X_m X_n})^2 K F_p] \cos(\psi_m - \psi_n) \; ; \\ \qquad \text{for } p > 0 \end{cases}$$

with

$$G_{mn} = \int_0^\infty \frac{w\sqrt{1-w^2}}{(w^2-u_m^2)(w^2-u_n^2)} (J'_p(Kw))^2 \, dw$$

$$F_p = \int_0^\infty \frac{(J_p(Kw))^2}{w\sqrt{1-w^2}} dw$$

b. TE to TM or TM to TE Mode Coupling

$$C_{mn}^{(ii)} = -\frac{\pi \gamma_m \gamma_n a^4}{Z_0 N_m X_m^2 X_n} Y_m Y'_n p K_{mn} \sin(\psi_m - \psi_n)$$

with

$$K_{mn} = \int_0^\infty \frac{w J_p^2(Kw)}{\sqrt{1-w^2}(w^2-u_n^2)} dw$$

c. TM to TM Mode Coupling

$$C_{mn}^{(ii)} = -\frac{2}{(2-\delta_{0p})} \frac{\pi a^3 \gamma_n \varepsilon_r'}{Z_0^2 N_m X_m X_n} K Y'_m Y'_n L_{mn} \cos(\psi_m - \psi_n)$$

with

$$L_{mn} = \int_0^\infty \frac{w^3 J_p^2(Kw)}{(w^2 - u_m^2)(w^2 - u_n^2)\sqrt{1-w^2}} dw$$

3.5 Evaluation of Contour Integrals In a Complex Plane

Thus far, analytical expressions for the coupling coefficients between two modes in a waveguide have been derived as shown in equations (3.12), (3.17) and (3.22). In these expressions, one term yet to be numerically calculated is the infinite integral along the w axis. An essential difficulty of numerical integration is the high oscillatory nature of the integrand. This comes from the presence of product of Bessel functions or first-order derivative of Bessel functions and is illustrated in Figures 3.2 to 3.5 which show the behavior of the integrands in G_{mn}, F_p, K_{mn} and L_{mn}, respectively. A logarithmic scale has been selected to magnify the degree of variation. When these functions are numerically integrated, their convergence with an increasing number of integration points is quite slow. It is, therefore, convenient to transform the integration path into a complex plane so that the integrated function is monotonic over the new contour. The deformation technique suggested by Mishustin [16] and Bird [12] is adapted to these particular integrals. Further references to the integration of complex variable can be found in a text book by McLachlan [21]. The deformation of integration path is similar for all cases.

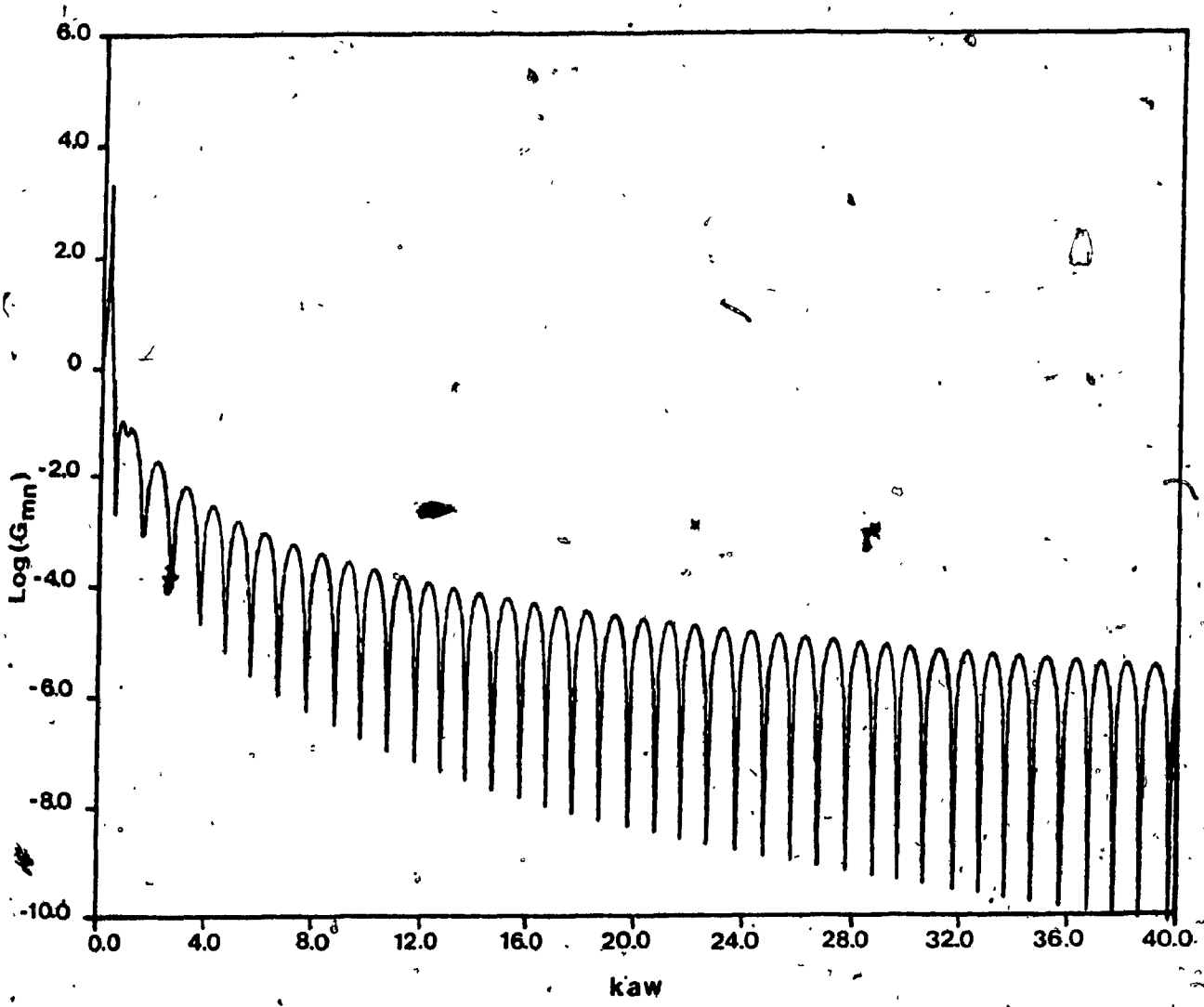

Figure 3.2 Variation of integrand in G_{mn} as a function of kaw

(TE_{11} mode coupling in one waveguide)

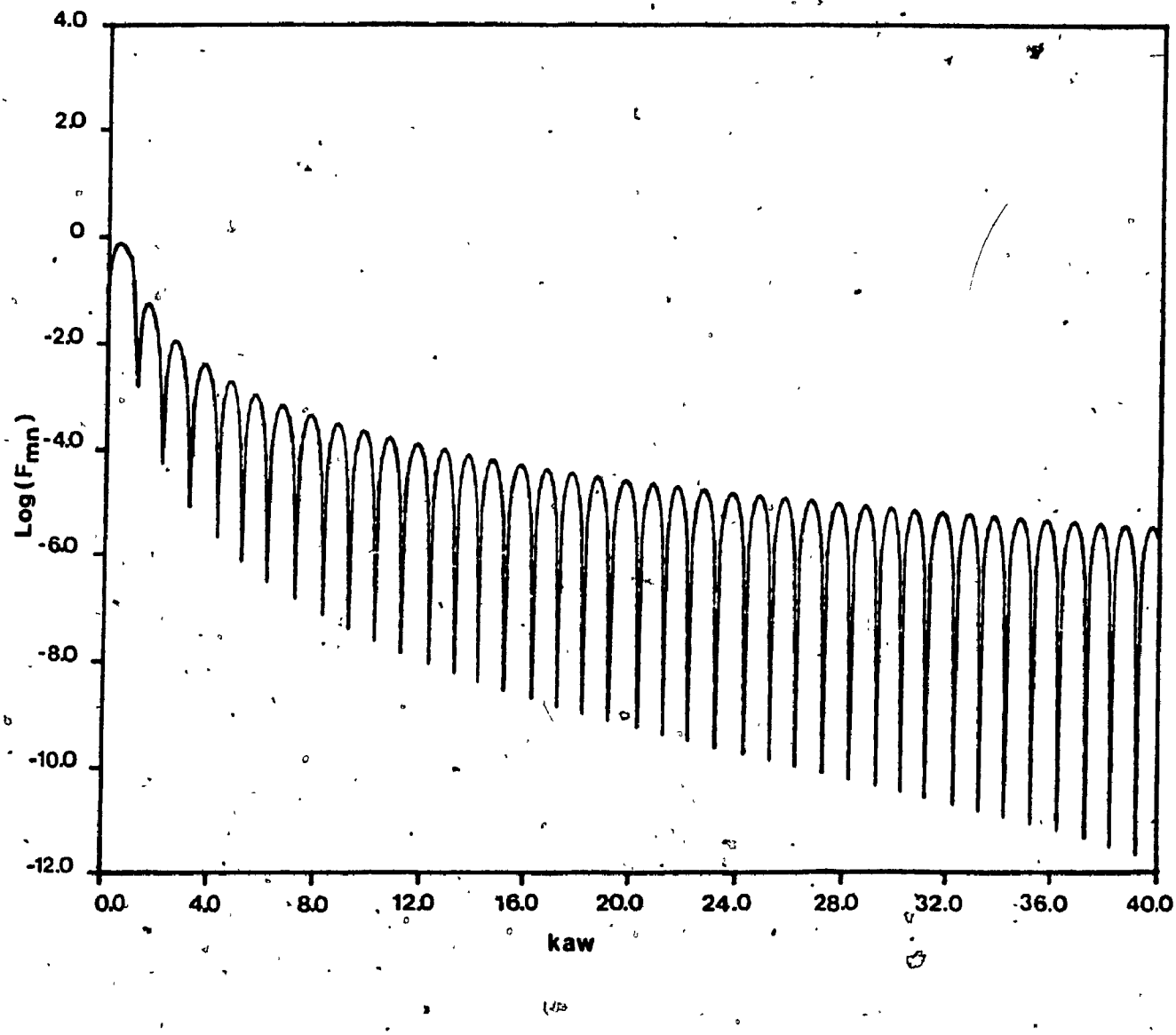

Figure 3.3 Variation of integrand in F_p as a function of kaw

(TE_{11} mode coupling in one waveguide)

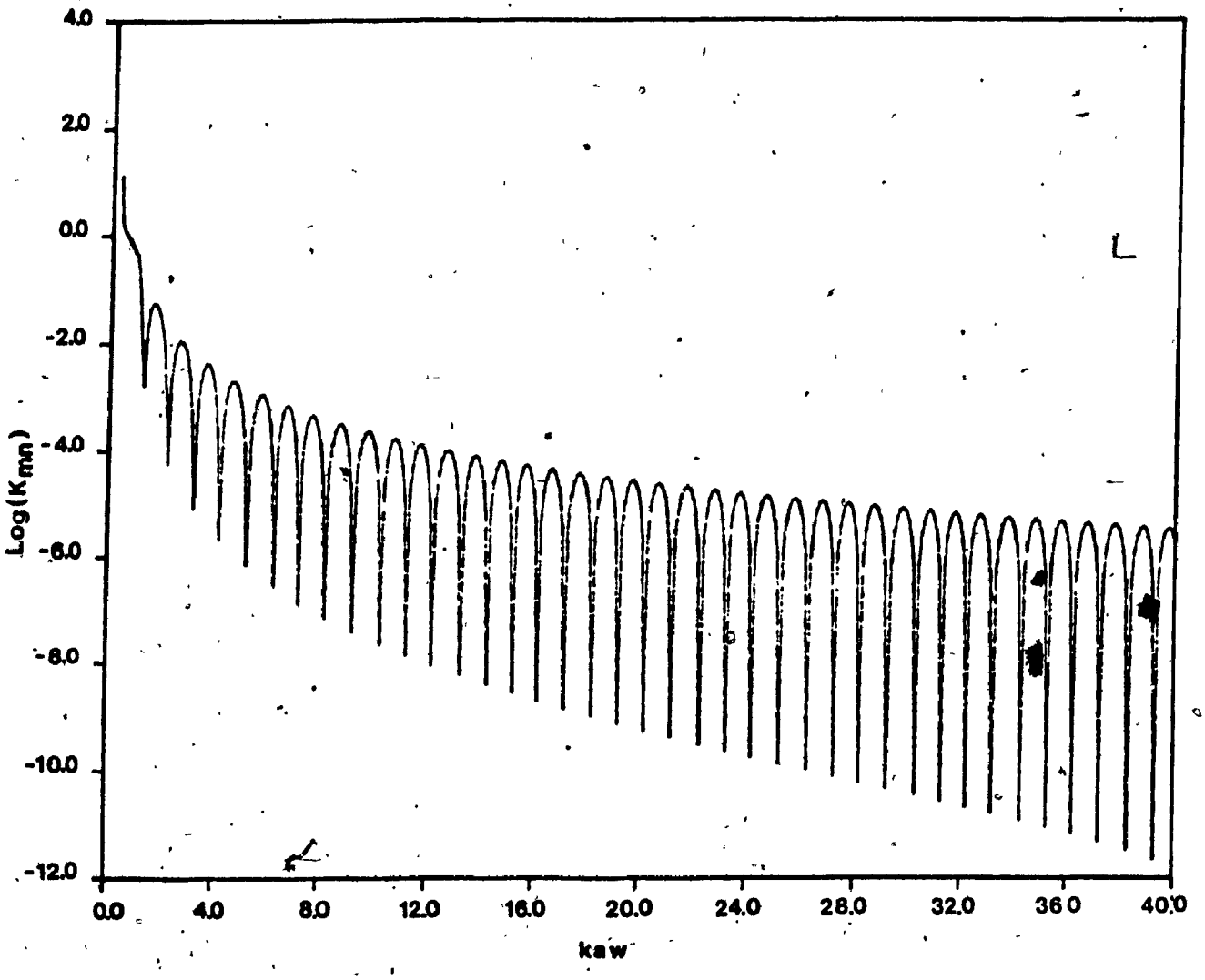

Figure 3.4 Variation of integrand in K_{mn} as a function of kaw

(TE_{11} to TM_{11} mode coupling in one waveguide)

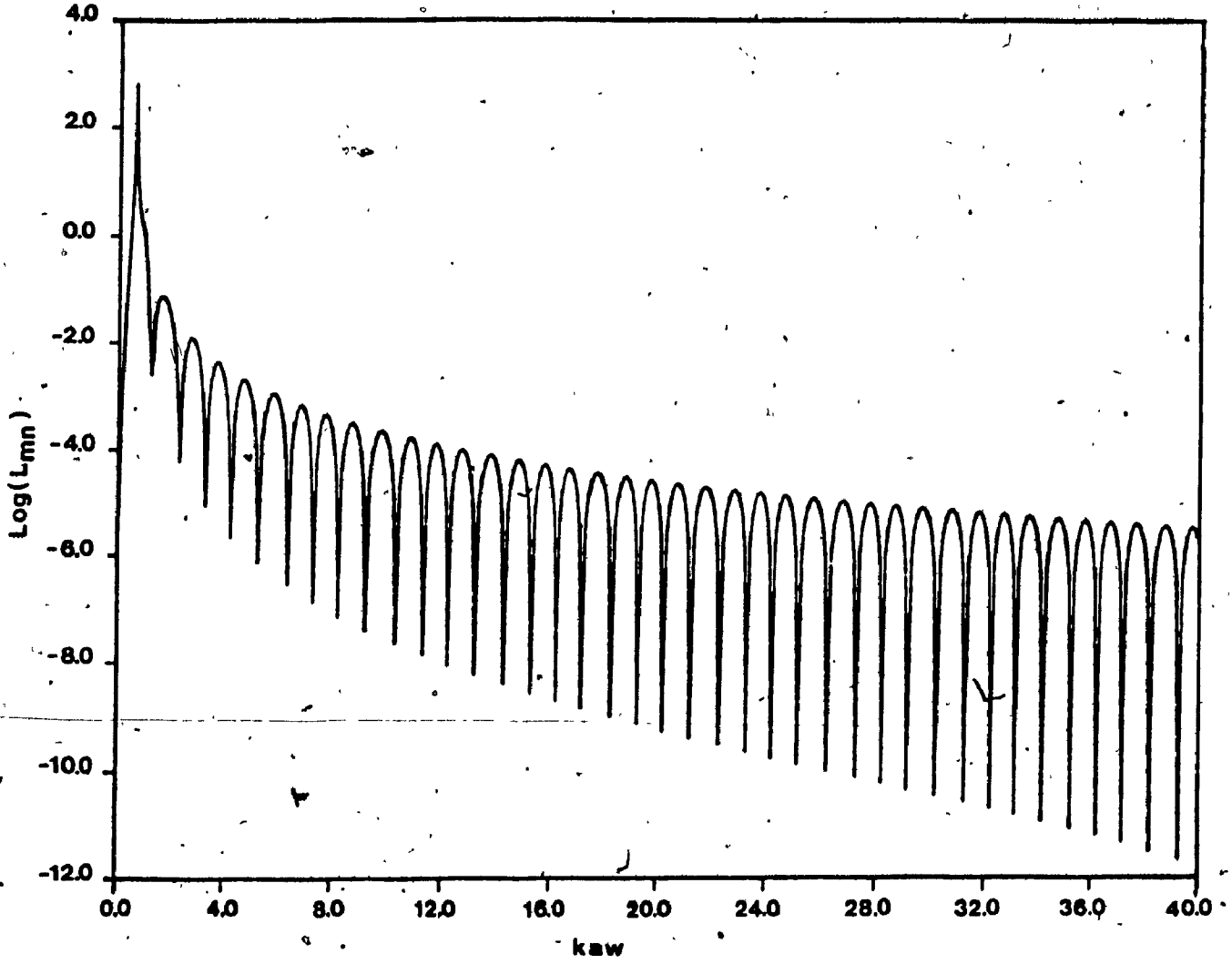

Figure 3.5 Variation of integrand in L_{mn} as a function of kaw

(TM_{11} mode coupling in one waveguide)

A detailed process will be presented only for the integral G_{mn}. For the remaining integrals, attention will be focused on key steps and final expressions.

3.5.1 Evaluation of G_{mn}

From (3.13),

$$G_{mn} = \int_0^\infty \frac{w\sqrt{1-w^2}}{(w^2-u_m^2)(w^2-u_n^2)} (J'_p(Kw))^2 \, dw$$

A relationship between cylindrical functions permits $J'_p(z)$ to be resolved into a summation of Hankel functions of the first and second kind, that is

$$J_p'(z) = \frac{1}{2}[H_p^{(1)}'(z) + H_p^{(2)}'(z)]$$

The integral is then altered to

$$G_{mn} = \frac{1}{2}\int_0^\infty \frac{w\sqrt{1-w^2}}{(w^2-u_m^2)(w^2-u_n^2)} J_p'(z)\,[H_p^{(1)}'(Kw) + H_p^{(2)}'(Kw)]\, dw \qquad (3.24)$$

$$= G_1 + G_2$$

We shall treat the integrals G_1 and G_2 separately.

a. Integral G_1

The integration contour of G_1, C_1 in Figure 3.6, contains no singularities, namely, a branch point at $w = 1$ and two simple poles at $w = u_m$ and $w = u_n$. By applying Cauchy's theorem, it may be found that in the plane $w > 0$ there are different contours that are equivalent to C_1. For the presence of

$H^{(1)'}_p(Kw)$, a suitable closed contour, as shown in Figure 3.6, in the upper half of the complex plane w is chosen. The contour comprising of C_1, C'_1 and an arc of radius R in the first quadrant encloses no singularities. Hence, the integral around this enclosed contour is zero. There is no contribution to the integral from the arc as the radius $R \to \infty$ since $H^{(1)}_p(Kw)$ tends to zero as $|w| \to \infty$ in the sector $0 < \arg(w) < \pi$. So, the contours C_1 and C'_1 described positively are equivalent.

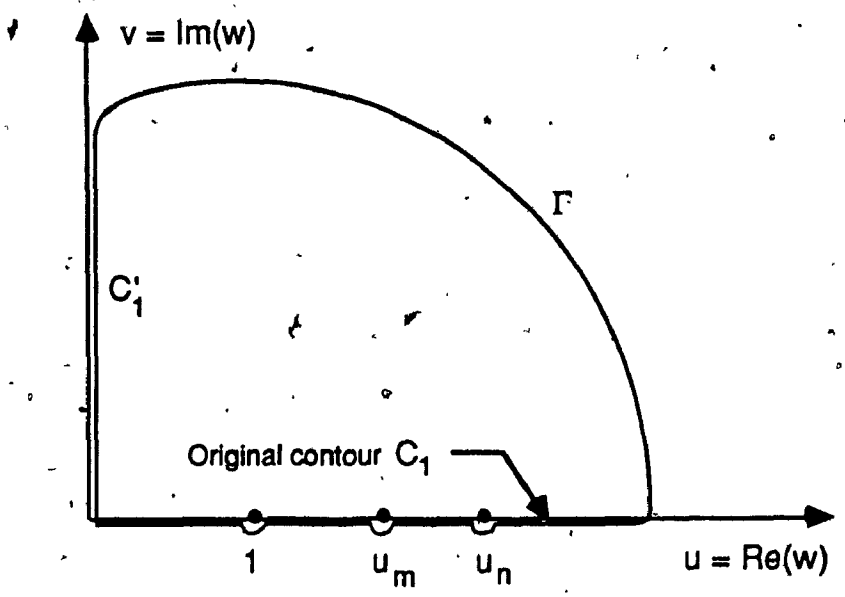

Figure 3.6 Deformation of integration path C_1 in a complex plane

Substituting $w = jv$ into G_1 to get

$$G_1 = -\frac{1}{2}\int_0^{\infty} \frac{v\sqrt{1+v^2}}{(v^2+u_m^2)(v^2+u_n^2)} J'_p(jKv)\, H_p^{(1)\,\prime}(jKv)\, dv \qquad (3.25)$$

From the following relationship, Ref [20]

$$J_p'(jKv) = -je^{jp\pi/2} I_p'(Kv)$$

$$H_p^{(1)'}(jKv) = -\frac{2}{\pi} e^{-jp\pi/2} K_p'(Kv)$$

where I'_p and K'_p are derivatives of the modified Bessel functions I_p and K_p,

$$J_p'(jKv)\, H_p^{(1)'}(jKv) = j\frac{2}{\pi} I_p'(Kv)\, K_p'(Kv)$$

As a result of these manipulations, the integral G_1 is modified to

$$G_1 = -j\frac{1}{\pi}\int_0^{\infty} \frac{v\sqrt{1+v^2}}{(v^2+u_m^2)(v^2+u_n^2)} I_p'(Kv)\, K_p'(Kv)\, dv \qquad (3.26)$$

b. Integral G_2

To evaluate G_2, a suitable contour which is equivalent to C_1 is selected. This equivalent contour is shown in Figure 3.7 as C'_2. In the region $-\pi < \arg(w) < 0$, the Hankel function $H^{(2)}_p(Kw)$ approaches zero for $|w| \to \infty$. This leads to the vanishing of the integral along Γ. The integral G_2 is then a summation of the integrals around the branch point, around the poles and along the branch cut. The integrals parallel to the Re(w) axis neutralize each other, since they are equal but opposite when the line separation $\to 0$. This is due to the function being analytic and single-valued, thereby returning to its original value after each pole is rounded.

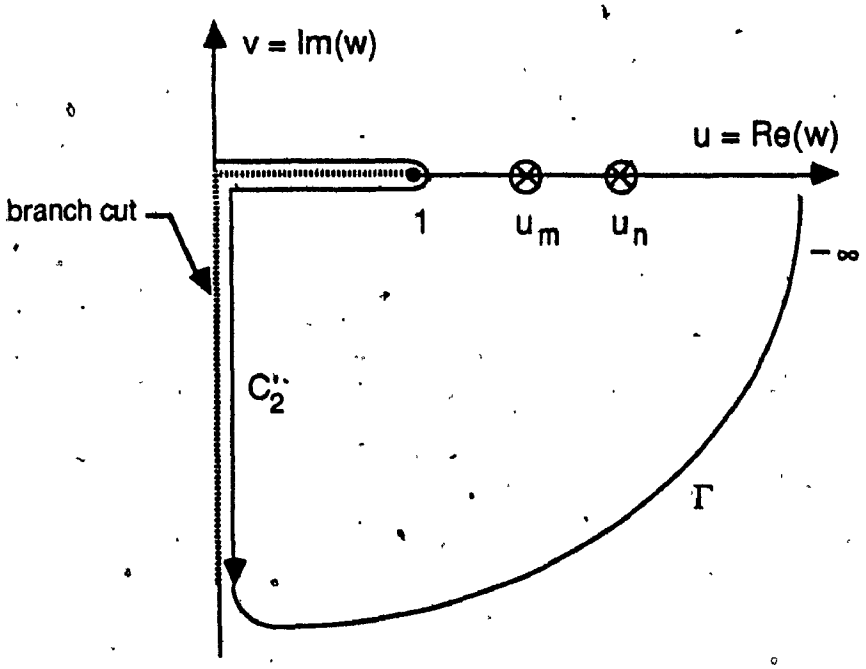

Figure 3.7 Deformation of integration path C_2 in a complex plane

The remaining terms of the integral along C'_2 are

$$G_2 = \int_0^1 \frac{u\sqrt{1-u^2}}{(u^2-u_m^2)(u^2-u_n^2)} J_p'(Ku)\, H_p^{(2)\prime}(Ku)\, du + \frac{1}{2}\int_0^\infty \frac{v\sqrt{v^2+1}}{(v^2+u_m^2)(v^2+u_n^2)} J_p'(-jKv)\, H_p^{(2)\prime}(-jKv)\, dv + j\pi \sum \text{Res}$$

For propagating modes, $0 < u_m < 1$ and $0 < u_n < 1$, the residues have no contribution to the total value of G_2. As

$$I_p'(Kv) = -j e^{jp\pi/2} J_p'(-jKv)$$

and $$K_p'(Kv) = -\frac{\pi}{2} e^{-jp\pi/2} H_p^{(2)\prime}(-jKv)$$

then,

$$G_2 = \int_0^1 \frac{u\sqrt{1-u^2}}{(u^2-u_m^2)(u^2-u_n^2)} J_p'(Ku)\, H_p^{(2)\prime}(Ku)\, du$$

$$-\frac{j}{\pi}\int_0^{\infty} \frac{v\sqrt{v^2+1}}{(v^2+u_m^2)(v^2+u_n^2)} I_p'(Kv)\, K_p'(Kv)\, dv$$

When either of the modes in the airfilled guide is evanescent, i.e. $u_m<1$ or $u_n<1$, the value of the integral at the poles must be accounted for. However, for $u_m \neq u_n$, the residues are zero, as being discussed below

$$\sum \text{Res}\,(G_2) = \left[\frac{F(w)}{Q'(w)}\right]_{w=u_m} + \left[\frac{F(w)}{Q'(w)}\right]_{w=u_n}$$

for $\quad F(w) = w\sqrt{1-w^2}\, J_p'(Kw)\, H_p^{(2)\prime}(Kw)$

and $\quad Q(w) = (w^2-u_m^2)(w^2-u_n^2)$

One may immediately realize that $F(w) = 0$ at $w = u_m$ and $w = u_n$, owing to the TE-mode boundary condition, $J'_p(\lambda_m a) = J'_p(\lambda_n a) = 0$. If $u_m = u_n$, i.e. self-coupling case, then the integrated function has a pole of order 2 at $w = u_m$. From the calculus of residues,

$$\text{Res}\, G_2 = \lim_{w \to u_m} \frac{d}{dw}\left[\frac{w\sqrt{1-w^2}\, J_p'(Kw)\, H_p^{(2)\prime}(Kw)}{(w+u_m)^2}\right]$$

Some manipulations with the differentiation and the limit lead to

$$\text{Res } G_2 = \frac{K\sqrt{1-u_m^2}}{4\,u_m} J_p''(X_m)\, H_p^{(2)\prime}(X_m)$$

$$= \frac{K\sqrt{u_m^2-1}}{4\,u_m} J_p''(X_m)\, Y_p'(X_m)$$

Finally, a complete solution of G_2 is obtained as,

$$G_2 = \int_0^1 \frac{u\sqrt{1-u^2}}{(u^2-u_m^2)(u^2-u_n^2)} J_p'(Ku)\, H_p^{(2)\prime}(Ku)\, du$$

$$- \frac{j}{\pi} \int_0^\infty \frac{v\sqrt{v^2+1}}{(v^2+u_m^2)(v^2+u_n^2)} I_p'(Kv)\, K_p'(Kv)\, dv$$

$$+ j\pi \frac{K\sqrt{u_m^2-1}}{4u_m} J_p''(X_m)\, Y_p'(X_m)\, \delta(u_m-u_n)\, H(u_m-1) \qquad (3.27)$$

The Kronecker delta function $\delta(u_m-u_n)$ and the Heaviside step function $H(u_m-1)$ are used to signify that the residue term is present only when the conditions $u_m = u_n$ and $u_m > 1$ are met.

3.5.2 Evaluation of F_p

The integral F_p is rewritten here for convenience,

$$F_p = \int_0^\infty \frac{J_p^2(Kw)}{w\sqrt{1-w^2}}\, dw$$

$$= \frac{1}{2} \int_0^\infty \frac{1}{w\sqrt{1-w^2}} J_p(Kw)\, [\, H_p^{(1)}(Kw) + H_p^{(2)}(Kw)\,]\, dw$$

$$= F_1 + F_2$$

Using the equivalent contours, as described in Section 3.5.1 above, for each integral to arrive at

$$F_p = \int_0^1 \frac{J_p(Ku)\, H_p^{(2)}(Ku)}{u\sqrt{1-u^2}}\, du - j\frac{2}{\pi}\int_0^\infty \frac{I_p(Kv)\, K_p(Kv)}{v\sqrt{1+v^2}}\, dv \qquad (3.28)$$

3.5.3 Evaluation of K_{mn}

From (3.18)

$$K_{mn} = \int_0^\infty \frac{w\, J_p^2(Kw)}{\sqrt{1-w^2}\,(w^2-u_n^2)}\, dw$$

$$= \frac{1}{2}\int_0^\infty \frac{w\, J_p(Kw)\, H_p^{(1)}(Kw)}{\sqrt{1-w^2}\,(w^2-u_n^2)}\, dw + \frac{1}{2}\int_0^\infty \frac{w\, J_p(Kw)\, H_p^{(2)}(Kw)}{\sqrt{1-w^2}\,(w^2-u_n^2)}\, dw$$

$$= K_1 + K_2$$

The deformation of the integration path of K_1 into the upper-half of the complex plane w leads to,

$$K_1 = -\frac{j}{\pi}\int_0^\infty \frac{v\, I_p(Kv)\, H_p^{(1)}(Kv)}{\sqrt{1+v^2}\,(v^2+u_m^2)}\, dv$$

Due to the presence of $H^{(2)}{}_p(Kw)$, the integration path of K_2 is deformed into the lower-half of the w-plane. This gives

$$K_2 = \int_0^1 \frac{u\, J_p(Ku)\, H_p^{(2)}(Ku)}{\sqrt{1-u^2}\,(u^2-u_n^2)}\, du - \frac{j}{\pi}\int_0^\infty \frac{v I_p(Kv)\, K_p(Kv)}{\sqrt{1+v^2}\,(v^2+u_n^2)}\, dv$$

The residue has no contribution to K_2 since

$$\operatorname*{Res}_{w=u_n} K_2 = \left.\frac{F(w)}{Q(w)}\right|_{w=u_n}$$

where $F(w) = w J_p(Kw) H_p^{(2)}(Kw)$

$$Q(w) = \sqrt{1-w^2}\,(w+u_n)$$

At $w = u_n$, $F(u_n) = u_n J_p(\lambda_n a) H^{(2)}_p(Ku_n) = 0$, owing to the TM-mode boundary condition.

Thus,

$$K_{mn} = \int_0^1 \frac{u J_p(Ku) H_p^{(2)}(Ku)}{\sqrt{1-u^2}\,(u^2-u_m^2)}\,du - j\frac{2}{\pi}\int_0^\infty \frac{v I_p(Kv) K_p(Kv)}{\sqrt{1+v^2}\,(v^2+u_n^2)}\,dv \qquad (3.29)$$

3.5.4 Evaluation of L_{mn}

The integral to be evaluated in the case of TM to TM mode coupling is

$$L_{mn} = \int_0^\infty \frac{w^3 J_p^2(Kw)}{(w^2-u_m^2)(w^2-u_n^2)\sqrt{1-w^2}}\,dw$$

As before, by means of a relationship between cylindrical functions, L_{mn} is modified to

$$L_{mn} = \frac{1}{2}\int_0^{\infty} \frac{w^3 J_p(Kw)\, H_p^{(1)}(Kw)}{\sqrt{1-w^2}\,(w^2-u_m^2)(w^2-u_n^2)}\,dw +$$

$$\frac{1}{2}\int_0^{\infty} \frac{w^3 J_p(Kw)\, H_p^{(2)}(Kw)}{\sqrt{1-w^2}\,(w^2-u_m^2)(w^2-u_n^2)}\,dw$$

$$= L_1 + L_2$$

For L_1, the equivalent path to the original one is along the imaginary axis in the positive sense, thus

$$L_1 = \frac{j}{\pi}\int_0^{\infty} \frac{v^3 I_p(Kv)\, K_p(Kv)}{\sqrt{1+v^2}\,(v^2+u_m^2)(v^2+u_n^2)}\,dv$$

For L_2, the equivalent integration path is a composition of that passes on both sides of the branch cut, along the negative imaginary axis and around the poles. If the poles u_m and u_n lie on the branch cut, then

$$L_2 = \frac{1}{2}\int_0^{1} \frac{u^3 J_p(Ku)\, H_p^{(2)}(Ku)}{\sqrt{1-u^2}\,(u^2-u_m^2)(u^2-u_n^2)}\,du$$

$$-\frac{j}{\pi}\int_0^{\infty} \frac{v^3 I_p(Kv)\, K_p(Kv)}{\sqrt{1+v^2}\,(v^2+u_m^2)(v^2+u_n^2)}\,dv$$

If either $0<u_m<1$ of $0<u_n<1$, then the contribution of the residues to the integral must be taken into account. Let the value of the integral obtained previously be L'_2. In this case,

$$L_2 = L'_2 + j\pi \sum \text{Residues}$$

When $u_m \neq u_n$, the residues are zero due to the TM boundary conditions, i.e. $J_p(\lambda_m a) = J_p(\lambda_n a) = 0$. When $u_m = u_n$, the integrand has a pole of order 2. The residue at the pole can be easily calculated by following,

$$\operatorname*{Res}_{w=u_m} L_2 = \lim_{w \to u_m} \frac{d}{dw} \left[\frac{w^3 J_p(Kw)\, H_p^{(2)}(Kw)}{\sqrt{1-w^2}\,(w+u_m)^2} \right]$$

$$= \frac{K u_m J'_p(X_m)\, Y_p(X_m)}{2\sqrt{u_m^2 - 1}}$$

The final result of the contour integral $L_{m\,n}$ is a summation of L_1 and L_2. This gives,

$$L_{mn} = \frac{1}{2} \int_0^1 \frac{u^3 J_p(Ku)\, H_p^{(2)}(Ku)}{\sqrt{1-u^2}\,(u^2 - u_m^2)(u^2 - u_n^2)}\, du$$

$$-j \frac{2}{\pi} \int_0^\infty \frac{v^3 I_p(Kv)\, K_p(Kv)}{\sqrt{1+v^2}\,(v^2 + u_m^2)(v^2 + u_n^2)}\, dv$$

$$+j\pi \frac{K u_m J'_p(X_m)\, Y_p(X_m)}{2\sqrt{u_m^2 - 1}}\, \delta(u_m - u_n)\, H(u_m - u_n) \qquad (3.30)$$

One may observe that in G_{mn}, F_p, K_{mn} and L_{mn}, there remains one integral along the imaginary axis. The function in these integrals is, however, monotonic over the integration path. Typical graphs of the modified integrands which are dependent on v are shown in Figures 3.8 to 3.11. The behavior of these functions allows the use of any standard numerical integration technique, such as Simpson, Gaussian quadrature or Romberg. Nevertheless, fast convergence is a main factor in selecting a suitable technique.

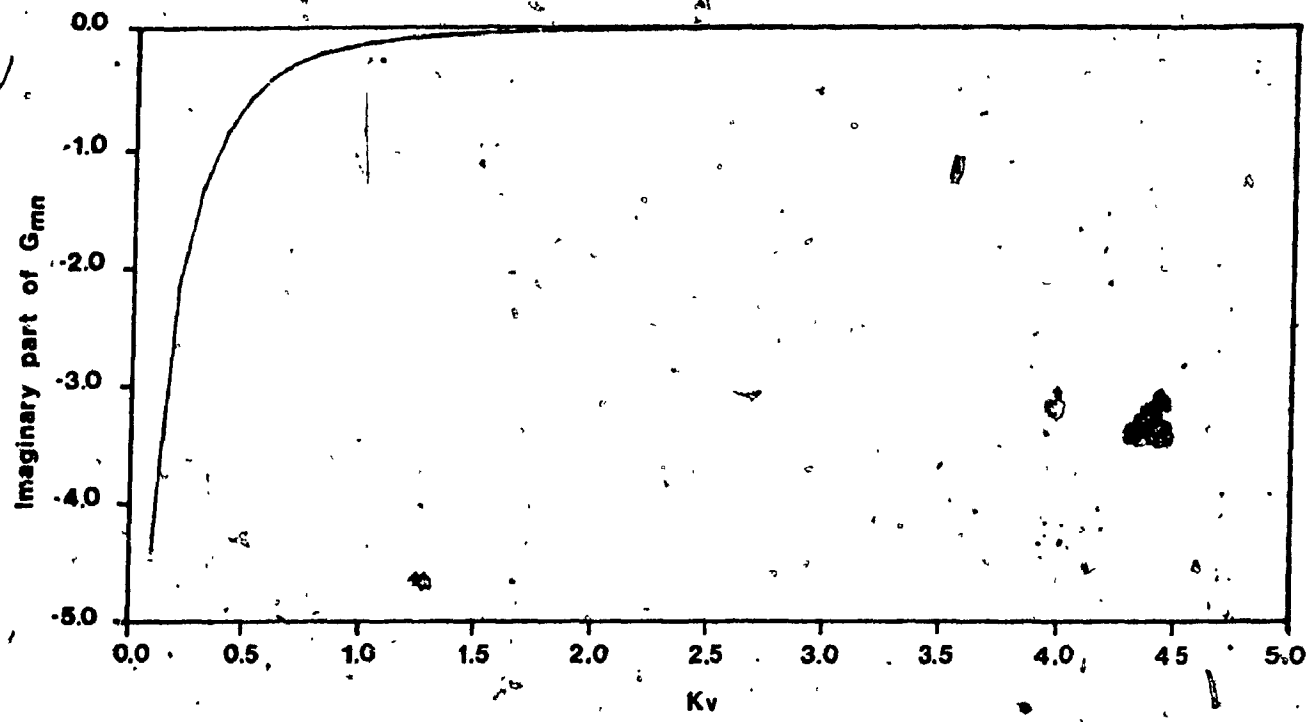

Figure 3.8 Variation of the imaginary integrand in G_{mn} as a function of Kv
(TE_{11} to TE_{11} mode coupling in one waveguide)

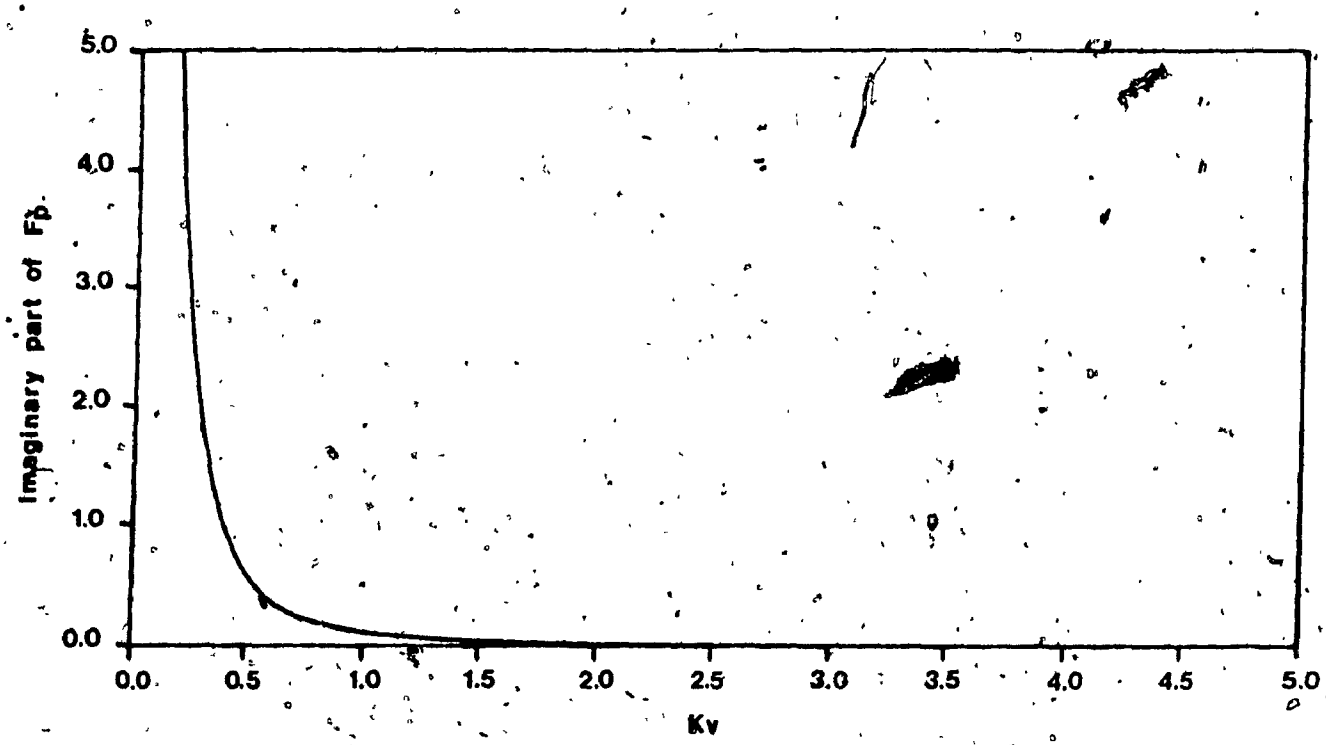

Figure 3.9 Variation of the imaginary integrand in F_p as a function of Kv
(TE_{11} to TE_{11} mode coupling in one waveguide)

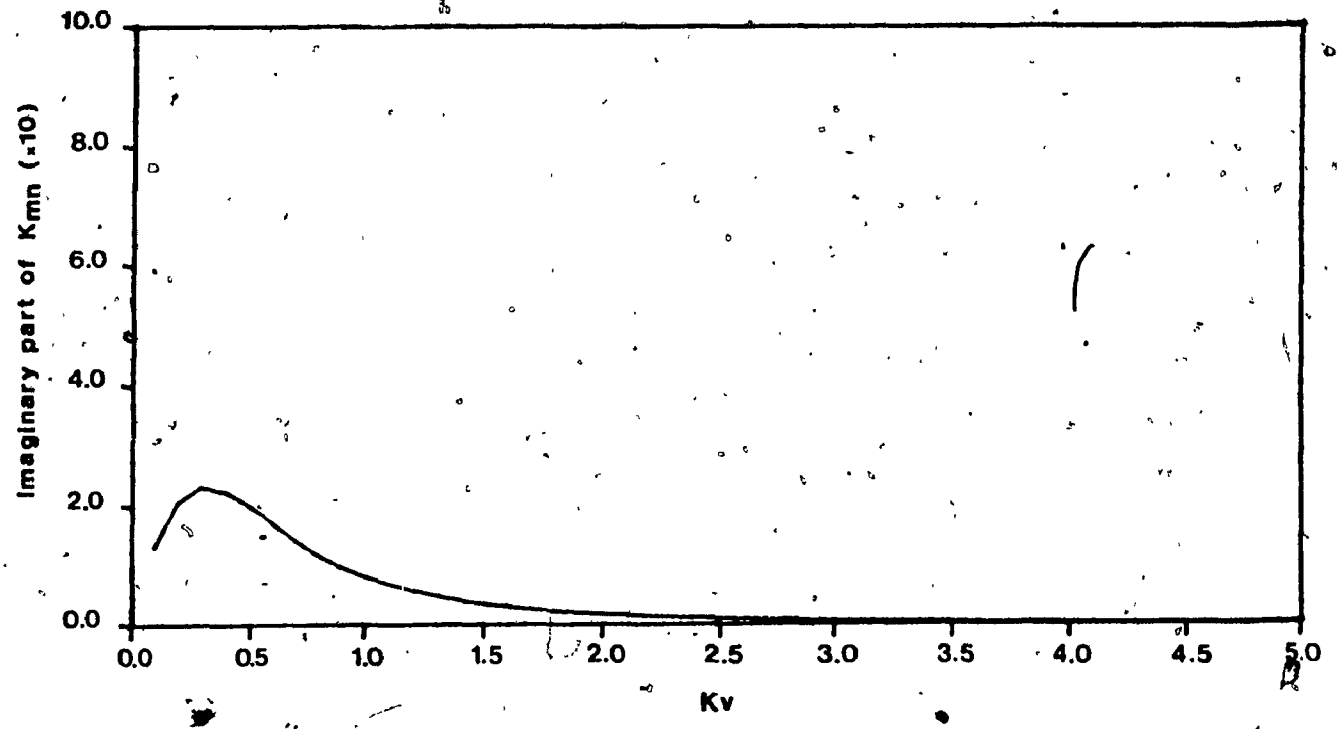

Figure 3.10 Variation of the imaginary integrand in K_{mn} as a function of Kv
(TE_{11} to TM_{11} mode coupling in one waveguide)

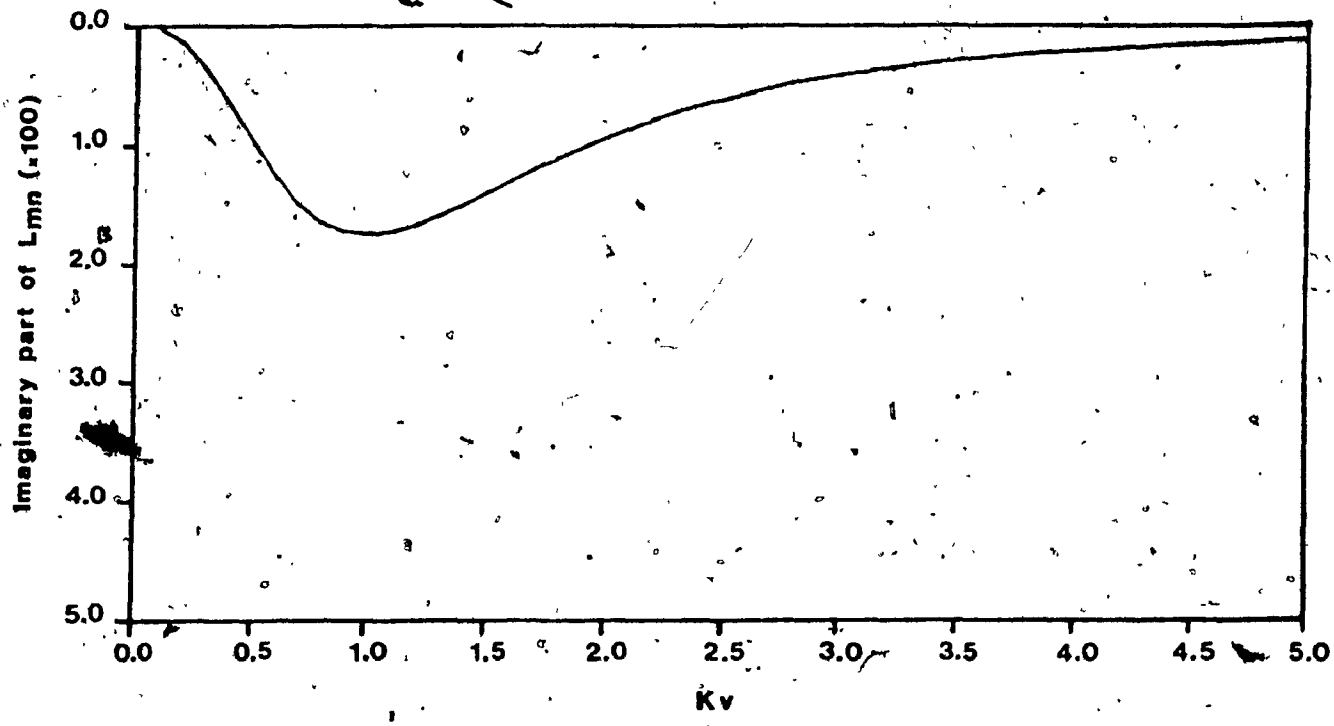

Figure 3.11 Variation of the imaginary integrand in L_{mn} as a function of Kv
(TM_{11} to TM_{11} mode coupling in one waveguide)

Further inspection of these functions reveals that they decrease rapidly with increasing v. Providing that $10/K < X \leq v$, these functions can be evaluated approximately for the range $X \leq v < \infty$ by means of large-argument approximation to the product $I'_p K'_p$ or $I_p K_p$. The augmented approximate term is named as "tail" integral in later discussion. The derivation of the "tail" integral in G_{mn} presented here can be applied fairly easily to subsequent cases.

From (3.27), the remainder of the integral along the imaginary axis is

$$G_{tail} = \int_X^\infty \frac{v\sqrt{1+v^2}}{(v^2+u_m^2)(v^2+u_n^2)} I_p'(Kv)\, K_p'(Kv)\, dv \qquad (3.31)$$

The asymtotic expansion for large argument of $I'_p(Kv)K'_p(Kv)$ is

$$I'_p(Kv)\, K'_p(Kv) \equiv -\frac{1}{2Kv}\left[1 + \frac{1}{2}\,\frac{4p^2-3}{(2Kv)^2} + \text{higher order term}\right]$$

Thus,

$$v\sqrt{1+v^2}\, I_p'(Kv)\, K_p'(Kv) \equiv v^2\sqrt{1+\frac{1}{v^2}}\left[-\frac{1}{2Kv}\left(1+\frac{4p^2-3}{2(2Kv)^2}\right)\right] \qquad (3.32)$$

For $v >> 1$,

$$\sqrt{1+\frac{1}{v^2}} \equiv 1+\frac{1}{2v^2}$$

Equation (3.33) then becomes

$$v\sqrt{1+v^2}\; I'_p(Kv)\, K'_p(Kv) \;\cong\; -\frac{1}{2K}\left[v + \frac{p^2-3/4}{2K^2 v} + \frac{1}{2v}\right] \qquad (3.33)$$

For large values of v, the term containing v^{-3} is neglected.

The integral $G_{tail}(X)$ is finally represented by

$$G_{tail}(X) \cong -\frac{1}{2K}\left[I_1 + \frac{1}{2}\left(1 + \frac{p^2-3/4}{K^2}\right) I_2\right]$$

where

$$I_1 = \int_X^\infty \frac{v\, dv}{(v^2+u_m^2)(v^2+u_n^2)} \quad \text{and} \quad I_2 = \int_X^\infty \frac{dv}{v(v^2+u_m^2)(v^2+u_n^2)}$$

Analytical solutions for I_1 and I_2 are directly obtained through the integral calculus. The solutions are

$$I_1 = \begin{cases} \dfrac{1}{2(X^2+u_m^2)} & ; \text{for } u_m = u_n \\ \dfrac{1}{2(u_m^2-u_n^2)}\left[\ln(X^2+u_m^2) - \ln(X^2+u_n^2)\right] & ; \text{for } u_m \neq u_n \end{cases} \qquad (3.34)$$

and

$$I_2 = \begin{cases} -\dfrac{1}{u_m^2}\left[I_1 + \dfrac{1}{2u_m^2}\ln\left(\dfrac{X^2}{X^2+u_m^2}\right)\right] & ; \text{for } u_m = u_n \\ -\dfrac{1}{(u_m u_n)^2}\left[\ln(X) + \dfrac{u_n^2\ln(X^2+u_m^2) - u_m^2\ln(X^2+u_n^2)}{2(u_m^2-u_n^2)}\right] & ; \text{for } u_m \neq u_n \end{cases} \qquad (3.35)$$

Following the above procedure, the remainders or "tail" integrals

along the imaginary axis of F_p, K_{mn} and L_{mn} are derived to be,

$$F_{tail} = \int_X^\infty \frac{1}{2\,Kv^3}\left[1 - \frac{1}{2v^2}\left(1 + \frac{p^2 - 1/4}{K^2}\right)\right] dv$$

$$= \frac{1}{4\,KX^2}\left[1 - \frac{1}{4X^2}\left(1 + \frac{p^2 - 1/4}{K^2}\right)\right] \qquad (3.36)$$

$$K_{tail} = \int_X^\infty \frac{v\, I_p(Kv)\, K_p(Kv)}{\sqrt{1+v^2}\,(v^2 + u_n^2)}\, dv$$

$$= \frac{1}{2K}\left[\frac{1}{u_n^2}\ln\left(\frac{X^2 + u_n^2}{X^2}\right) - \frac{1}{4u_n^2}\left(1 + \frac{p^2 - 1/4}{K^2}\right)\left(\frac{1}{X^2} + \frac{1}{u_n^2}\ln\left(\frac{X^2}{X^2 + u_n^2}\right)\right)\right] \qquad (3.37)$$

and

$$L_{tail} = \int_X^\infty \frac{v^3\, I_p(Kv)\, K_p(Kv)}{\sqrt{1+v^2}\,(v^2 + u_m^2)(v^2 + u_n^2)}\, dv$$

$$= \frac{1}{2K} I_1 - \frac{1}{4K}\left(1 + \frac{p^2 - 1/4}{K^2}\right) I_2 \qquad (3.38)$$

where I_1 and I_2 have been given in equations (3.34) and (3.35), respectively.

3.6 Summary

A rigorous analysis has been made to compute the intermodal coupling in a waveguide. This is the first step in a detailed treatment of the mutual coupling in a finite planar antenna array. The analysis has, at considerable length, considered all possible coupling between modes that might exist in the waveguides. The resultant self-coupling coefficients constitute the diagonal block matrices in the total coupling coefficient matrix

[C]. It was shown that only modes that have similar azimuthal period can interact with each other. Furthermore, no coupling is possible between two orthogonally polarized modes.

The self-coupling coefficients are derived exactly and suitable for implementation. Integration of highly oscillatory functions is avoided by means of a contour deformation technique. As a result, the functions of those related integrals become monotonic over the equivalent integration path and thus permit the use of any standard numerical integration formula with a significantly smaller number of integration points. The numerical integration is further speeded up by realizing that the monotonic integrands rapidly vanish at large arguments. Analytical expressions can then be developed to represent the total value of the remaining integrals whose argument is tending toward infinity. This is the special merit of the contour deformation.

CHAPTER 4

ANALYSIS OF MUTUAL COUPLING IN AN ANTENNA ARRAY

4.1 Introduction

The analysis presented earlier in Chapter 3 is very useful in studying the input admittance of a circular waveguide opening into an infinite flange. It can also be used to obtain more accurate radiation patterns of such an antenna. The main objective of this research, however, has yet to be addressed. That is, the calculation of coupled power from one waveguide to the others in an array environment.

The discussion in the following Section will, therefore, be concentrated on extending the analysis to include more than one waveguide aperture. The derivation can be commenced from equation (2.28), which expresses the coupling coefficient between mode m in the i-th waveguide and mode n in the j-th waveguide. However, in following the derivation one will realize that one of the Bessel functions contains an argument that is not expressed explicitly in terms of the integration variables. To separate the variable associated with one of the apertures, Graf's addition theorem [20] for cylindrical functions is employed. An elaborate review of this useful theorem will be given in Section 4.2. Rigorous analyses of possible mode interactions between apertures are presented in subsequent Sections 4.3 and 4.4. Contour integration is once again found useful in dealing with infinite integrals that are present in the expressions of cross-coupling coefficients $C^{(ij)}_{mn}$. The oscillatory nature of

the required integrands are then suppressed. This makes numerical integration very efficient. The deformation of a contour integration path, that follows in a similar manner to that described in Section 3.5, is the topic of Section 4.6.

4.2 The TE to TE Mode Coupling Between Separated Apertures

Before advancing toward the derivation of the mode cross-coupling coefficients, it is felt worthwhile to look at Graf's addition theorem for Bessel functions. This brief review will find its use in later analyses. With reference to Figure 4.1,

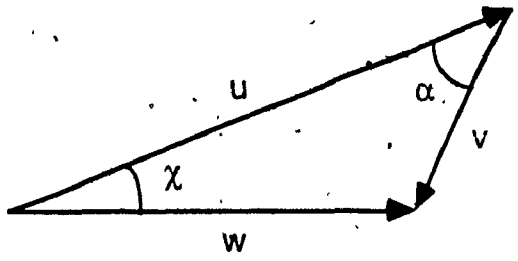

Figure 4.1 Graf's addition theorem

Graf's addition theorem is given as [20]

$$J_p(w) \begin{matrix}\cos\\ \sin\end{matrix} (p\chi) = \sum_{k=-\infty}^{\infty} J_{p+k}(u)\, J_k(v) \begin{matrix}\cos\\ \sin\end{matrix} (k\alpha) \qquad (4.1)$$

where the arguments are as shown in Figure 4.1.

The restrictions $|ve^{\pm j\alpha}| < |u|$ are not necessary for Bessel function with integer or zero order. Some derivatives of (4.1) that will be of significance are

$$J_p(w)\cos(-p\chi+\theta) = \sum_{k=-\infty}^{\infty} J_{p+k}(u)\,J_k(v)\cos(-k\alpha+\theta) \tag{4.2}$$

and

$$J_p(w)\sin(-p\chi+\theta) = \sum_{k=-\infty}^{\infty} J_{p+k}(u)\,J_k(v)\sin(-p\chi+\theta) \tag{4.3}$$

Expanding equation (2.28) to include separated waveguides and using equation (2.29),

$$C_{mn}^{(ij)} = \frac{j\omega\varepsilon_0}{2\pi}\frac{Z_n}{N_m}\int_0^{\infty}\frac{\xi\,d\xi}{\sqrt{\xi^2-k^2}}\iint_{D_i}\bar{\Psi}_m^{(i)}\cdot\bar{F}_n^{(j)}\,dS$$

Relevant components of vector $\bar{F}(j)_n$ and $\bar{\Psi}(i)_m$ can be found in Chapter 2 and 3, respectively. To apply Graf's addition theorem, let us relate the arguments of equation (4.1) to the present problem. For notations shown in Figure 4.2,

$$\Phi = \phi_{ij} - \chi \quad \text{and} \quad \alpha = \phi_i - \phi_{ij} - \pi \tag{4.4}$$

From equation (2.30), for TE modes

$$F_{nx}^{(j)} = \frac{j\pi\gamma_n}{\lambda_n}\Big[-J_{p-1}(\xi\rho)\,Q_{p-1}\cos(-(p-1)\chi+(p-1)\phi_{ij}-\psi_n) + J_{p+1}(\xi\rho)\,Q_{p+1}\cos(-(p+1)\chi+(p+1)\phi_{ij}-\psi_m)\Big] \tag{4.5a}$$

$$F_{ny}^{(j)} = \frac{j\pi\gamma_n}{\lambda_n}\Big[\, J_{p-1}(\xi\rho)\, Q_{p-1} \sin(-(p-1)\chi + (p-1)\phi_{ij} - \psi_n) + J_{p+1}(\xi\rho)\, Q_{p+1} \sin(-(p+1)\chi + (p+1)\phi_{ij} - \psi_m)\Big] \qquad (4.5b)$$

$$F_{nz}^{(j)} = \frac{2\pi\gamma_n}{k} J_p(\xi\rho)\, Q_p \cos(-p\chi + p\phi_{ij} - \psi_n) \qquad (4.5c)$$

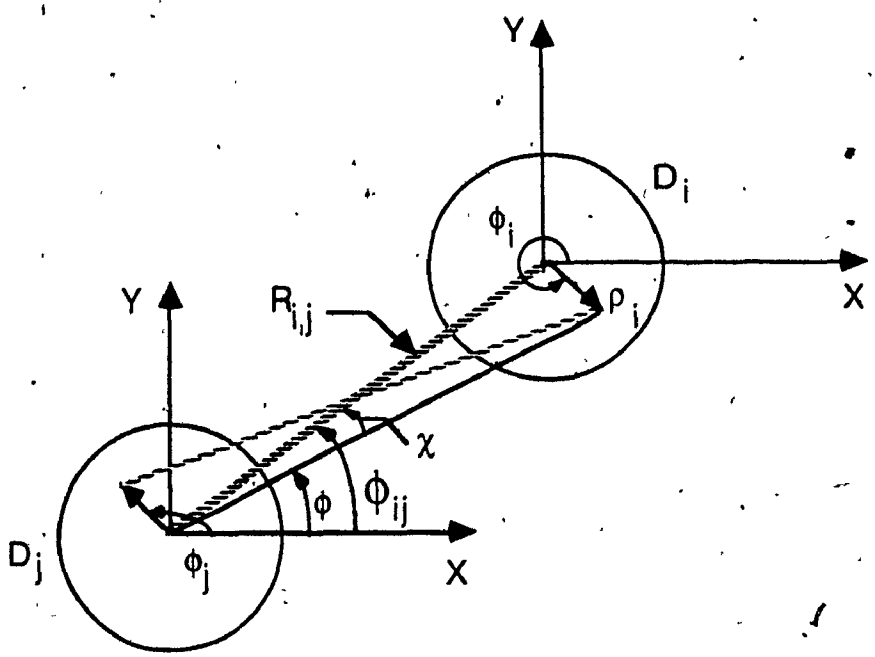

Figure 4.2 Relevant vector notations for Graf's theorem

In the above equations, Q_p, Q_{p-1} and Q_{p+1} are the Lommel integrals of order p, p-1 and p+1, respectively.

Let us make the following substitutions into equations (4.2) and (4.3),

$$u = R_{ij}\xi \qquad v = \rho_i \xi \qquad w = \rho\xi \qquad \text{and} \qquad \alpha = \phi - \pi - \phi_{ij}$$

and then introduce the new formulae into equation (4.5) giving

$$F_{nx}^{(j)} = \frac{j\pi\gamma_n}{\lambda_n}\left[-Q_{p-1}\sum_{k=-\infty}^{\infty} J_{p+k-1}(\xi R_{ij})\, J_k(\xi\rho_i)\cos(-k\alpha+(p-1)\phi_{ij}-\psi_n) + Q_{p+1}\sum_{k=-\infty}^{\infty} J_{p+k+1}(\xi R_{ij})\, J_k(\xi\rho_i)\cos(-k\alpha+(p+1)\phi_{ij}-\psi_m)\right] \quad (4.6a)$$

$$F_{ny}^{(i)} = \frac{j\pi\gamma_n}{\lambda_n}\left[Q_{p-1}\sum_{k=-\infty}^{\infty} J_{p+k-1}(\xi R_{ij})\, J_k(\xi\rho_i)\sin(-k\alpha+(p-1)\phi_{ij}-\psi_n) + Q_{p+1}\sum_{k=-\infty}^{\infty} J_{p+k+1}(\xi R_{ij})\, J_k(\xi\rho_i)\sin(-k\alpha+(p+1)\phi_{ij}-\psi_m)\right] \quad (4.6b)$$

$$F_{nz}^{(i)} = \frac{2\pi\gamma_n}{k} Q_p\sum_{k=-\infty}^{\infty} J_{p+k}(\xi R_{ij})\, J_k(\xi\rho_i)\cos(-k\alpha+p\phi_{ij}-\psi_n) \quad (4.6c)$$

Now, notice that

$$\cos(-k\alpha+(p-1)\phi_{ij}-\psi_n) = (-1)^k\cos(k\phi_i-(k+p-1)\phi_{ij}+\psi_n) \quad (4.7a)$$

$$\cos(-k\alpha+(p+1)\phi_{ij}-\psi_n) = (-1)^k\cos(k\phi_i-(k+p+1)\phi_{ij}+\psi_n) \quad (4.7b)$$

$$\sin(-k\alpha+(p-1)\phi_{ij}-\psi_n) = (-1)^{k+1}\sin(k\phi_i-(k+p-1)\phi_{ij}+\psi_n) \quad (4.7c)$$

$$\sin(-k\alpha+(p+1)\phi_{ij}-\psi_n) = (-1)^{k+1}\sin(k\phi_i-(k+p+1)\phi_{ij}+\psi_n) \quad (4.7d)$$

$$\cos(-k\alpha+p\phi_{ij}-\psi_n) = (-1)^k\cos(k\phi_i-(k-p)\phi_{ij}+\psi_n) \quad (4.7e)$$

The use of equation (4.7), in conjunction with rearrangement of related terms, simplifies equation (4.6) to

$$F_{nx}^{(j)} = \frac{j\pi\gamma_n}{\lambda_n}\left\{\sum_k (-1)^k J_k(\xi\rho_i)\left[-J_{p+k-1}(\xi R_{ij})\, Q_{p-1}\cos(k\phi_i+\psi_{p-1}) + J_{p+k+1}(\xi R_{ij})\, Q_{p+1}\cos(k\phi_i+\psi_{p+1})\right]\right\} \quad (4.8a)$$

$$F_{ny}^{(j)} = \frac{j\pi\gamma_n}{\lambda_n}\left\{\sum_k (-1)^{k+1} J_k(\xi\rho_i)\left[J_{p+k-1}(\xi R_{ij})\, Q_{p-1}\sin(k\phi_i+\psi_{p-1}) + J_{p+k+1}(\xi R_{ij})\, Q_{p+1}\sin(k\phi_i+\psi_{p+1})\right]\right\} \quad (4.8b)$$

$$F_{nz}^{(j)} = \frac{2\pi\gamma_n}{k}\sum_k (-1)^k Q_p J_{p+k}(\xi R_{ij}) J_k(\xi\rho_i)\cos(k\phi_i+\psi_p) \quad (4.8c)$$

with $\psi_p = -(k+p)\phi_{ij} + \psi_n$.

The integration on the scalar product $\bar{\Psi}^{(i)}_m . \bar{F}^{(j)}_n$ over the coupled aperture i–th is now ready to be calculated. As before, let us define the function $\Gamma(\xi)$ as

$$\Gamma(\xi) = \iint_{D_i} \bar{\Psi}^{(i)}_m . \bar{F}^{(j)}_n \rho d\rho d\phi$$

The evaluation of $\Gamma(\xi)$ is quite lengthy yet straightforward. It is most convenient to calculate the surface integral involving the x- and y-dependent terms together. This results from the similarity of their expressions. The z-dependent term is treated separately. In the end, a combination of the resultant components gives

$$\Gamma(\xi) = C\left\{-\frac{J_p'(\xi a)\,J_l'(\xi a)\,a^2}{(\xi^2-\lambda_m^2)(\xi^2-\lambda_n^2)}\left(1-\frac{\xi^2}{k^2}\right)\left[S_{l,p}^{(1)}+D_{l,p}^{(1)}\right]\right.$$

$$\left.-\frac{pl}{(\xi\lambda_m\lambda_n)^2}J_p(\xi a)\,J_l(\xi a)\left[-S_{l,p}^{(1)}+D_{l,p}^{(1)}\right]\right\} \qquad (4.9)$$

where newly-introduced symbols represent

$$C = 2\pi^2\gamma_m\gamma_n J_p(\lambda_n a)\,J_l(\lambda_m a)$$

$$S_{l,p}^{(1)} = (-1)^l J_{p+l}(\xi R_{ij})\cos((p+l)\phi_{ij}-\psi_m-\psi_n)$$

$$D_{l,p}^{(1)} = J_{p-l}(\xi R_{ij})\cos((p-l)\phi_{ij}+\psi_m-\psi_n)$$

The cross-coupling coefficient $C^{(ij)}_{mn}$ for two TE modes is now

$$C_{mn}^{(ij)} = \frac{j\omega\varepsilon_0}{2\pi}\frac{Z_n}{N_m}\int_0^{\infty}\frac{\xi\,d\xi}{\sqrt{\xi^2-k^2}}\,C\left\{\frac{-J_p'(\xi a)\,J_l'(\xi a)\,a^2}{(\xi^2-\lambda_m^2)(\xi^2-\lambda_n^2)}\left(1-\frac{\xi^2}{k^2}\right)\left[S_{l,p}^{(1)}+D_{l,p}^{(1)}\right]\right.$$

$$\left.-\frac{pl}{(\xi\lambda_m\lambda_n)^2}J_p(\xi a)\,J_l(\xi a)\left[-S_{l,p}^{(1)}+D_{l,p}^{(1)}\right]\right\} \qquad (4.10)$$

Introduce the variables X_m, X_n, K, u_m, u_n and w, whose definitions have been given in Chapter 3, into equation (4.10) and regroup all constants to get

$$C_{mn}^{(ij)} = -\frac{\pi a^3\gamma_m J_p(\lambda_n a)\,J_l(\lambda_m a)}{N_m}\left[\frac{G_{mn}}{K}+\frac{pl\,K}{(X_mX_n)^2}F_{mn}\right] \qquad (4.11)$$

where

$$G_{mn} = \int_0^{\infty} \frac{w\sqrt{1-w^2}}{(w^2-u_m^2)(w^2-u_n^2)} J_p'(Kw)\, J_l'(Kw)\, (S_{l,p}^{(1)} + D_{l,p}^{(1)})\, dw \qquad (4.12)$$

and

$$F_{mn} = \int_0^{\infty} \frac{J_p(Kw)\, J_l(Kw)}{w\sqrt{1-w^2}} \left[-S_{l,p}^{(1)} + D_{l,p}^{(1)} \right] dw$$

for $l > 0$ and $p > 0$.

4.3 The TE to TM or TM to TE Mode Coupling Between Separated Apertures

The innermost surface integral, i.e. $\Gamma(\xi)$, in $C^{(ij)}{}_{mn}$ is evaluated by following the procedure presented in Section 4.2. For TE modes in the j-th aperture, the components of $F^{(j)}{}_n$ are given in equations (4.8a), (4.8b) and (4.8c), inclusively. The vector $\Psi^{(i)}{}_m$ of TM modes in the i-th aperture can be derived from equation (2.23) using

$$\bar{\Psi}_m^{(i)} = \frac{1}{Z_m}\, \hat{z} \times [\, \bar{\Psi}_m^{(i)} \,]^{TE}$$

with components of $[\, \Psi_m^{(i)} \,]^{TE}$ are given in equation (3.2).

The final form of $\Gamma(\xi)$ is derived as

$$\Gamma(\xi) = C \left[\frac{J_p(\xi a)\, J_l(\xi a)}{(\xi^2 - \lambda_m^2)} (-S_{l,p}^{(2)} + D_{l,p}^{(2)}) \right] \qquad (4.13)$$

where

$$C = \frac{2\pi^2 \gamma_m \gamma_n a p}{Z_m \lambda_n^2 \lambda_m} J_p(\lambda_n a) J_l'(\lambda_m a)$$

$$S_{l,p}^{(2)} = (-1)^{\frac{p-l}{2}} J_{p+l}(\xi R_{ij}) \sin((p+l)\phi_{ij} - \psi_m \pm \psi_n)$$

$$D_{l,p}^{(2)} = J_{p-l}(\xi R_{ij}) \sin((p-l)\phi_{ij} + \psi_m - \psi_n)$$

From equation (2.29), the cross-coupling coefficient between a TM mode in the i-th aperture to a TE mode in the j-th aperture is

$$C_{mn}^{(ij)} = \frac{\pi a^4 Z_n \gamma_m \gamma_n}{Z_0 Z_m N_m X_n^2 X_m} p J_p(\lambda_n a) J_l'(\lambda_m a) K_{mn} \qquad (4.14)$$

where K_{mn} is given as

$$K_{mn} = \int_0^\infty \frac{w J_p(Kw) J_l(Kw)}{\sqrt{1-w^2}\,(w^2 - u_m^2)} (-S_{l,p}^{(2)} + D_{l,p}^{(2)})\, dw \qquad (4.15)$$

When the indices are interchanged in equation (4.14), i.e. the mutual coupling between a TE mode in the j-th aperture and a TM mode in the j-th aperture, the cross-coupling coefficient $C^{(ij)}{}_{mn}$ becomes,

$$C_{mn}^{(ij)} = -\frac{\pi a^4 \gamma_m \gamma_n}{Z_0 N_m X_m^2 X_n} l J_l(\lambda_m a) J_p'(\lambda_n a) K_{mn}' \qquad (4.16)$$

where

$$K'_{mn} = \int_0^\infty \frac{w\, J_l(Kw)\, J_p(Kw)}{\sqrt{1-w^2}\,(w^2-u_n^2)} \left(S^{(2)}_{l,p} + D^{(2)}_{l,p} \right) dw \qquad (4.17)$$

4.4 The TM to TM Mode Coupling Between Separated Apertures

Last among the possible mutual couplings is between two TM modes in two apertures. The i-th aperture is assumed to carry mode m whose azimuthal variation is l. The j-th aperture, on the other hand, is assumed to carry mode n whose azimuthal variation is p. With reference to equation (2.29), the surface integral over the scalar function $\Psi^{(i)}_m . F^{(j)}_n$ should be evaluated first.

For TM modes, the components of $F^{(j)}_n$ are derived from equations (3.14a) and (3.14b) with changes in angular notation mentioned in (4.4). Simple algebraic manipulations lead to

$$F^{(j)}_{nx} = -\frac{j\pi\gamma_n}{Z_n \lambda_n} \left[Q_{p-1} \sum_k J_{p+k-1}(\xi R_{ij})\, J_k(\xi\rho_i)\, (-1)^{k+1} \sin(k\phi_i + \psi_{p-1}) + Q_{p+1} \sum_k J_{p+k+1}(\xi R_{ij})\, J_k(\xi\rho_i)\, (-1)^{k+1} \sin(k\phi_i + \psi_{p+1}) \right] \qquad (4.18a)$$

$$F^{(j)}_{ny} = \frac{j\pi\gamma_n}{Z_n \lambda_n} \left[-Q_{p-1} \sum_k J_{p+k-1}(\xi R_{ij})\, J_k(\xi\rho_i)\, (-1)^{k} \cos(k\phi_i + \psi_{p-1}) + Q_{p+1} \sum_k J_{p+k+1}(\xi R_{ij})\, J_k(\xi\rho_i)\, (-1)^{k} \cos(k\phi_i + \psi_{p+1}) \right] \qquad (4.18b)$$

The final expression of $\Gamma(\xi)$ is obtained as

$$\Gamma(\xi) = C\left[\frac{\xi^2}{(\xi^2-\lambda_m^2)(\xi^2-\lambda_n^2)} J_p(\xi a) J_1(\xi a) (S_{1,p}^{(1)} + D_{1,p}^{(1)})\right] \quad (4.19)$$

where

$$C = -\frac{2\pi^2 \gamma_m \gamma_n a^2}{Z_m Z_n \lambda_m \lambda_n} J_1'(\lambda_m a) J_p'(\lambda_n a)$$

$S^{(1)}_{1,p}$ and $D^{(1)}_{1,p}$ are similar to those in the TE-to-TE mutual coupling case.

Finally, the cross-coupling coefficient $C^{(ij)}_{mn}$ is given by

$$C_{mn}^{(ij)} = \frac{j\omega\varepsilon_0}{2\pi} \frac{Z_n}{N_m} \int_0^\infty \frac{\xi}{\sqrt{\xi^2-k^2}} \Gamma(\xi)\, d\xi$$

$$= -\frac{\pi a^3 \varepsilon_r \gamma_n}{N_m Z_0^2 X_m X_n} K J_1'(\lambda_m a) J_p'(\lambda_n a) L_{mn} \quad (4.20)$$

L_{mn} is a compact form of

$$L_{mn} = \int_0^\infty \frac{w^3 J_p(Kw) J_1(Kw)}{\sqrt{1-w^2}\,(w^2-u_m^2)(w^2-u_n^2)} (S_{1,p}^{(1)} + D_{1,p}^{(1)})\, dw \quad (4.21)$$

The development of the cross-coupling coefficients between two modes in separated waveguides is now complete. For future reference, essential expressions of the coefficients are summarized in Table 4.1. For definitions of various constants, refer to Section 4.2.

Table 4.1

CROSS-COUPLING COEFFICIENTS BETWEEN MODES

IN SEPARATED WAVEGUIDES

a. TE to TE cross coupling

$$C_{mn}^{(ij)} = -\frac{\pi a^3 \gamma_m J_p(\lambda_n a) J_1(\lambda_m a)}{N_m} \left| \frac{G_{mn}}{} + \frac{p\,1\,K}{(X_m X_n)^2} F_{mn} \right|$$

$$G_{mn} = \int_0^\infty \frac{w\sqrt{1-w^2}}{(w^2-u_m^2)(w^2-u_n^2)} J_p'(Kw)\, J_1'(Kw)\, (S_{1,p}^{(1)} + D_{1,p}^{(1)})\, dw$$

$$F_{mn} = \int_0^\infty \frac{J_p(Kw)\, J_1(Kw)}{w\sqrt{1-w^2}} (-S_{1,p}^{(1)} + D_{1,p}^{(1)})\, dw$$

b. TE to TM or TM to TE cross coupling

When mode n is TE and mode m is TM, then

$$C_{mn}^{(ij)} = \frac{\pi a^4 Z_n \gamma_m \gamma_n}{N_m Z_m Z_0 K^2 X_m} p\, J_1'(\lambda_m a)\, J_p(\lambda_n a)\, K_{mn}$$

$$K_{mn} = \int_0^\infty \frac{w J_1(Kw)\, J_p(Kw)}{\sqrt{1-w^2}\,(w^2-u_m^2)} (-S_{1,p}^{(2)} + D_{1,p}^{(2)})\, dw$$

When mode m is TE and mode n is TM, then

$$C_{mn}^{(ij)} = -\frac{\pi a^4 \gamma_m \gamma_n}{N_m Z_0 X_m^2 X_n} l\, J_p'(\lambda_n a)\, J_l(\lambda_m a)\, K_{mn}$$

$$K_{mn} = \int_0^{\infty} \frac{w\, J_p(Kw)\, J_l(Kw)}{\sqrt{1-w^2}\,(w^2-u_n^2)} (S_{l,p}^{(2)} + D_{l,p}^{(2)})\, dw$$

c. TM to TM cross coupling

$$C_{mn}^{(ij)} = -\frac{\pi a^3 \varepsilon_r \gamma_n}{N_m Z_0^2 X_m X_n} K\, J_p'(\lambda_n a)\, J_l'(\lambda_m a)\, L_{mn}$$

$$L_{mn} = \int_0^{\infty} \frac{w^3\, J_p(Kw)\, J_l(Kw)}{\sqrt{1-w^2}\,(w^2-u_m^2)(w^2-u_n^2)} (S_{l,p}^{(1)} + D_{l,p}^{(1)})\, dw$$

with

$$S_{l,p}^{(1)} = (-1)^l J_{p+l}(\xi R_{ij}) \cos((p+l)\phi_{ij} - \psi_m - \psi_n)$$

$$D_{l,p}^{(1)} = J_{p-l}(\xi R_{ij}) \cos((p-l)\phi_{ij} + \psi_m - \psi_n)$$

$$S_{l,p}^{(2)} = (-1)^l J_{p+l}(\xi R_{ij}) \sin((p+l)\phi_{ij} - \psi_m - \psi_n)$$

$$D_{l,p}^{(2)} = J_{p-l}(\xi R_{ij}) \sin((p+l)\phi_{ij} + \psi_m - \psi_n)$$

4.5 Evaluation of Contour Integral in a Complex Plane

Rigorous analysis in previous Sections has arrived at analytical formulae for the coupling coefficients $C^{(ij)}_{mn}$. These resultant coefficients contain one or two infinite integrals of the type found in equations (3.13), (3.18) and (3.23). These integrals involve functions having triple products of Bessel functions of different order. According to the results of the earlier finding, these functions are of a high oscillatory nature. Direct numerical integration is not an advisable method. A more efficient method is to adopt the contour integration technique, in which the integration variables are transformed to a complex domain. As has been studied in depth in Chapter 3, there are equivalent contours to the original ones, when certain conditions are fulfilled. The contour deformation in Chapter 3 is applicable to the present contours.

The first step in the evaluation of the infinite integrals is to rephrase the Bessel function $J_{p+k}(\xi R_{ij})$ and $J_{p-l}(\xi R_{ij})$ as a sum of Hankel functions of the first and second kind. Depending on the presence of the Hankel function in the modified integrand, an equivalent contour to the original one can be suitably selected. A note of attention is necessary, for each coupling integral there are two transformations; one for the term $J_{p+l}(\xi R_{ij})$ and one for the term $J_{p-l}(\xi R_{ij})$. Furthermore, in the latter case, two conditions should be distinguished; that is when $(p-l)>0$ and when $(p-l)<0$. In the subsequent Sections, we shall present the calculation of the infinite integrals in terms of contour integration. The presentation of the process leading to final expressions is minimized as much as possible.

4.5.1 Evaluation of G_{mn} and F_{mn}

In the course of computing the TE-to-TE cross-coupling coefficients, we shall have to integrate two integrals, namely G_{mn} and F_{mn}. The process of evaluating these integrals is quite similar in nature.

Let us first look at G_{mn}. From equation (4.12), the original form of G_{mn} is

$$G_{mn} = \int_0^{\infty} \frac{w\sqrt{1-w^2}}{(w^2-u_m^2)(w^2-u_n^2)} J_p'(Kw)\, J_l'(Kw)\, (S_{l,p}^{(1)} + D_{l,p}^{(1)})\, dw$$

$$= G_{mn}^{(1)} + G_{mn}^{(2)} \qquad (4.22)$$

$G^{(1)}_{mn}$ and $G^{(2)}_{mn}$ denote two integrals

$$G_{mn}^{(1)} = G_1 \int_0^{\infty} \frac{w\sqrt{1-w^2}}{(w^2-u_m^2)(w^2-u_n^2)} J_p'(Kw)\, J_l'(Kw)\, J_{p+l}(kR_{ij}w)\, dw \qquad (4.23a)$$

$$G_{mn}^{(2)} = G_2 \int_0^{\infty} \frac{w\sqrt{1-w^2}}{(w^2-u_m^2)(w^2-u_n^2)} J_p'(Kw)\, J_l'(Kw)\, J_{p-l}(kR_{ij}w)\, dw \qquad (4.23b)$$

The two constants G_1 and G_2 are given by

$$G_1 = (-1)^l \cos((p+l)\phi_{ij} - \psi_m - \psi_n)$$

$$G_2 = \cos((p-l)\phi_{ij} + \psi_m - \psi_n)$$

In $G^{(1)}_{mn}$ and $G^{(2)}_{mn}$, the Bessel functions $J_{p+l}(kR_{ij}w)$ and $J_{p-l}(kR_{ij}w)$ are, respectively, rephrased as

$$J_{p+1}(kR_{ij}w) = \frac{1}{2}[H^{(1)}_{p+1}(kR_{ij}w) + H^{(2)}_{p+1}(kR_{ij}w)] \qquad (4.24a)$$

$$J_{p-1}(kR_{ij}w) = \frac{1}{2}[H^{(1)}_{|p-1|}(kR_{ij}w) + H^{(2)}_{|p-1|}(kR_{ij}w)]\begin{cases} 1 & ,(p-1)>0 \\ (-1)^{1-p} & ,(p-1)<0 \end{cases} \qquad (4.24b)$$

Each integral $G^{(1)}_{mn}$ and $G^{(2)}_{mn}$ is now regarded as a sum of two integrals, following the substitution of (4.24) into (4.23). With reference to Figure 3.6 and Figure 3.7, a suitable equivalent contour for the integral involving $H^{(1)}_{\nu}(z)$ is the positive imaginary axis, whereas that for the integral involving $H^{(2)}_{\nu}(z)$ is a composition of branches along the barrier, around the poles and the negative imaginary axis.

Having defined all the terms and selected equivalent contours, the calculation of $G^{(1)}_{mn}$ and $G^{(2)}_{mn}$ can be done fairly easy. The solution of $G^{(1)}_{mn}$ is first obtained as,

$$G^{(1)}_{mn} = G_1\Big[\int_0^1 \frac{u\sqrt{1-u^2}}{(u^2-u_m^2)(u^2-u_n^2)} J_p'(Ku)\, J_l'(Ku)\, H^{(2)}_{p+l}(kR_{ij}u)\, du$$

$$- j\frac{2}{\pi}\int_0^{\infty} \frac{v\sqrt{1+v^2}}{(v^2+u_m^2)(v^2+u_n^2)} I_p'(Kv)\, I_l'(Kv)\, K_{p+l}(kR_{ij}v)\, dv\Big] \qquad (4.25)$$

The residues at poles, i.e. when $u_m>1$ or $u_n>1$, have no contribution to the total value of $G^{(1)}_{mn}$. In other words,

(i) When $u_m \neq u_n$, the integrated function has simple poles at $w = u_m$ and $w = u_n$. The original function being :

$$G(w) = \frac{g_1(w)}{g_2(w)} = \frac{w\sqrt{1-w^2}\, J_p'(Kw)\, J_l'(Kw)}{(w+u_m)(w+u_n)(w-u_m)(w-u_n)} H_{p+l}^{(2)}(kR_{ij}w)$$

The residues at poles are

$$\operatorname*{Res}_{w=u_m} G(w) = \frac{g_1(w)}{g_2(w)}(w-u_m)\Big|_{w=u_m}$$

$$\operatorname*{Res}_{w=u_n} G(w) = \frac{g_1(w)}{g_2(w)}(w-u_n)\Big|_{w=u_n}$$

At $w = u_m$ and $w = u_n$,

$$J_p'(Ku_n) = J_p'(\lambda_n a) = 0$$

$$J_l'(Ku_m) = J_l'(\lambda_m a) = 0$$

due to the TE boundary condition. The value of residues is, thus, zero.

(ii) When $u_m = u_n$, the integrated function has a pole of order 2 at $w = u_m$ (or $w = u_n$). The original function becomes,

$$G(w) = \frac{g_1(w)}{g_2(w)} = \frac{w\sqrt{1-w^2}}{(w^2-u_m^2)^2} J_p'(Kw)\, J_l'(Kw)\, H_{p+l}^{(2)}(kR_{ij}w)$$

The residue is calculated by following,

$$\operatorname*{Res}_{w=u_m} G(w) = \frac{d}{dw}\left[\frac{g_1(w)}{g_2(w)}\right]_{w=u_m}$$

At $w = u_m$, $g'_1(u_m) = 0$, due to $J'_p(Ku_m) = J'_p(\lambda_m a) = 0$ for TE modes. The residue of the function at its pole is again zero.

In a manner similar to that followed above, the integral $G^{(2)}_{mn}$ is calculated as

$$G^{(2)}_{mn} = G_2 \begin{cases} G^{(21)}_{mn} - j\frac{2}{\pi}(-1)^l G^{(22)}_{mn} & (p-l)\geq 0 \\ (-1)^{l-p}\left[G^{(21)}_{mn} - j\frac{2}{\pi}(-1)^p G^{(22)}_{mn}\right] & (p-l)<0 \end{cases} \qquad (4.26)$$

where

$$G^{(21)}_{mn} = \int_0^1 \frac{u\sqrt{1-u^2}}{(u^2-u_m^2)(u^2-u_n^2)} J_p'(Ku)\, J_l'(Ku)\, H^{(2)}_{|p-l|}(kR_{ij}u)\, du$$

$$G^{(22)}_{mn} = \int_0^\infty \frac{v\sqrt{1+v^2}}{(v^2+u_m^2)(v^2+u_n^2)} I_p'(Kv)\, I_l'(Kv)\, K_{|p-l|}(kR_{ij}v)\, dv$$

Direct numerical integration can now be applied to terms in equations (4.25) and (4.26). The oscillation of the integrated functions has been minimized by this transformation process.

We shall proceed further with the evaluation of the second integral F_{mn}. From equation (4.12)

$$F_{mn} = \int_0^{\infty} \frac{J_p(Kw)\, J_l(Kw)}{w\sqrt{1-w^2}} \left(-S^{(1)}_{l,p} + D^{(1)}_{l,p} \right) dw$$

$$= F^{(1)}_{mn} + F^{(2)}_{mn}$$

The new integrals $F^{(1)}_{mn}$ and $F^{(2)}_{mn}$ are explicitly expressed as

$$F^{(1)}_{mn} = F_1 \int_0^{\infty} \frac{J_p(Kw)\, J_l(Kw)}{w\sqrt{1-w^2}} J_{p+l}(kR_{ij}w)\, dw$$

$$F_1 = (-1)^{l+1} \cos((p+l)\phi_{ij} - \psi_m - \psi_n)$$

and

$$F^{(2)}_{mn} = F_2 \int_0^{\infty} \frac{J_p(Kw)\, J_l(Kw)}{w\sqrt{1-w^2}} J_{p-l}(kR_{ij}w)\, dw$$

$$F_2 = \cos((p-l)\phi_{ij} + \psi_m - \psi_n)$$

Without much difficulty, the solutions of these integrals are

$$F^{(1)}_{mn} = F_1 \left[\int_0^{1} \frac{J_p(Ku)\, J_l(Ku)}{u\sqrt{1-u^2}} H^{(2)}_{p+l}(kR_{ij}u)\, du \right.$$

$$\left. - j\frac{2}{\pi} \int_0^{\infty} \frac{I_p(kv)\, I_l(kv)}{v\sqrt{1+v^2}} K_{p+l}(kR_{ij}v)\, dv \right] \qquad (4.27)$$

$$F_{mn}^{(2)} = F_2 \begin{cases} F_{mn}^{(21)} - j\frac{2}{\pi}(-1)^l F_{mn}^{(22)} & (p-l)>0 \\ (-1)^{(l-p)}\left[F_{mn}^{(21)} - j\frac{2}{\pi}(-1)^p F_{mn}^{(22)} \right] & (p-l)<0 \end{cases} \quad (4.28)$$

where

$$F_{mn}^{(21)} = \int_0^{\infty} \frac{J_p(Ku)\, J_l(Ku)}{u\sqrt{1-u^2}} H_{|p-l|}^{(2)}(kR_{ij}u)\, du$$

$$F_{mn}^{(22)} = \int_0^{\infty} \frac{I_p(Kv)\, I_l(Kv)}{v\sqrt{1+v^2}} K_{|p-l|}(kR_{ij}v)\, dv$$

4.5.2 Evaluation of K_{mn}

The coupling coefficient between TE to TM or TM to TE contains one infinite integral, namely K_{mn}. Little expansion is required in order to arrive at a solution for this integral. Let us first rewrite the original form of K_{mn}

$$K_{mn} = \int_0^{\infty} \frac{w\, J_p(Kw)\, J_l(Kw)}{\sqrt{1-w^2}\,(w^2-u_m^2)} \left(-S_{l,p}^{(2)} + D_{l,p}^{(2)} \right) dw$$

$$= K_{mn}^{(1)} + K_{mn}^{(2)}$$

The complete expressions of $K^{(1)}_{mn}$ and $K^{(2)}_{mn}$ are

$$K_{mn}^{(1)} = K_1 \int_0^{\infty} \frac{w\, J_l(Kw)\, J_p(Kw)}{\sqrt{1-w_2}\,(w^2-u_m^2)} J_{p+l}(kR_{ij}w)\, dw$$

$$K_1 = (-1)^{l+1} \sin((p+l)\phi_{ij} - \psi_m - \psi_n)$$

and

$$K^{(2)}_{mn} = K_2 \int_0^{\infty} \frac{w\, J_1(Kw)\, J_p(Kw)}{\sqrt{1-w^2}\,(w^2-u_m^2)} J_{p-1}(kR_{ij}w)\, dw$$

$$K_2 = \sin((p-1)\phi_{ij} + \psi_m - \psi_n)$$

Following the procedure adopted previously, the solutions of $K^{(1)}_{mn}$ and $K^{(2)}_{mn}$ are found quite easily. For $K^{(1)}_{mn}$,

$$K^{(1)}_{mn} = K_1 \left[\int_0^{1} \frac{u\, J_p(Ku)\, J_1(Ku)}{\sqrt{1-u^2}\,(u^2-u_m^2)} H^{(2)}_{p+1}(kR_{ij}u)\, du \right.$$

$$\left. - j\frac{2}{\pi} \int_0^{\infty} \frac{vI_p(Kv)\, I_1(Kv)}{\sqrt{1+v^2}\,(v^2+u_m^2)} K_{p+1}(kR_{ij}v)\, dv \right] \qquad (4.29)$$

The residue of the function at pole $w = u_m$ is zero. Since

$$\operatorname*{Res}_{w=u_m} = \frac{w\, J_p(Kw)\, J_1(Kw)}{\sqrt{1-w^2}\,(w+u_m)} H^{(2)}_{p+1}(kR_{ij}w)\Big|_{w=u_m}$$

For TM modes, $J_1(Ku_m) = J_1(\lambda_m a) = 0$.

The solution of $K^{(2)}_{mn}$ is separated into two cases; one represents the condition $(p-1)>0$ and the other represents the condition $(p-1)<0$. The calculation of $K^{(2)}_{mn}$ at those conditions is essentially similar. In combining the two solutions, we obtain a generalized expression as,

$$K_{mn}^{(2)} = K_2 \begin{cases} [K_{mn}^{(21)} - j\frac{2}{\pi}(-1)^p K_{mn}^{(22)}] & (p-1)>0 \\ (-1)^{1-p}[K_{mn}^{(21)} - j\frac{2}{\pi}(-1)^1 K_{mn}^{(22)}] & (p-1)<0 \end{cases} \quad (4.30)$$

where

$$K_{mn}^{(21)} = \int_0^1 \frac{u J_1(Ku)\, J_p(Ku)}{\sqrt{1-u^2}\,(u^2-u_m^2)} H_{|p-1|}^{(2)}(kR_{ij}u)\, du$$

$$K_{mn}^{(22)} = \int_0^\infty \frac{v\, I_p(Kv)\, I_1(Kv)}{\sqrt{1+v^2}\,(v^2+u_m^2)} K_{|p-1|}(kR_{ij}v)\, dv$$

The value of K_{mn} is now obtained by simply adding those of $K^{(1)}{}_{mn}$ and $K^{(2)}{}_{mn}$. Although numerical integration is still required, the rate of convergence of these integrals is maximized — an aim that one always searches for in a computation-intensive problem such as the present one.

4.5.3 Evaluation of L_{mn}

The integral L_{mn} which occurs in the TM to TM coupling coefficient expression takes the form:

$$L_{mn} = \int_0^\infty \frac{w^3 J_p(Kw)\, J_1(Kw)}{\sqrt{1-w^2}\,(w^2-u_m^2)(w^2-u_n^2)} (S_{1,p}^{(1)} + D_{1,p}^{(1)})\, dw$$

$$= L_{mn}^{(1)} + L_{mn}^{(2)}$$

$L^{(1)}{}_{mn}$ and $L^{(2)}{}_{mn}$ are given as

$$L^{(1)}_{mn} = L_1 \int_0^{\infty} \frac{w^3 J_p(Kw) J_1(Kw)}{\sqrt{1-w^2}\,(w^2-u_m^2)(w^2-u_n^2)} J_{p+1}(kR_{ij}w)\,dw$$

$$L_1 = (-1)^l \cos((p+1)\phi_{ij} - \psi_m - \psi_n)$$

and

$$L^{(2)}_{mn} = L_2 \int_0^{\infty} \frac{w^3 J_p(Kw) J_1(Kw)}{\sqrt{1-w^2}\,(w^2-u_m^2)(w^2-u_n^2)} J_{p-1}(kR_{ij}w)\,dw$$

$$L_2 = \cos((p-1)\phi_{ij} + \psi_m - \psi_n)$$

The calculations of $L^{(1)}_{mn}$ and $L^{(2)}_{mn}$ is easily carried out, following the use of equivalent contours to the original paths (along the w-axis). The final results are shown to be

$$L^{(1)}_{mn} = L_1 \left[\int_0^1 \frac{u^3 J_p(Ku) J_1(Ku)}{\sqrt{1-u^2}\,(u^2-u_m^2)(u^2-u_n^2)} H^{(2)}_{p+1}(kR_{ij}u)\,du \right.$$

$$\left. - j\frac{2}{\pi} \int_0^{\infty} \frac{v^3 I_p(Kv) I_1(Kv)}{\sqrt{1+v^2}\,(v^2+u_m^2)(v^2+u_n^2)}\,dv \right] \qquad (4.31)$$

When either of the modes in the airfilled waveguides is evanescent, i.e. $u_m>1$ or $u_n>1$, the value of the function at the poles have contribution to the total value of $L^{(1)}_{mn}$. Let the function be identified as

$$L(w) = \frac{w^3 J_p(Kw) J_1(Kw)}{\sqrt{1-w^2}\,(w^2-u_m^2)(w^2-u_n^2)} H^{(2)}_{p+1}(kR_{ij}w)$$

(i) When $u_m \neq u_n$, the function has two simple poles at $w=u_m$ and $w=u_n$. The residues at the poles are

$$\operatorname*{Res}_{w=u_m} L(w) = \frac{w^3 J_p(Kw) J_1(Kw)}{\sqrt{1-w^2}\,(w+u_m)(w^2-u_n^2)} H_{p+1}^{(2)}(kR_{ij}w)\Big|_{w=u_m}$$

$$\operatorname*{Res}_{w=u_n} L(w) = \frac{w^3 J_p(Kw) J_1(Kw)}{\sqrt{1-w^2}\,(w+u_n)(w^2-u_m^2)} H_{p+1}^{(2)}(kR_{ij}w)\Big|_{w=u_n}$$

At $w=u_m$ and $w=u_n$, $J_p(\lambda_n a) = J_1(\lambda_m a) = 0$ due to the TM boundary condition of the corresponding modes. Thus, the residues at the poles all vanish. No additional term is required in equation (4.31).

(ii) When $u_m=u_n$ (then p=1), L(w) becomes

$$L(w) = \frac{l_2(w)}{l_1(w)} = \frac{w^3 J_p(Kw) J_1(Kw)}{\sqrt{1-w^2}\,(w^2-u_m^2)^2} H_{p+1}^{(2)}(kR_{ij}w)$$

The residue at the pole $w = u_m$ (order 2) is evaluated as follows:

$$\operatorname*{Res}_{w=u_m} L(w) = \frac{d}{dw}\left[(w-u_m)^2 \frac{w^3 J_p(Kw) J_1(Kw)}{\sqrt{1-w^2}\,(w+u_m)^2(w-u_m)^2} H_{p+1}^{(2)}(kR_{ij}w)\right]_{w=u_m}$$

For TM modes, $J_p(Ku_m) = J_p(\lambda_n a) = 0$. Therefore, the residue vanishes.

The final result of $L^{(2)}_{mn}$ is summarized below :

$$L_{mn}^{(2)} = L_2 \begin{cases} [L_{mn}^{(21)} - j\frac{2}{\pi}(-1)^l L_{mn}^{(22)}] \ , \ (p-l) > 0 \\ [L_{mn}^{(21)} - j\frac{2}{\pi}(-1)^p L_{mn}^{(22)}] \ , \ (p-l) < 0 \end{cases} \tag{4.32}$$

where

$$L_{mn}^{(21)} = \int_0^1 \frac{u^3 J_p(Ku) J_l(Ku)}{\sqrt{1-u^2}\,(u^2-u_m^2)(u^2-u_n^2)} H_{|l-p|}^{(2)}(kR_{ij}u)\,du$$

and

$$L_{mn}^{(22)} = \int_0^\infty \frac{v^3 I_p(Kv) I_l(Kv)}{\sqrt{1+v^2}\,(v^2+u_m^2)(v^2+u_n^2)} K_{|l-p|}(kR_{ij}v)\,dv$$

CHAPTER 5

RADIATION FROM AN ANTENNA ARRAY

5.1 Introduction

For the class of radiators known as "aperture antennas", the radiated far field is calculated in terms of the known field distribution over the aperture of the antenna. In all important practical cases the waveguide allows propagation of only one mode, called the dominant mode. Over a cross section inside the waveguide sufficiently far from the aperture, any component of the field is a vector sum of those associated with the incident and the reflected waves of the dominant mode. In the aperture, however, additional higher-mode fields exist locally, excited by the discontinuity in the guide. It is quite reasonable to assume that the higher-mode fields contribute a smaller fraction to the total radiation field as the aperture dimensions increase. Rigorous solution of the boundary problem is deemed necessary for apertures of a fraction of a wavelength.

In essence, the analysis thus far is a rigorous one. Possible existing higher modes are assumed in the computation of the coupling coefficients $C^{(ij)}_{mn}$. These coefficients are, in turn, related to the set up of the scattering matrix [S], as has been discussed earlier in Chapter 2. Having formed the [S] matrix, the amplitudes of reflected waves (including that of the dominant mode) are directly derived. A complete description of the aperture tangential electric field distribution E_t is then available for the computation of radiation fields.

5.2 Radiation Field

In the unbounded, source-free region (z>0), the transverse magnetic field H_t at a point P(x,y,z) is given by

$$\bar{H}_t(R) = \frac{j}{2\pi\omega\mu_0}(\nabla_t\nabla_t + k^2)\cdot\bar{z}\times\iint_{-\infty}^{\infty}\bar{E}_t(R,0)\,G\,dS'$$

By using equation (2.13) to replace the total tangential electric field and by following the procedure outlined in Appendix B to eliminate the ∇_t operator, the above equation can be rewritten as:

$$\bar{H}_t(R) = \frac{j\omega\varepsilon_0}{2\pi}\sum_i\sum_m A_m^{(i)} Z_m \iint_{D_i}\left(h'_m G + j\frac{\gamma_m}{k}h'_{mz}\nabla_t G\right)dS'$$

With reference to Figure 2.3

$$\bar{R} = \bar{r} - \bar{r}'$$

$$\nabla_t G(|\bar{r}-\bar{r}'|) = \nabla_t G(|\bar{R}|) = -j\frac{k}{R}G(R)\,(x\,\bar{i}_x + y\,\bar{i}_y)\left(1+\frac{1}{jkR}\right)$$

In a coordinate system whose origin is located at the center of the aperture i-th (x_{oi},y_{oi}), let point P be defined by (r_i, θ_i, ϕ_i). Then it is quite obvious that

$$|\bar{R}| = |\bar{r}-\bar{r}'| = |\bar{r}_i - \bar{\rho}'|$$

For the far-zone fields, the usual approximation

$$|\bar{R}| \approx \bar{r}_i - \bar{r}_i\cdot\bar{\rho}' \approx r_i - \rho'\sin\theta_i\cos(\phi_i - \phi')$$

is valid, then

$$G(R) \approx \frac{e^{-jkR}}{R} \approx \frac{e^{-jkr_i}}{r_i} e^{jk\bar{r}_i \cdot \bar{\rho}}$$

Furthermore,

$$\frac{x\,\bar{i}_x + y\,\bar{i}_y}{r} \approx \sin\theta_i\,(\cos\phi_i\,\bar{i}_x + \sin\phi_i\,\bar{i}_y)$$

Introducing equation (5.2) and the far-zone approximations into equation (5.1) to get

$$H_t(x,y,z) = \frac{j\omega\varepsilon_0}{2\pi} \sum_i \sum_m A_m^{(i)} Z_m \iint_{D_i} G(r_i)\, e^{jk\bar{r}_i \cdot \bar{\rho}'} \left[\left(h_{mx} + \frac{\gamma_m}{k} \sin\theta_i \cos\phi_i\, h'_{mz}\right)\bar{i}_x\right.$$

$$\left. + \left(h_{m,y} + \frac{\gamma_m}{k} \sin\theta_i \sin\phi_i\, h'_{m\,z}\right)\bar{i}_y\right] dS' \qquad (5.3)$$

It is also noted that only the first order $1/r_i$ is retained in the development of equation (5.3).

Let $f^{(i)}_{mx}$ and $f^{(i)}_{my}$ be the transverse components of $\bar{f}^{(i)}_m$,

$$f^{(i)}_{mx} = \iint_{D_i} G(r_i)\, e^{jk\bar{r}_i \cdot \bar{\rho}'} \left(h'_{mx} + \frac{\gamma_m}{k} \sin\theta_i \cos\phi_i\, h'_{mz}\right) dS'$$

and

$$f^{(i)}_{my} = \iint_{D_i} G(r_i)\, e^{jk\bar{r}_i \cdot \bar{\rho}'} \left(h'_{my} + \frac{\gamma_m}{k} \sin\theta_i \sin\phi_i\, h'_{mz}\right) dS'$$

From the general sense of the analysis, the vector $f^{(i)}_m$ is separated to that of TE modes and TM modes. We shall investigate this vector categorically for TE and TM modes below.

a. TE modes

Substitute the components of h^{TE}_m, given in Appendix A, into equation (5.4) to get,

$$f^{(i)}_{mx} = G(r_i)\iint_{D_i}\Big[\frac{j\gamma_m}{2\lambda_m}\big[-J_{p-1}(\lambda_m\rho')\cos((p-1)\phi' - \psi_m) + J_{p+1}(\lambda_m\rho')\cos((p+1)\phi' - \psi_m)\big] + \frac{\gamma_m}{k}J_p(\lambda_m\rho')\cos(p\phi' - \psi_m)\sin\theta_i\cos\phi_i\Big]e^{jw\rho'\cos(\phi' - \phi_i)}dS' \quad (5.5a)$$

$$f^{(i)}_{my} = G(r_i)\iint_{D_i}\Big[\frac{j\gamma_m}{2\lambda_m}\big[J_{p-1}(\lambda_m\rho')\sin((p-1)\phi' - \psi_m) + J_{p+1}(\lambda_m\rho')\sin((p+1)\phi' - \psi_m)\big] + \frac{\gamma_m}{k}J_p(\lambda_m\rho')\cos(p\phi' - \psi_m)\sin\theta_i\sin\phi_i\Big]e^{jw\rho'\cos(\phi' - \phi_i)}dS' \quad (5.5b)$$

where $w = k\sin\theta_i$.

These are evaluated with the help of the Bessel-Fourier series

$$e^{jw\rho'\cos(\phi' - \phi_i)} = J_0(w\rho') + 2\sum_{m=1}^{\infty} j^m J_m(w\rho')\cos m(\phi' - \phi_i),$$

and the Lommel integral formula

$$Q_n = \int_0^x x J_n(\alpha x) J_n(\beta x)\,dx = \frac{x}{\alpha^2 - \beta^2}\Big[J_n(\alpha x)\frac{d}{dx}J_n(\beta x) - J_n(\beta x)\frac{d}{dx}J_n(\alpha x)\Big]$$

Using these in equation (5.5), the components for the TE-mode $f^{(i)}_m$ are obtained as follows :

$$f^{(i)}_{mx} = G(r_i)\, j^p \frac{\pi \gamma_m}{\lambda_m} \left[-Q_{p-1} \cos((p-1)\phi_i - \psi_m) - Q_{p+1} \cos((p+1)\phi_i - \psi_m) + \frac{2\lambda_m}{k} \sin\theta_i \cos\phi_i\, Q_p \cos(p\phi_i - \psi_m) \right] \quad (5.6a)$$

$$f^{(i)}_{my} = G(r_i)\, j^p \frac{\pi \gamma_m}{\lambda_m} \left[Q_{p-1} \sin((p-1)\phi_i - \psi_m) - Q_{p+1} \sin((p+1)\phi_i - \psi_m) + \frac{2\lambda_m}{k} \sin\theta_i \sin\phi_i\, Q_p \cos(p\phi_i - \psi_m) \right] \quad (5.6b)$$

If $V^{(i)}_{mx}$, $V^{(i)}_{my}$ and $V^{(i)}_{mz}$ are introduced to represent

$$V^{(i)}_{mx} = -Q_{p-1} \cos((p-1)\phi_i - \psi_m) - Q_{p+1} \cos((p+1)\phi_i - \psi_m)$$

$$V^{(i)}_{my} = Q_{p-1} \sin((p-1)\phi_i - \psi_m) - Q_{p+1} \sin((p+1)\phi_i - \psi_m)$$

$$V^{(i)}_{mz} = \frac{2\lambda_m}{k} Q_p \cos(p\phi_i - \psi_m)$$

then

$$f^{(i)}_{mx} = G(r_i)\, j^p \frac{\pi \gamma_m}{\lambda_m} [\, V^{(i)}_{mx} + V^{(i)}_{mz} \sin\theta_i \cos\phi_i \,] \quad (5.7a)$$

$$f^{(i)}_{my} = G(r_i)\, j^p \frac{\pi \gamma_m}{\lambda_m} [\, V^{(i)}_{my} + V^{(i)}_{mz} \sin\theta_i \sin\phi_i \,] \quad (5.7b)$$

b. <u>TM modes</u>

We now proceed with the calculation of $\bar{f}^{(i)}_m$ for the TM modes. It is evidence that the TM-mode $\bar{f}^{(i)}_m$ can be derived from that of TE modes. Recalling that

$$\bar{h}_m^{(TM)} = \frac{1}{Z_m} i_z \times \bar{h}_m^{(TE)}$$

then,

$$f_{mx}^{(i)} = -G(r_i)\, j^p \frac{\pi \gamma_m}{\lambda_m} \frac{1}{Z_m} V_{my}^{(i)} \qquad (5.8a)$$

$$f_{my}^{(i)} = G(r_i)\, j^p \frac{\pi \gamma_m}{\lambda_m} \frac{1}{Z_m} V_{mx}^{(i)} \qquad (5.8b)$$

Let us now return to equation (5.3). The transverse components of the radiated magnetic field are :

$$H_x = \frac{j\omega\varepsilon_0}{2\pi} \sum_i \sum_m A_m^{(i)} Z_m f_{mx}^{(i)} \qquad (5.9a)$$

$$H_y = \frac{j\omega\varepsilon_0}{2\pi} \sum_i \sum_m A_m^{(i)} Z_m f_{my}^{(i)} \qquad (5.9b)$$

From Maxwell's equation (continuity of magnetic flux), for a source-free region.

$$\nabla . \bar{H} = 0$$

It is, therefore, possible to obtain the axial component H_z using this equation. The solution is found to be,

$$H_z = -\frac{j\omega\varepsilon_0}{2\pi} \sum_i \sum_m A_m^{(i)} Z_m \tan\theta_i \left(f_{mx}^{(i)} \cos\phi_i + f_{my}^{(i)} \sin\phi_i \right) \qquad (5.9c)$$

Again, only the first-order $1/r_i$ term is retained. This is a valid consideration for far-zone fields.

It is convenient to express the field in terms of its spherical components; thus we have

$$H_r = 0 \tag{5.10a}$$

$$H_\theta = \frac{j\omega\varepsilon_0}{2\pi} \sum_i \sum_m A_m^{(i)} Z_m \frac{1}{\cos\theta_i} (f_{mx}^{(i)} \cos\phi_i + f_{my}^{(i)} \sin\phi_i) \tag{5.10b}$$

$$H_\phi = \frac{j\omega\varepsilon_0}{2\pi} \sum_i \sum_m A_m^{(i)} Z_m (- f_{mx}^{(i)} \sin\phi_i + f_{my}^{(i)} \cos\phi_i) \tag{5.10c}$$

The electric field in the radiation zone is related as in a spherical TEM wave, i.e. by

$$\bar{E} = - Z_0 (\bar{i}_r \times \bar{H})$$

which has the following components

$$E_r = 0 \tag{5.12a}$$

$$E_\theta = j \frac{k}{2\pi} \sum_i \sum_m A_m^{(i)} Z_m (- f_{mx}^{(i)} \sin\phi_i + f_{my}^{(i)} \cos\phi_i) \tag{5.12b}$$

$$E_\phi = j \frac{k}{2\pi} \sum_i \sum_m A_m^{(i)} Z_m \frac{1}{\cos\theta_i} (f_{mx}^{(i)} \cos\phi_i + f_{my}^{(i)} \sin\phi_i) \tag{5.12c}$$

Equation (5.12) states that the total far field is due to the combination of elemental fields from all modes at all apertures. The elemental field due to the m-th TE or TM mode in the i-th aperture are essentially given by equation (5.12), with the substitution of appropriate components of $\bar{f}^{(i)}_m$.

From equations (5.7), the contributions from the m-th TE mode in the i-th aperture to the total radiation field can be shown to be

$$E^{(i)}_{\theta,m} = j^{p+1} k^2 Z_0 a^3 A^{(i)}_m G(r_i) \left[\frac{p J_p(\lambda_m a_i) J_p(w a_i)}{w (\lambda_m a_i)^2} \right] \sin(p\phi_i - \psi_m) \quad (5.13a)$$

$$E^{(i)}_{\phi,m} = -j^{p+1} k^2 Z_0 G(r_i) \cos\theta_i \left[\frac{J_p(\lambda_m a_i) J_p'(w a_i)}{w^2 - \lambda_m^2} \right] \cos(p\phi_i - \psi_m) \quad (5.13b)$$

Similarly, the contributions from the m-th TM mode in the i-th aperture to the total radiation field is

$$E^{(i)}_{\theta,m} = -j^{p+1} k^2 A^{(i)}_m \frac{\gamma_m a_i}{\lambda_m (w^2 - \lambda_m^2)} J_p'(\lambda_m a_i) J_p(w a_i) G(r_i) \sin\theta_i \cos(p\phi_i - \psi_m) \quad (5.14a)$$

$$E^{(i)}_{\phi,m} = 0 \quad (5.14b)$$

5.2 Co-polar and Cross-polar Definitions

The radiation fields from an antenna can be completely specified in terms of two vector components. The definition of the two components at a point in space and their identification in terms of a co-polarized and cross-polarized component is not universally agreed upon. In his paper, Ludwig [22] has clarified and discussed some of the popular choices. Ludwig's third definition of cross polarization is often preferred for antennas which are operated in a predominantly linearly polarized mode.

Consider an antenna under test being mounted at the origin of a model tower, as shown in Figure 5.2 (ref. [23]). This antenna radiates an

electromagnetic field that has both E_x and E_y components along the z axis or boresight direction. Assuming that on-axis the radiated field is linearly polarized along the y direction. If a small receiving dipole is moved off axis in any direction but is not rotated, i.e. it is always kept oriented parallel to the yz plane, then it receives a component of the radiated field that is called the *co-polarized field*. The field component that is perpendicular to this polarization is called the *cross-polarized field*. Instead of being moved off axis the receiving dipole can be kept fixed while the transmitting antenna is rotated around x axis (i.e. varying θ angle) at some particular angle ϕ. Let the radiated field at the point P specified by the angles θ and ϕ be $E(\theta,\phi) = E_\theta(\theta,\phi)\, i_\theta + E_\phi(\theta,\phi)\, i_\phi$. When the point P is rotated so it coincides with the z axis the field $E(\theta,\phi)$ can be resolved into x and y components, which, from Figure 5.2b, are readily seen to be given by

$$E_x = E_\theta \cos\phi - E_\phi \sin\phi \qquad (5.15a)$$

$$E_y = E_\theta \sin\phi + E_\phi \cos\phi \qquad (5.15b)$$

The reference polarization is along the y axis, then E_x is the cross-polarized field, and E_y is the desired co-polarized field.

5.3 Relationship Between Spherical and Azimuth–Elevation Coordinates

The field coordinate system that is used in the analysis is the spherical system (r,θ,ϕ). For some practical applications, it is preferable to use the Elevation and Azimuth coordinate system. This system is illustrated in Figure 5.3. Its relationship to the spherical system is expressed by

$$\theta = \cos^{-1} [\cos(El) \cos(Az)]$$

$$\phi = \tan^{-1} [\sin(Az) / \tan(El)]$$

Later, in the computer program, Elevation–Azimuth are used to describe the location of the far-field point but are converted into Theta–Phi coordinates prior to the field calculation.

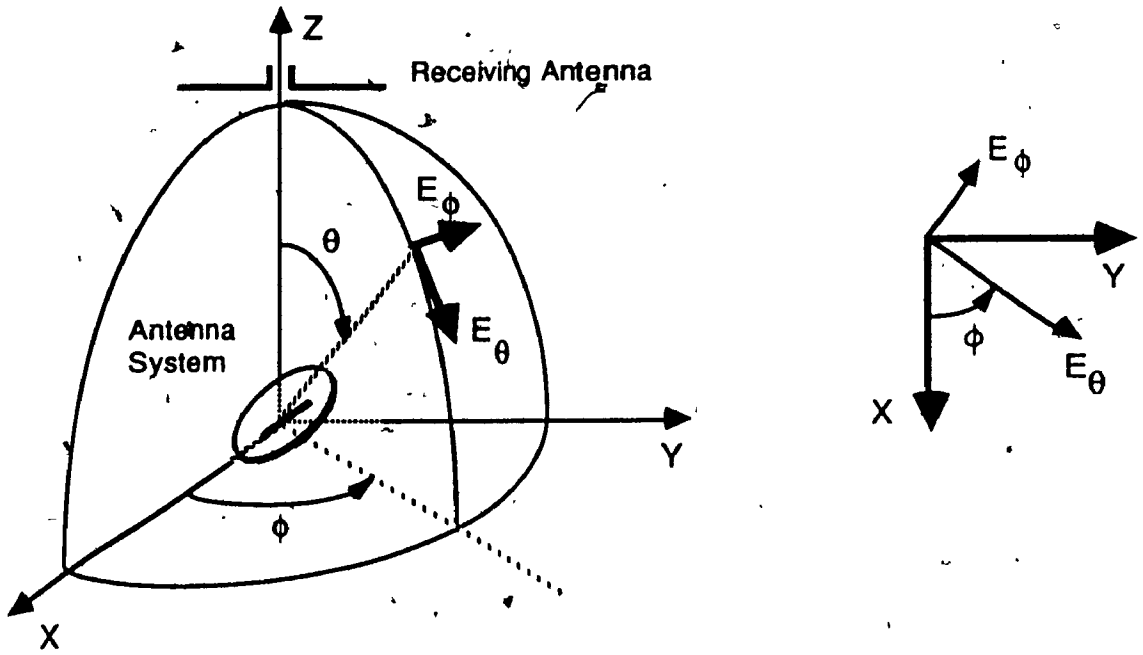

Figure 5.1 Illustration of field components radiated by an antenna system

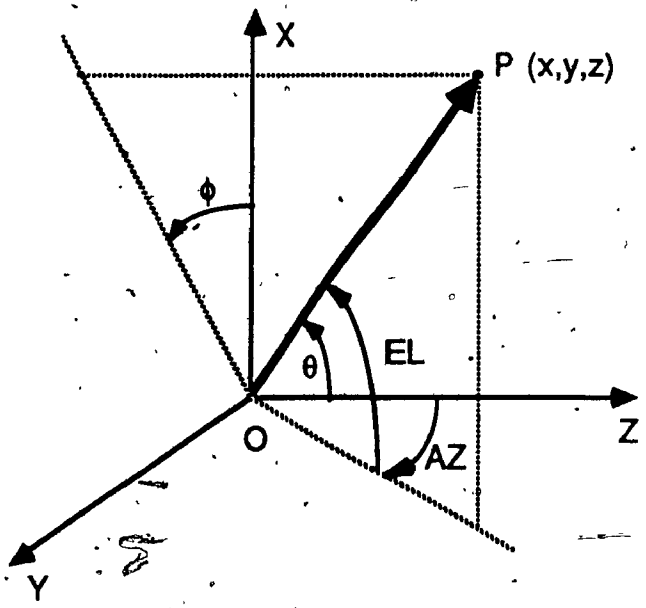

Figure 5.2 Elevation and Azimuth Coordinates of an observation point P

CHAPTER 6

NUMERICAL RESULTS

A computer program has been written based on the analysis presented in previous sections. There is sufficient data from which it is possible to verify the analysis. Numerical results corresponding to various array configurations will be presented in this Chapter. The choice of parameters in test cases conforms with those of experiments.

All computations are performed on a DEC VAX 11/780 computer, where single precision is used. The speed and availability of personal computers also permits the calculation on these of less complicated cases such as the admittance of a flanged circular waveguide. The solution for the complex amplitudes b's of reflected modes in

$$[b] = [I+C]^{-1}\,[I-C]\,[a]$$

is solved directly, which is faster and more accurate than computing the inverse of [I+C].

6.1 TE_{11} Input Admittance of a Flanged Circular Waveguide

Experimental results for this case have been reported by Bailey and Swift [15]. The waveguide is terminated in a finite ground plane in their experiment. However, later comparison with computed data reveals that a ground plane one wavelength square is sufficient for approximating an

infinite ground plane for impedance measurement. The input admittance, normalized to the waveguide characteristic admittance, is expressed by

$$Y_{in} = G - jB = \frac{1-\Gamma}{1+\Gamma} = \frac{1-\frac{b}{a}}{1+\frac{b}{a}}$$

where a and b are the amplitude of the incident and reflected waves, respectively.

The theory developed by these workers did not include the effect of the TE_{11} mode coupling to higher order modes, i.e. TM_{11}, TE_{12}, TM_{12}, etc. The predicted results from the present work are given in Figure 6.1. Two sets of data are given, one obtained from a single-mode approximation and one obtained from a six-mode approximation. It is evident that the latter agrees well with experiment, and in particular, it predicts the admittance is real at only one point when $d/\lambda = 0.765$ wavelength (or $ka = 2.404$, which is the cut-off wavenumber of TM_{01} mode). This is also recorded by the experiment. Furthermore, the six-mode approximation shows that the susceptance B is capacitive at higher frequencies instead of being inductive and approaching zero monotonically in the one-mode approximation.

The assumption of reflected evanescent modes is quite apparent from the above result. These modes have some effect upon the calculation of the scattering matrix coefficients and hence the reflection coefficient of the propagating mode.

6.2 H-plane Coupling Between Two Circular Waveguides

Two identical waveguides separated by a distance R are driven by a TE_{11} mode in one waveguide and are radiating into free space. The field in both waveguides is assumed to be polarized in the x direction (vertical polarization). Figure 6.2 depicts the experimental arrangement. A comparison between the measured results by Bailey [24] and the predicted results by the present software is made in Figures 6.3 and 6.4, where the former represents the amplitude and the latter represents the phase. The scattering coefficients are obtained by solving

$$[S] = [I + C]^{-1} [I - C]$$

It is observed that the computed magnitude and phase of S_{21} as a function of frequency, for various distances R, agree quite well with the measured ones. The mutual coupling is rather evident at lower frequencies, for the apertures exhibit smaller electrical size. The flat ground plane in the measurement was a 12-inch by 24-inch rectangular aluminium plate, thus diffractions from the edge cause some scatter in the data.

6.3 E-plane Coupling Between Two Circular Waveguides

Using a similar set-up as above, Bailey [25] has measured the scattered power between two waveguides placed side by side as shown in Figure 6.5. The waveguides are excited by a y-polarized (horizontal polarization) TE_{11} mode. Predicted results are compared with the experimental ones in Figure 6.6. Again, good correlation between the two sets of data is achieved.

In this particular investigation, it is quite interesting to notice that the magnitude of S_{21} is significantly higher than that in the H-plane

coupling case. The difference is of the order of 10 dB. The reason for this increase can be attributed to the nature of the aperture field distribution. In contrast to a highly tapered distribution in the H-plane, the field in the E-plane has strong edge illumination, causing a strong coupling in this plane.

The waveguides in the above cases are located quite far apart. Practical designs usually call for a much closer spacing, i.e, slightly greater than one diameter separation. A comparative study is made with the results reported earlier by Clarricoats *et al* [26]. The element spacing is now set at 2.1a. Figure 6.7 shows the magnitude of the scattering coefficient S_{21} of coupling between TE_{11} modes as a function of horn radius. In the E-plane case, the coupling decreases rapidly with increasing horn radius until the horn supports the TM_{11} mode, then the coupling approaches to a shallow maximum. In the H-plane case, the transition occurs at $a > 0.848$ wavelength when the TE_{12} mode is supported by the waveguide. In general, good agreement between the two sets of data is achieved.

6.4 Radiation Patterns From An Isolated and Seven-horn Antenna Array

The above experiments have signified that there are strong interactions between waveguides placed in the vicinity of each other. This mechanism is regarded as a cause for the disturbance in the antenna cross-polar patterns. The degree of cross-polar degradation will be assessed in the following studies.

6.4.1 Experiment conducted at SPAR Aerospace Ltd.

A seven-horn array antenna, whose layout is depicted in Figure 6.8, was built and tested at SPAR Aerospace Ltd. [2]. At the measurement

frequency 12.45 GHz the diameter and spacing between the elements correspond to 1.136 and 1.181 wavelength respectively. The experimental horns are conical, however their flare angle is quite small and it is justifiable to neglect the effect of phase error at the aperture in the computation. To establish a basis for comparison, the radiation patterns of an isolated horn are first recorded and shown in Figure 6.9. The cross-polar level in the ϕ = 45 degree plane (see Figure 5.2 for angle notation) is referenced to the co-polar level at the boresight angle. Good agreement, within measurement tolerances, is observed for all patterns. The measured cross-polar level is in the order of -30 dB, an expected value for a horn of this size.

Once the isolated horn performance is known, measurements were carried out in the array environment to quantify the mutual coupling effects on the radiation characteristics. Recorded patterns are illustrated in Figure 6.10. The center element of the array is driven by a TE_{11} mode whereas the peripheral elements are terminated by matched loads. Both predicted and measured results show a noticeable increase, 4 dB by prediction and 6 dB by measurement, in the cross-polar level. The high cross polarization component of the TE_{21} mode (which is supported by the waveguides at the measurement frequency) is believed to be the dominant reason for this change. The interaction of this higher mode to the dominant mode was included in the computation.

6.4.2 Experiment reported in publication

The radiation characteristics of an immersed horn in a cluster environment were also investigated experimentally by Adatia *at al* in their

1981 publication [27]. Although the measurements were performed over a frequency band of 14.0–14.5 GHz, particular results at 14.25 GHz, were presented. At this center frequency, the electrical dimensions of the horn diameter and horn spacing are 1.026 and 1.031 wavelength, respectively.

The contour plots of computed and measured co-polar and cross-polar radiated fields of an isolated horn are illustrated in Figures 6.11 to 6.13, inclusive. The agreement between the two sets is considered qualitatively similar, with the cross-polar lobes in the diagonal planes peaking at approximately -32 dB relative to the peak of the co-polar pattern.

The performance of the elements combined in a cluster is computed and presented in Figures 6.14 and 6.15. Measured data follows in Figure 6.16. It is initially observed that there is a slight modification to the co-polar radiated pattern from a near circular contours associated with an isolated element. The resultant elliptical contours are due to the difference in the edge illumination in the E- and H-plane of the array. The predicted change, however, is not as large as that in Figure 6.16. The measurement has shown significant distortion, particularly with the shoulder effects. Insofar as the cross-polar lobes are concerned, the prediction shows a shift of the lobes toward the boresight and a raising of the peak level to approximately -22dB below the co-polar peak. Once again the contour plots are not in close correlation with those from the measurement, despite a similarity in level.

In an attempt to further improve the computed results, the inclusion of higher modes is considered. Such consideration leads to results presented in Figures 6.17 and 6.18. The additional mode is TE_{21}. There is a slight improvement with regard to the degree of co-polar contour distortion

but that is still far from being a close match of the measured contours. The cross-polar contours, on the other hand, are closing on the recorded shape. The formation of a -22 dB cross-polar lobe much closer to the boresight is clearly predicted. In view of this positive result, it is believed that higher modes such as TM_{01} (has strong cross polarization) be included. Because such computation becomes very time consuming with increasing number of modes, it was not attempted.

6.5 Summary

This Chapter has presented numerical data, in terms of the scattering coefficient and radiation patterns, for various antenna configurations. The computed results are compared against measured and published data to validate the analysis and the software. The favorable comparisons have provided confidence that the present work is sufficiently accurate and it can be regarded as a supplemental package to aid the design and analysis of planar antenna arrays.

It is worthwhile to mention that the setting up of the coupling coefficient matrix accounts for nearly 90 percent of the total computing time. This is due to the many integrals involved in the formulae. The addition of higher modes in the computation is a must but care should be taken not to include arbitrary modes that will result in lengthening the computation, where their total contribution to the total radiated field is insignificant.

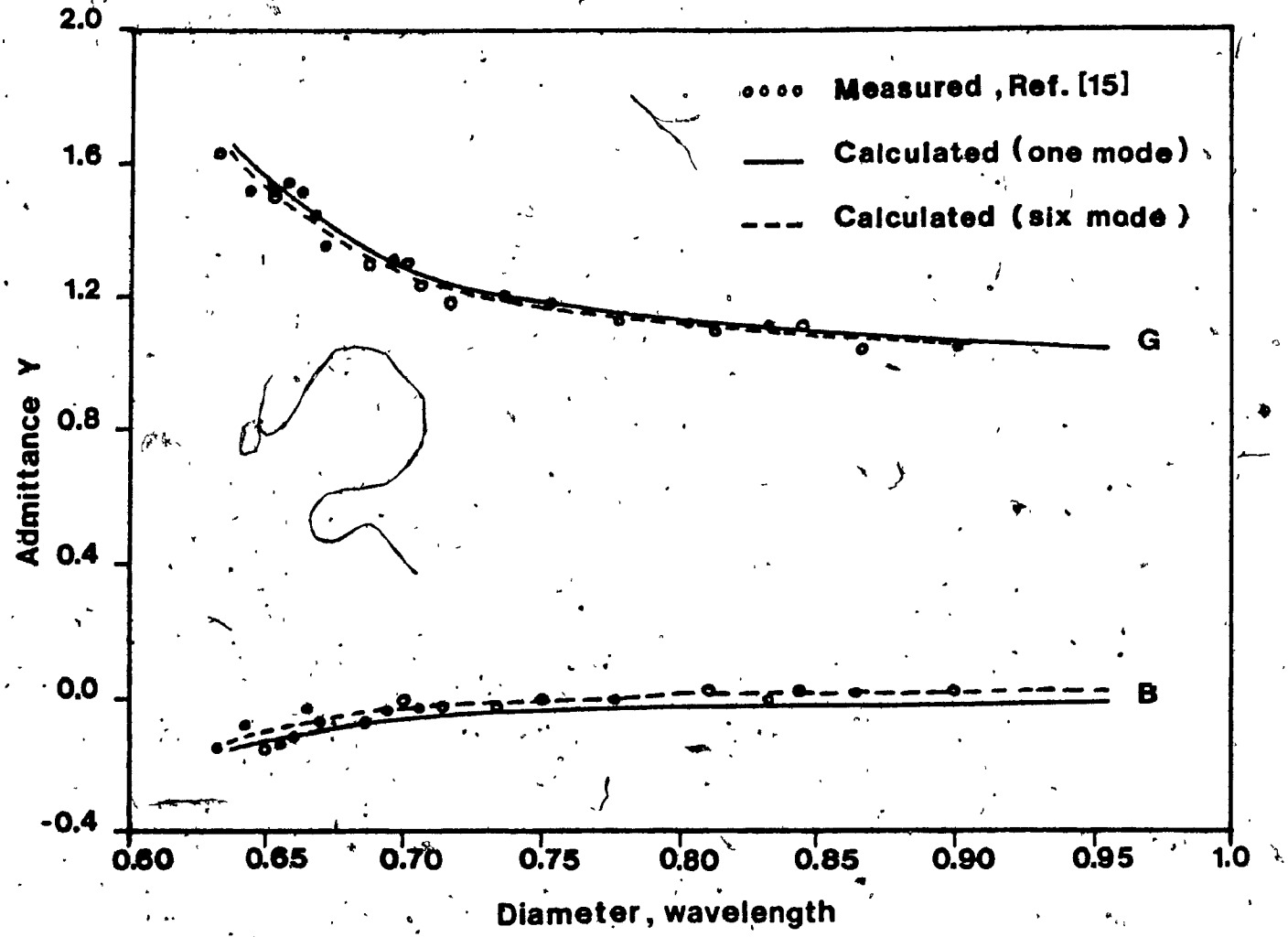

Figure 6.1 Input admittance of a flanged circular waveguide

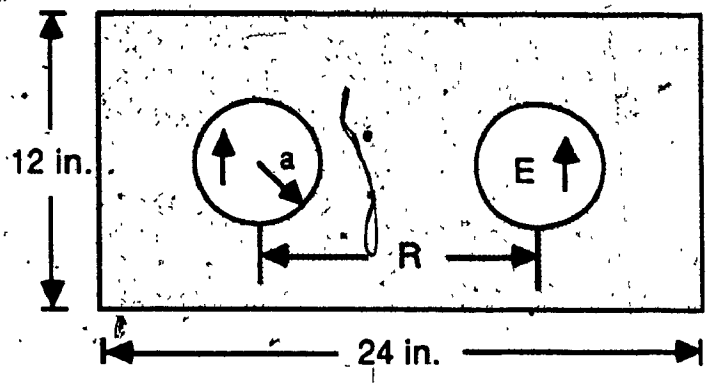

Figure 6.2 H-plane coupling — Experimental set up

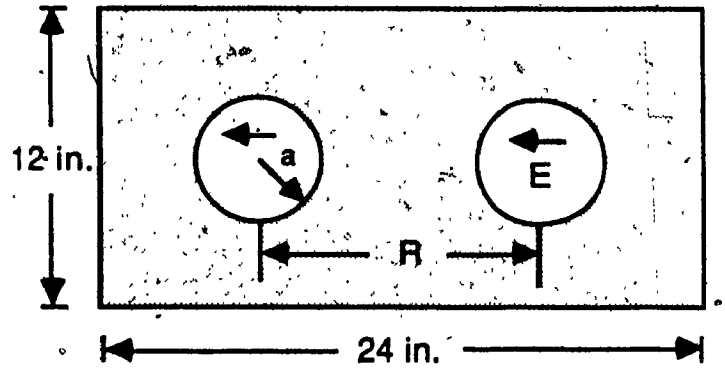

Figure 6.5 E-plane coupling – Experimental set up

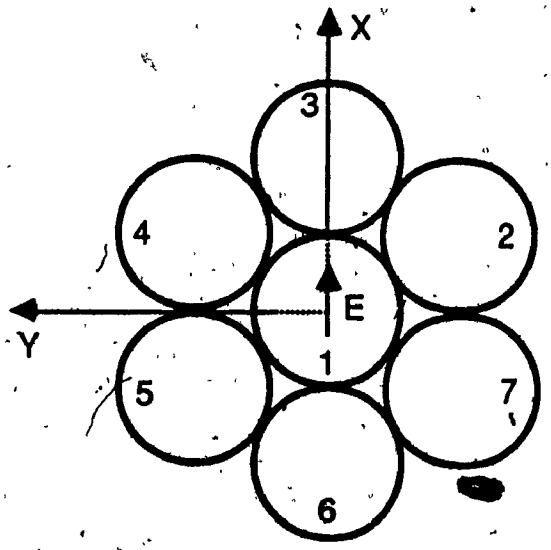

Figure 6.8 Seven-horn array antenna configuration

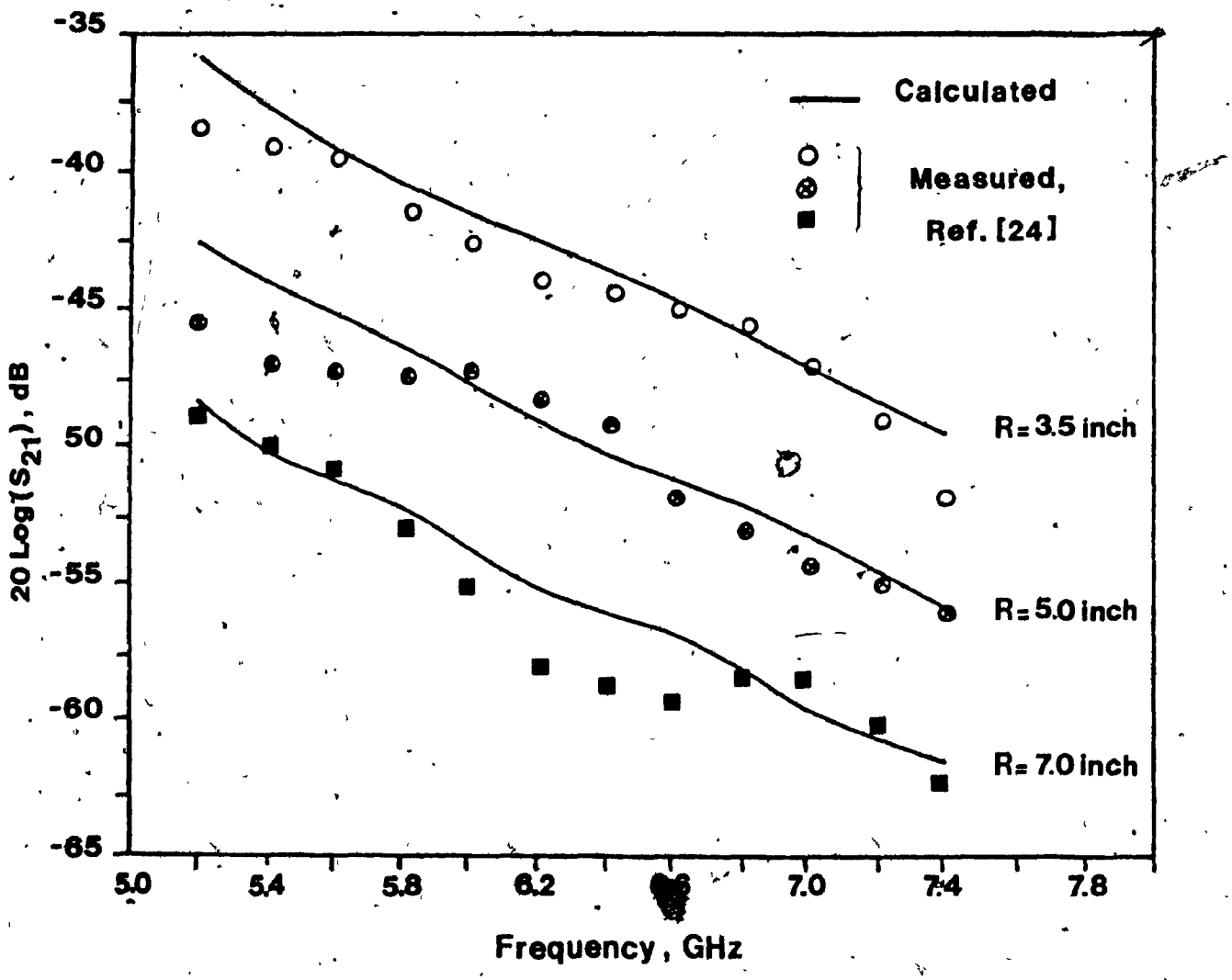

Figure 6.3 H-plane coupling of two identical waveguides separated by a distance R — Amplitude of S_{21} Waveguide radius a = 0.75 in.

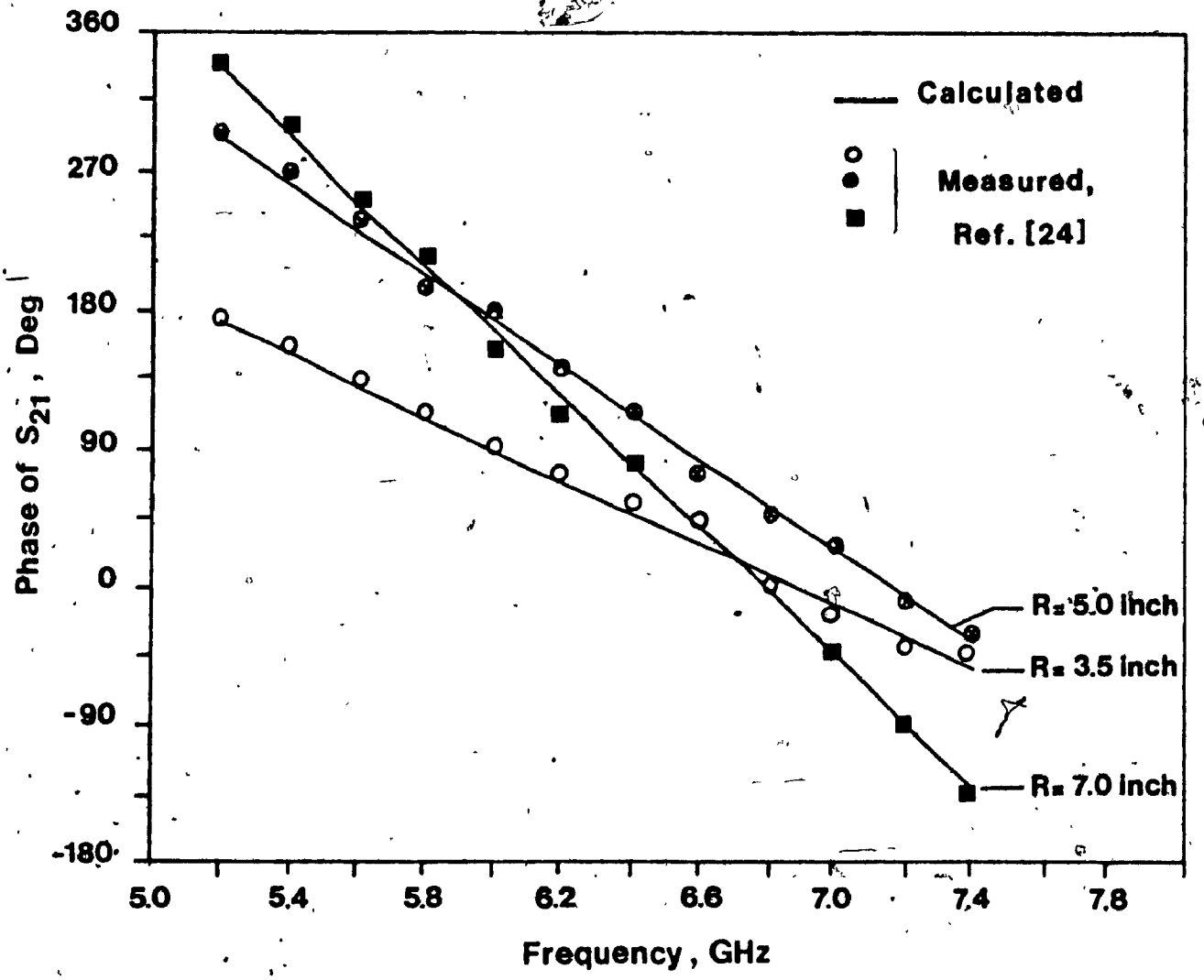

Figure 6.4 H-plane coupling of two identical waveguides separated by a distance R — Phase of S_{21}
Waveguide radius a = 0.75 in.

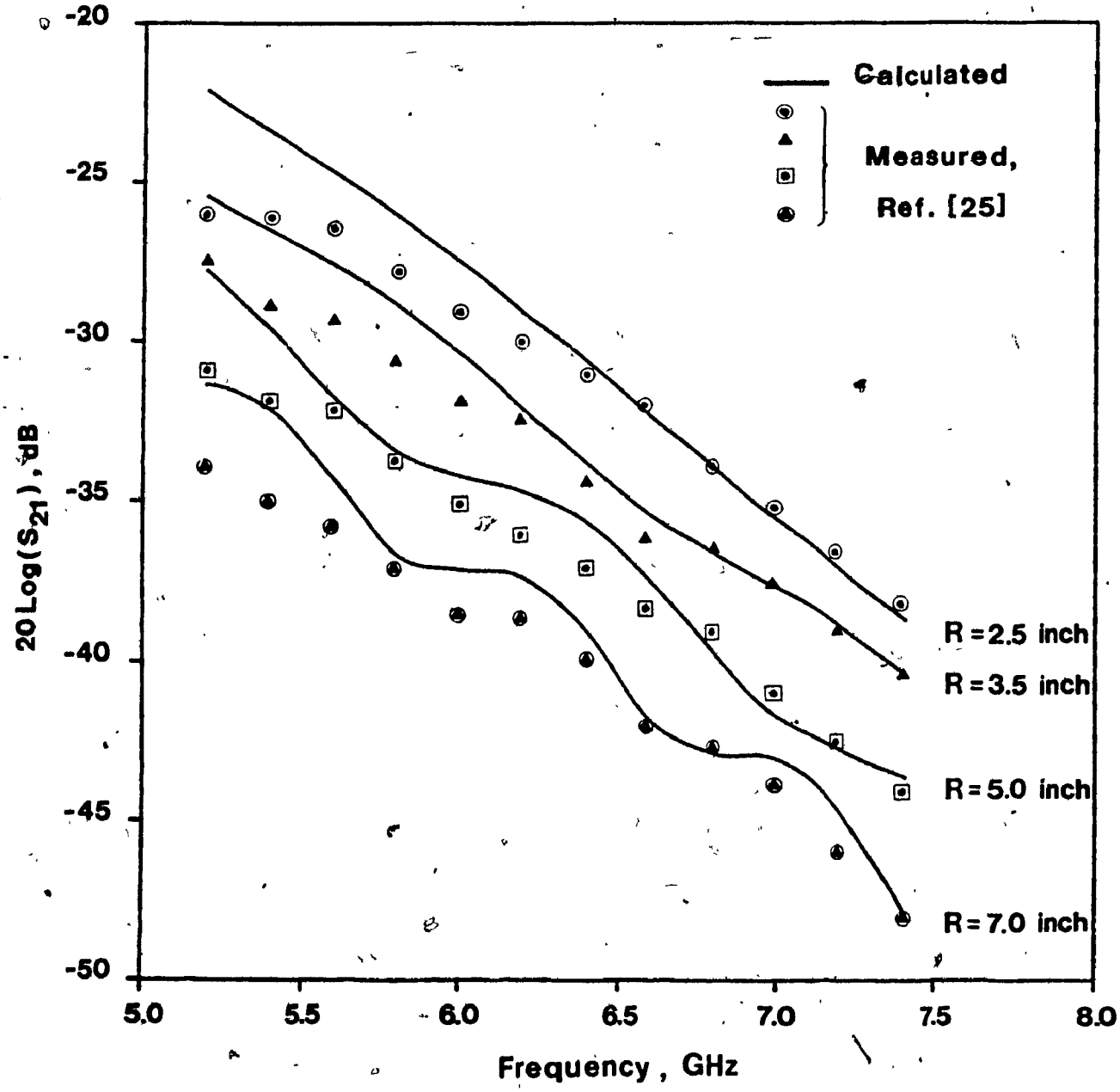

Figure 6.6 E-plane coupling of two identical waveguides separated by a distance R — Amplitude of S_{21} Waveguide radius a = 0.75 in.

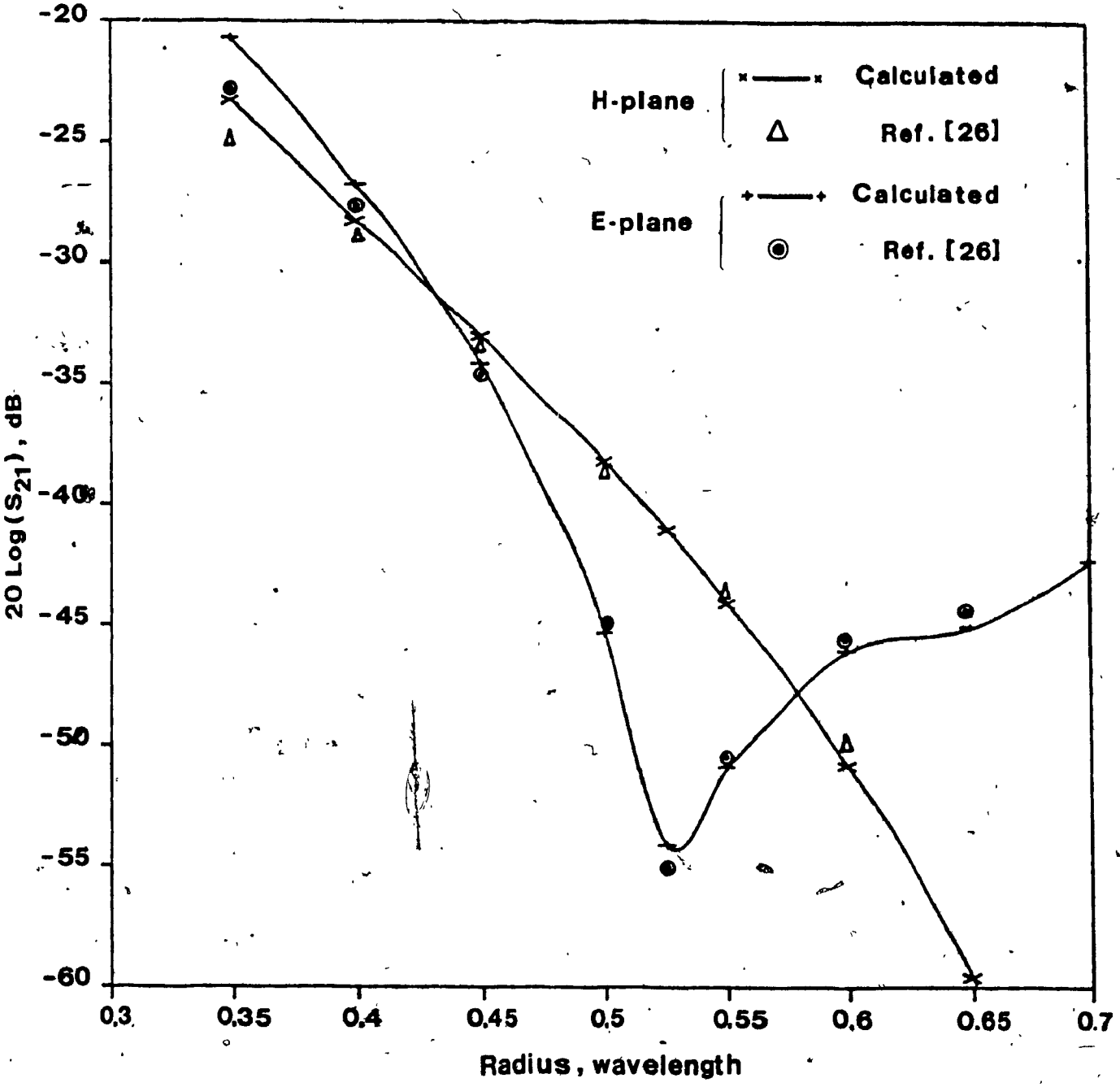

Figure 6.7 Scattering coefficient S_{21} of TE_{11} mode between two waveguides separated by a distance R=2.1a

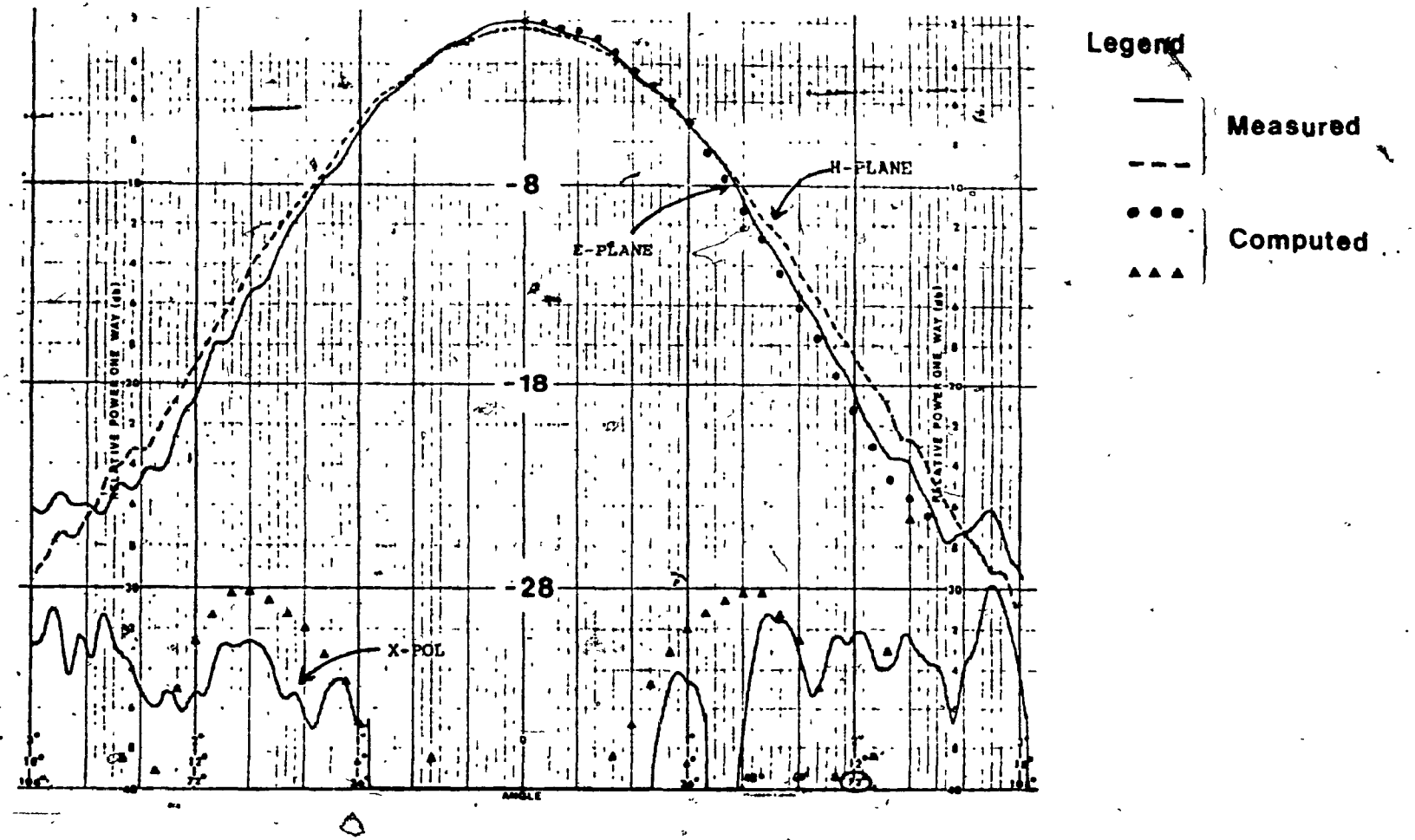

Figure 6.9 Radiation patterns of an isolated horn with linear polarization – Frequency f = 12.45 GHz

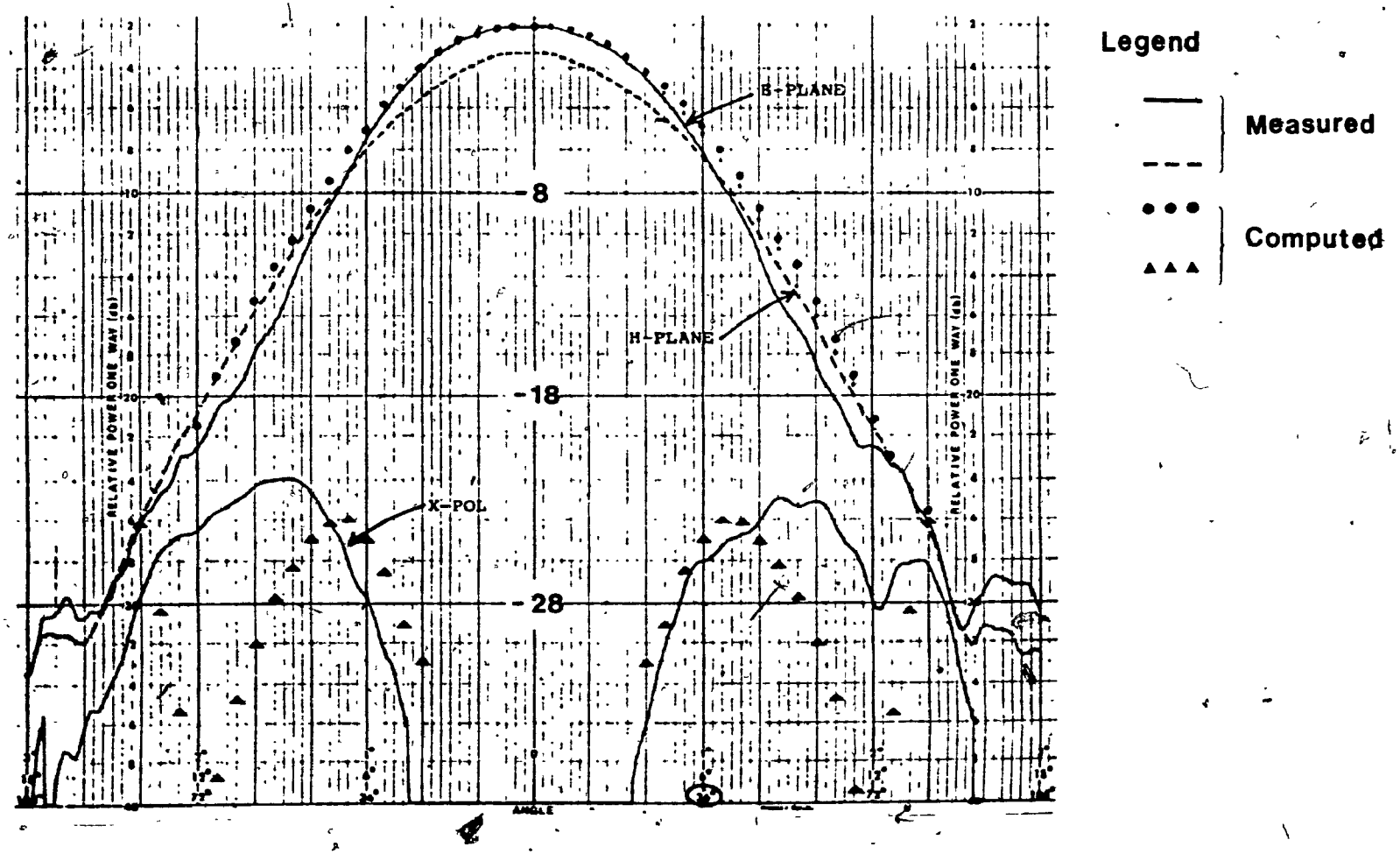

Figure 6.10 Radiation patterns of a horn array with linear polarization – Frequency f = 12.45 GHz

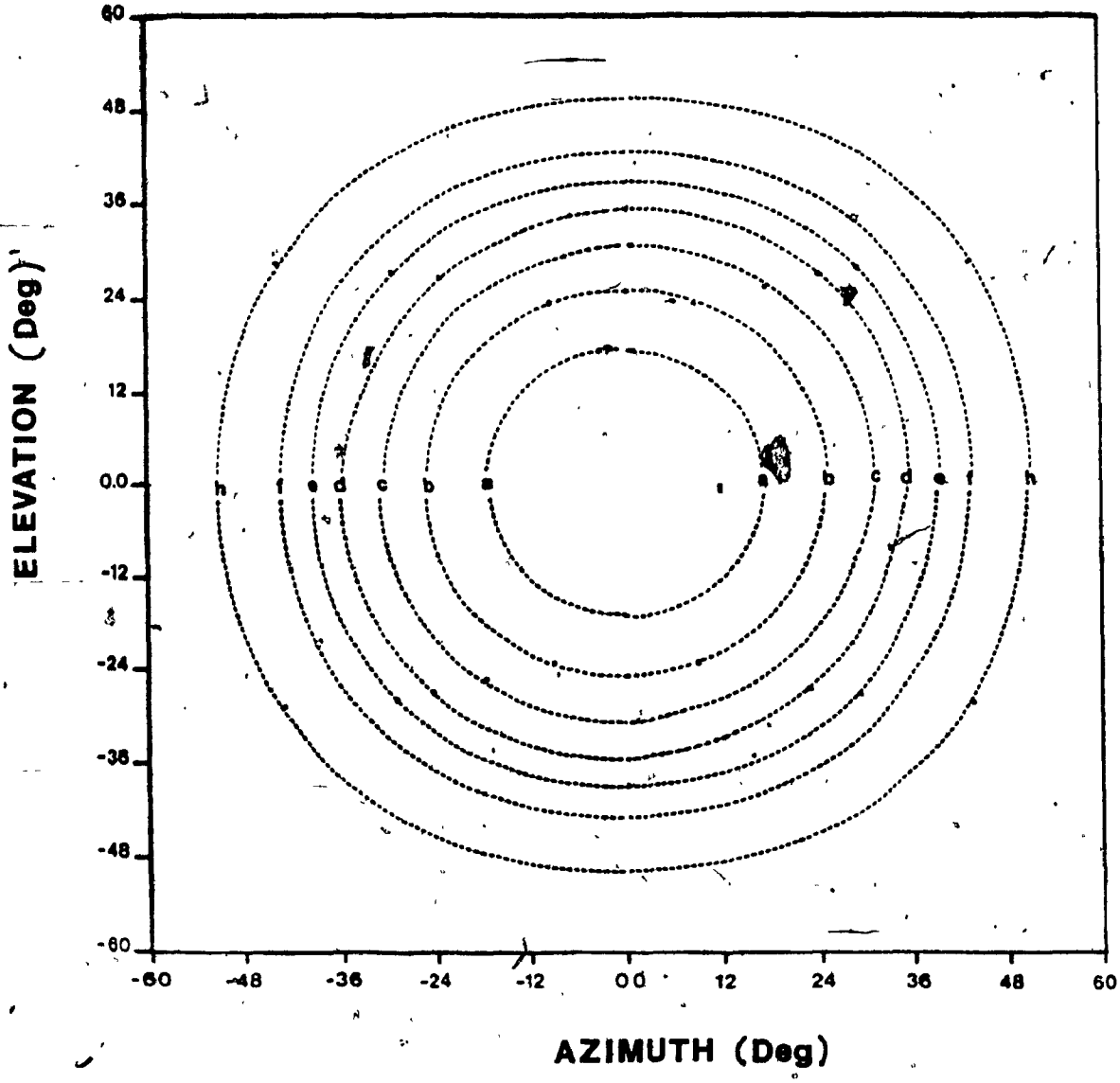

Contour Level (dB)

a	=	-1
b	=	-2
c	=	-3
d	=	-4
e	=	-5
f	=	-6
h	=	-8

Figure 6.11 Computed co-polar contour of an isolated conical horn
Linear polarization TE_{11} – Frequency f = 14.25 GHz
D = 1.026 wavelength

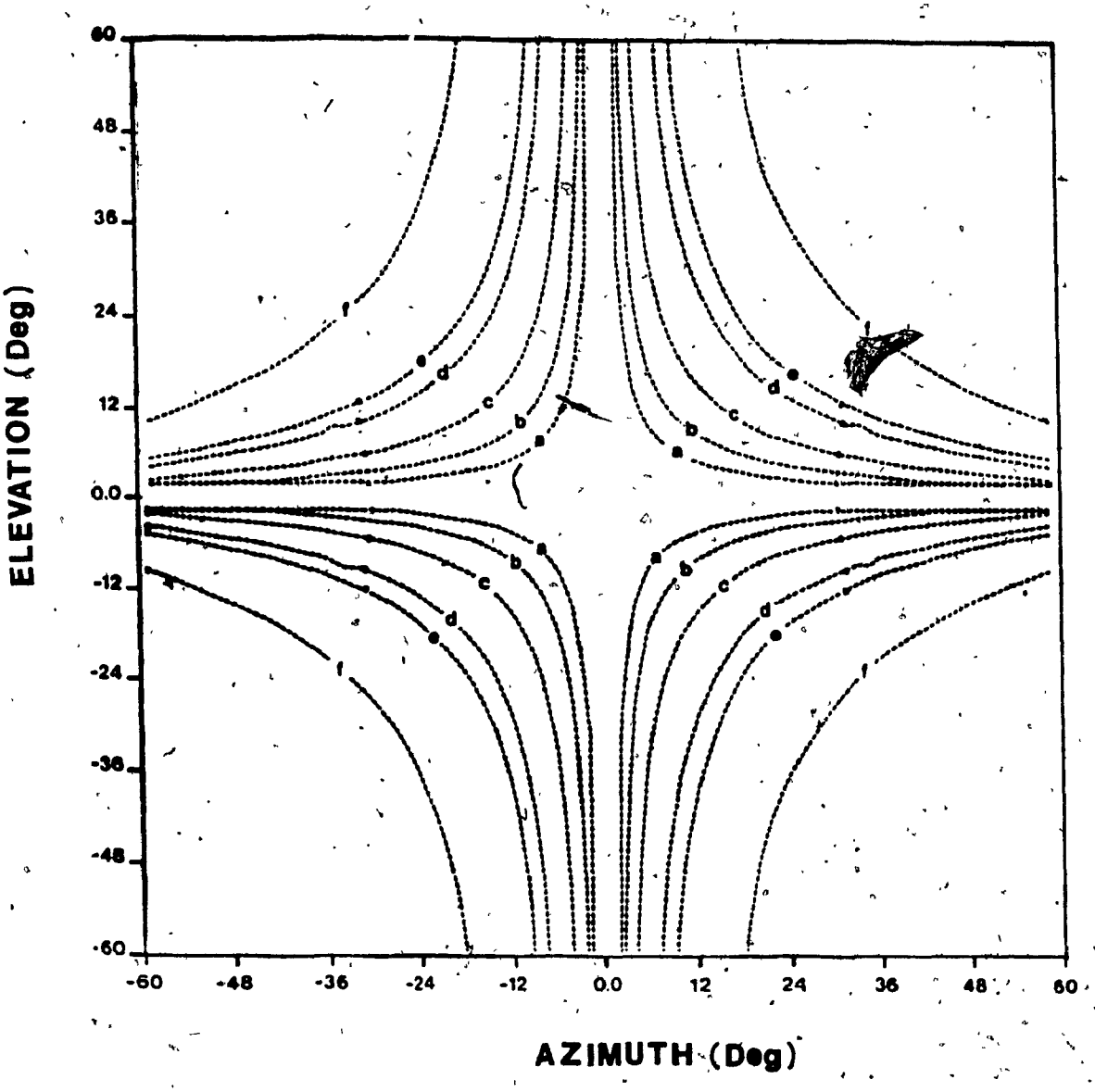

Contour Level (dB)

a	=	-55
b	=	-50
c	=	-45
d	=	-40
e	=	-38
f	=	-34

Figure 6.12. Computed cross-polar contour of an isolated conical horn
Linear polarization TE_{11} – Frequency f = 14.25 GHz
D = 1.026 wavelength

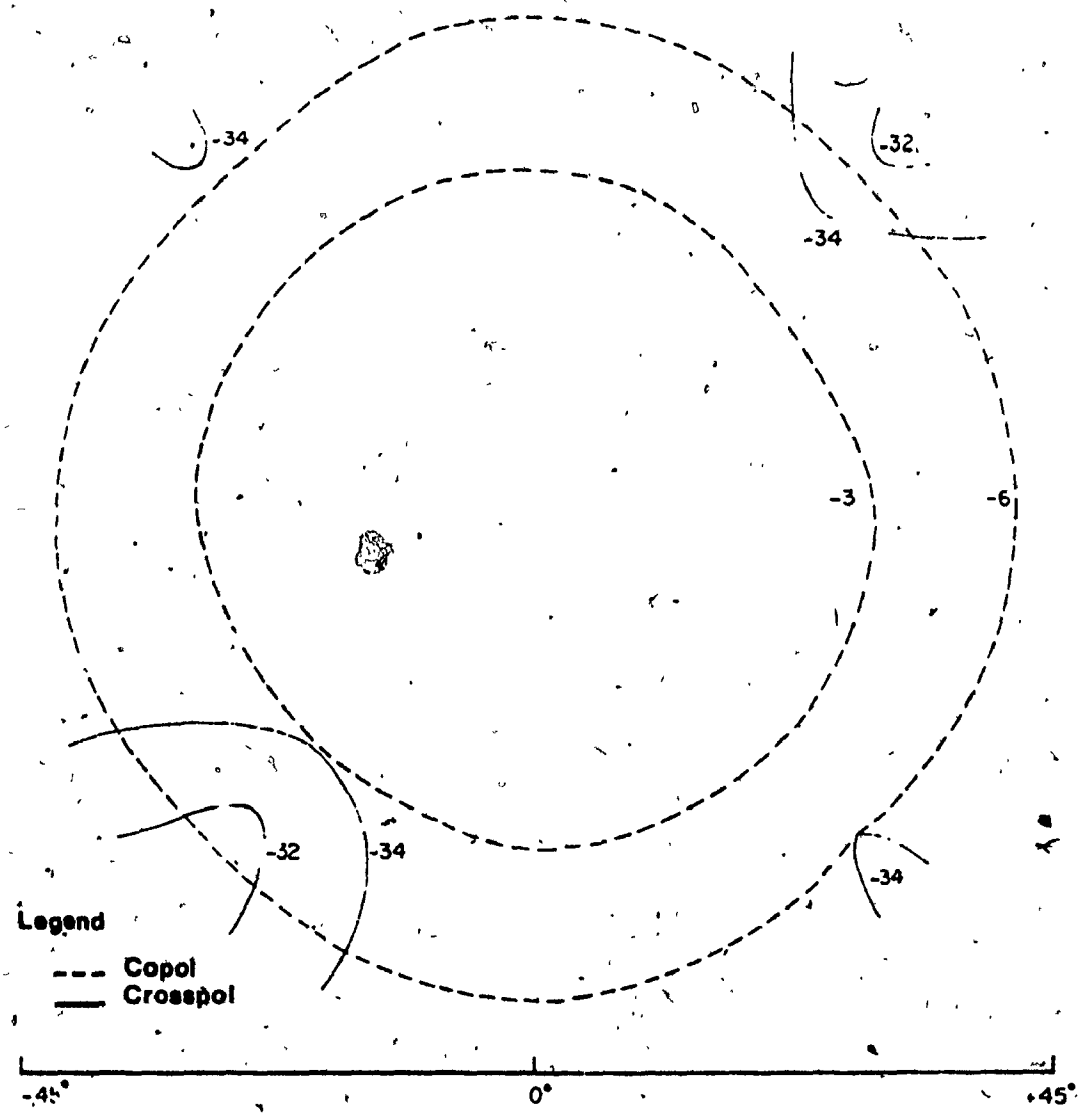

Figure 6.13 Measured co- and cross-polar contours of an isolated conical horn
Linear polarization TE_{11} – Frequency f = 14.25 GHz
D = 1.026 wavelength

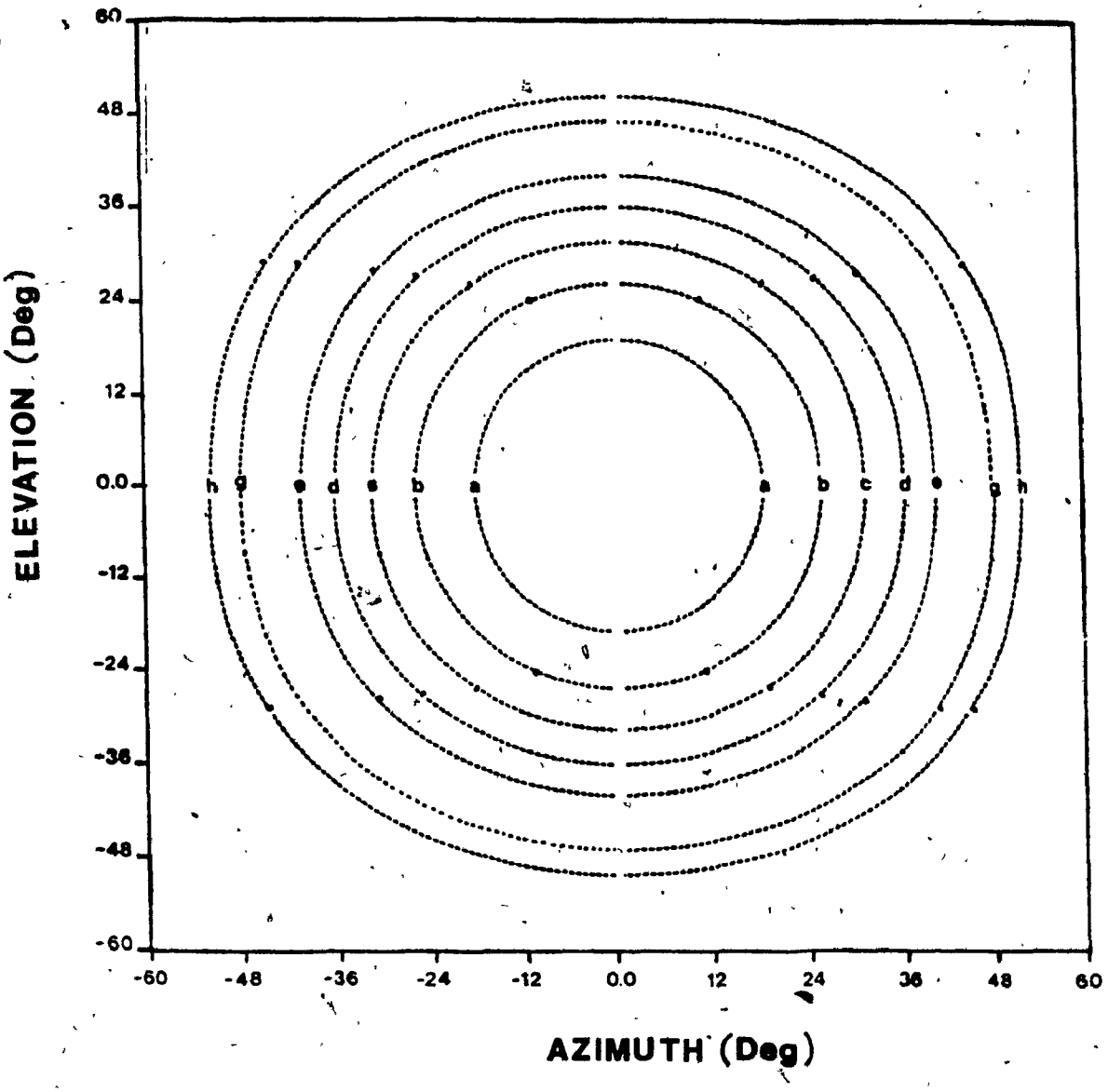

Contour Level (dB)

a	=	**-1**
b	=	**-2**
c	=	**-3**
d	=	**-4**
e	=	**-5**
g	=	**-7**
h	=	**-8**

Figure 6.14 Computed co-polar contour of a seven-horn array antenna
Linear polarization TE_{11} – Frequency f = 14.25 GHz
D = 1.026 wavelength

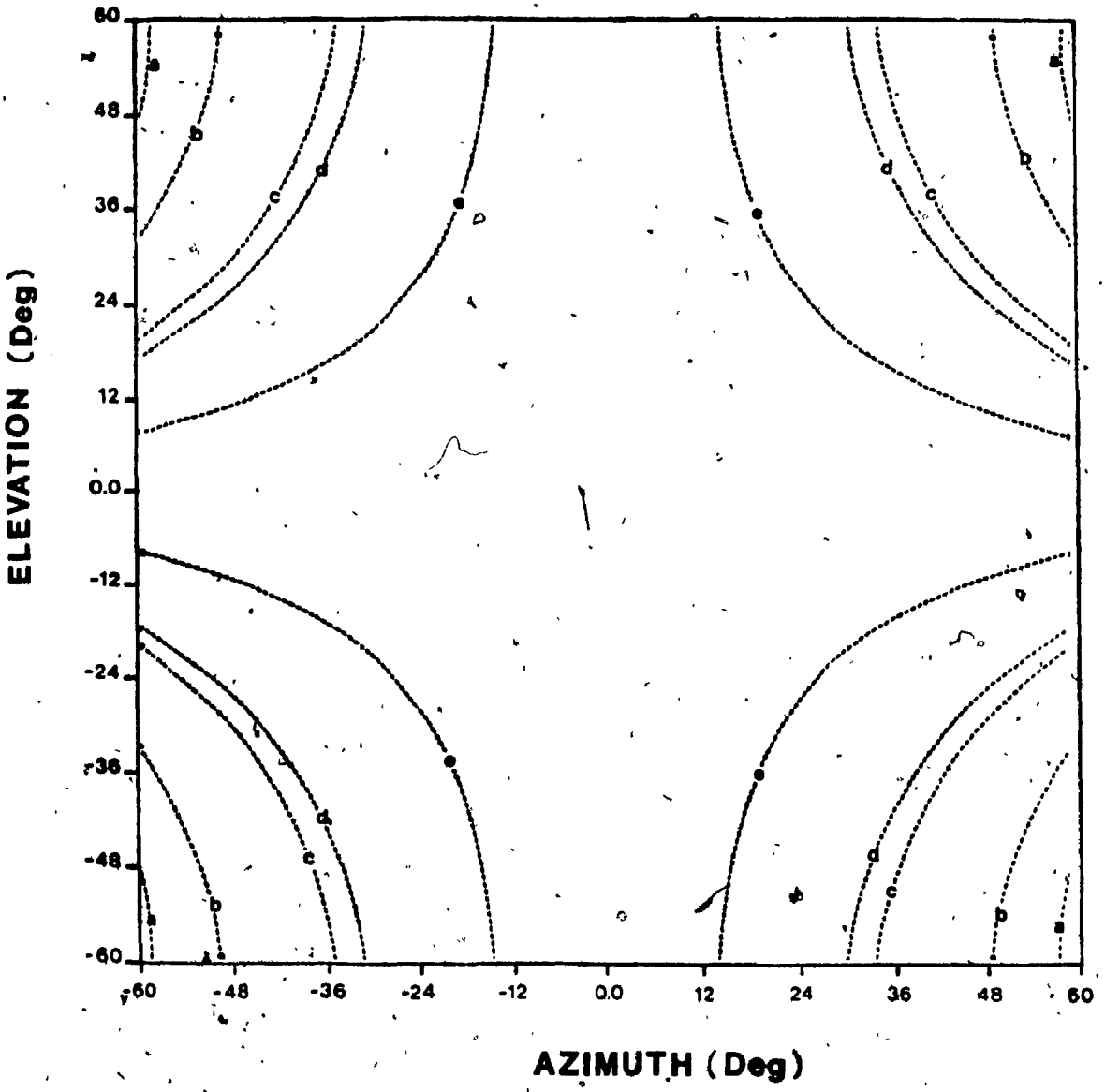

Figure 6.15 Computed cross-polar contour of a seven-horn array antenna
Linear polarization TE_{11} – Frequency f = 14.25 GHz
D = 1.026 wavelength

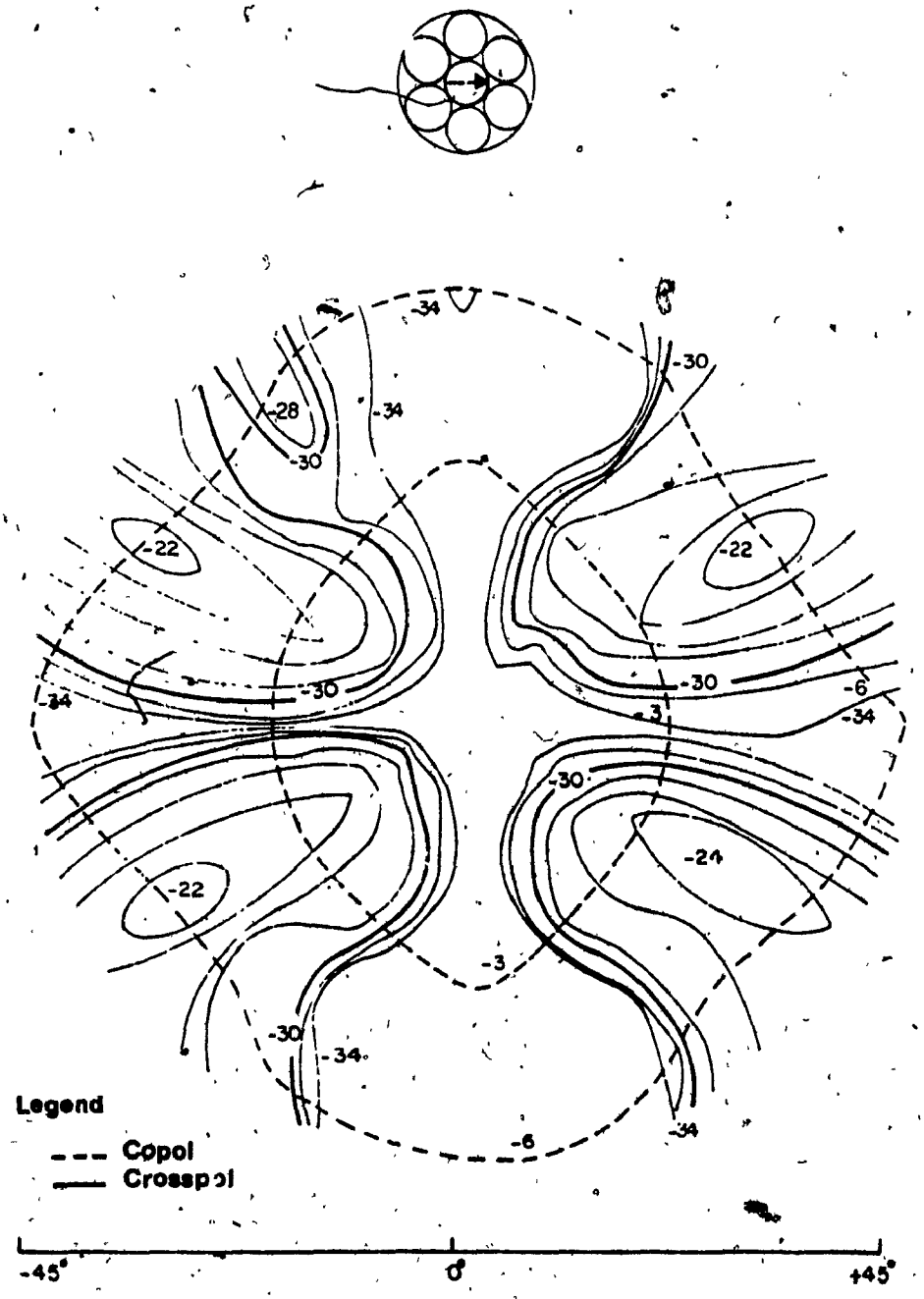

Figure 6.16 Measured co- and cross-polar contours of a seven-horn antenna
Linear polarization TE_{11} - Frequency f = 14.25 GHz
D = 1.026 wavelength

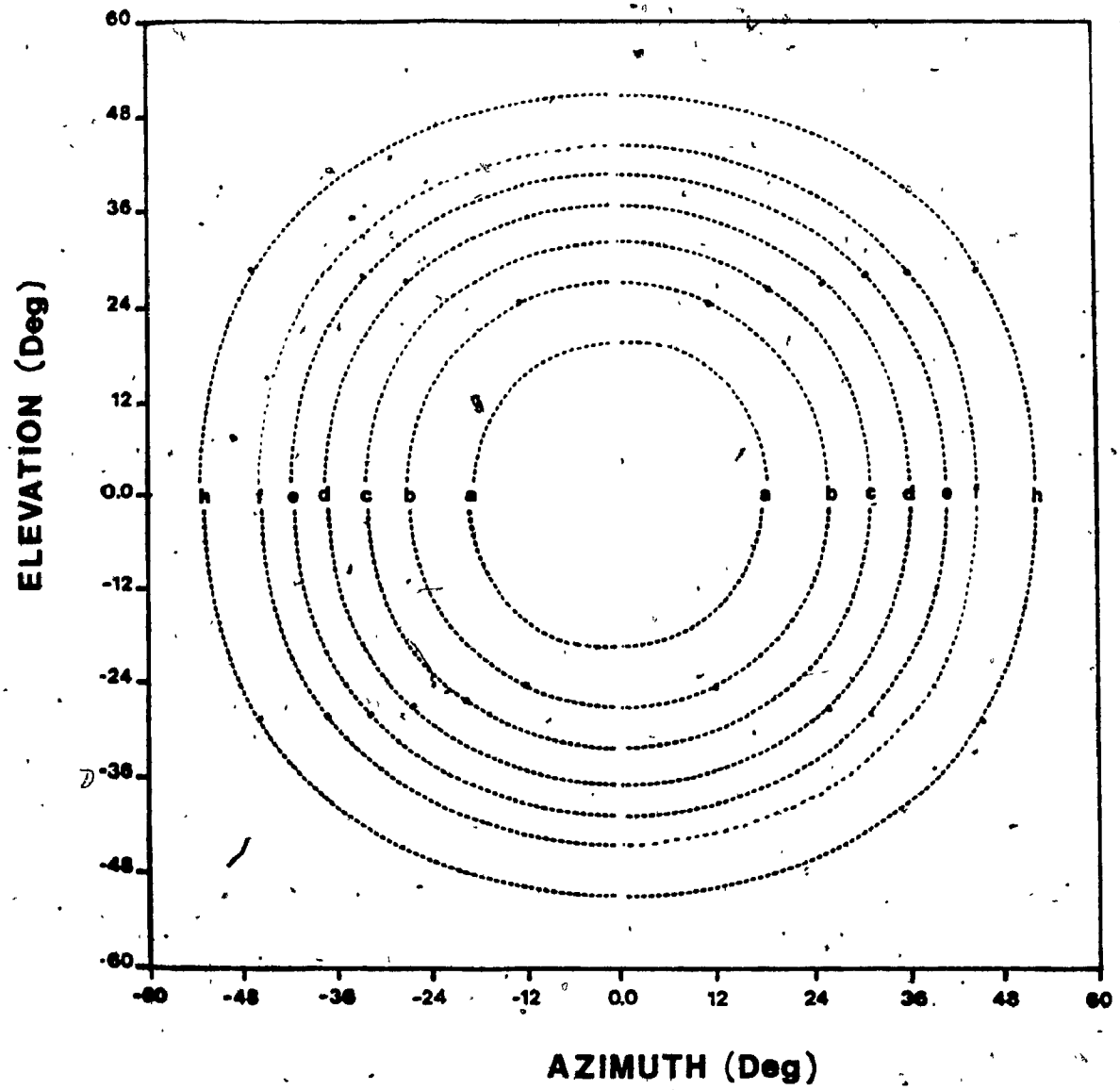

Contour Level (dB)

a	=	-1
b	=	-2
c	=	-3
d	=	-4
e	=	-5
f	=	-6
h	=	-8

Figure 6.17 Computed co-polar contour of a seven-horn array antenna
Including higher-order mode TE_{21}

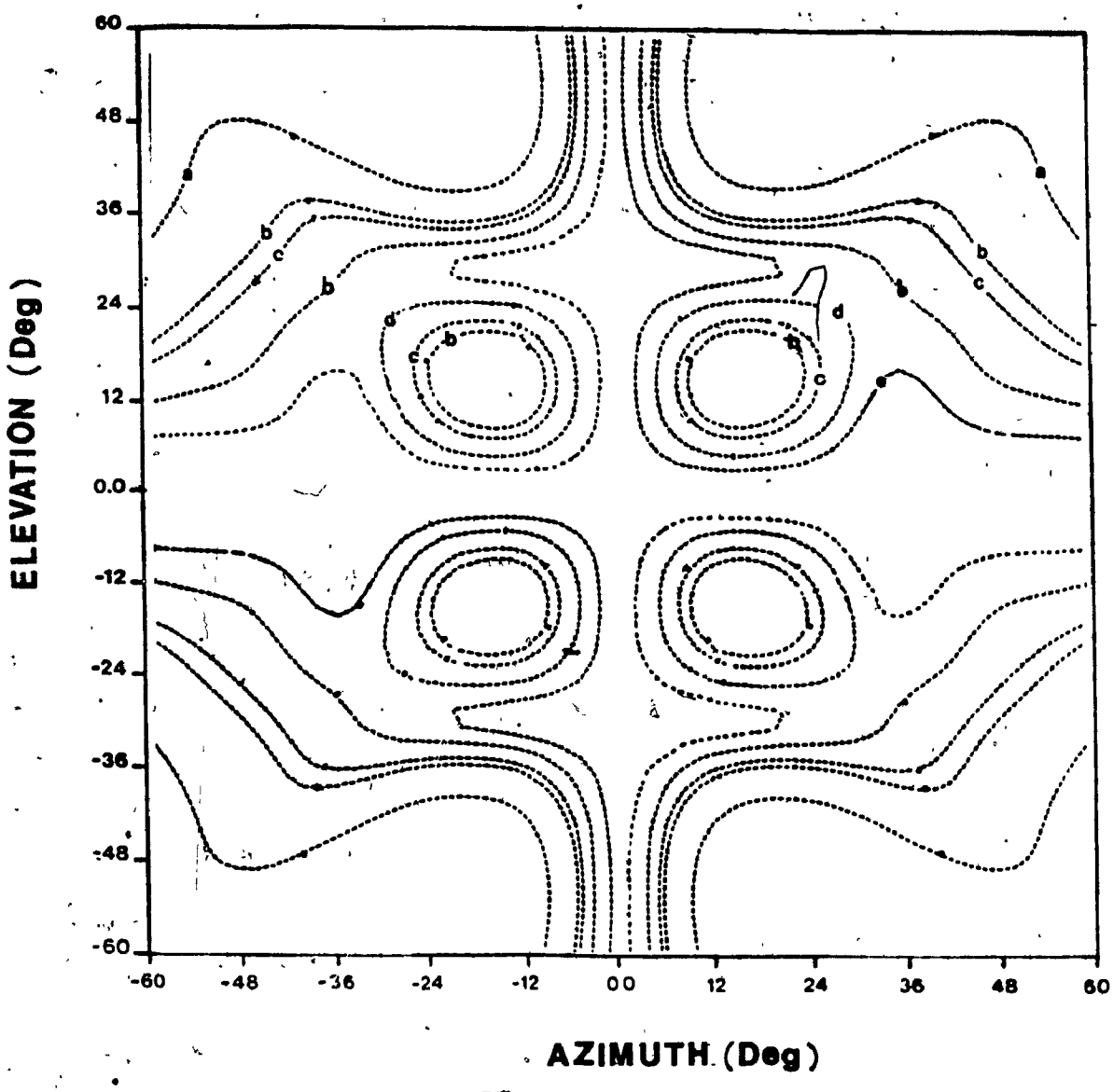

Contour Level (dB)

a	=	**-22**
b	=	**-26**
c	=	**-27**
d	=	**-30**
e	=	**-34**

Figure 6.18 Computed cross-polar contour of a seven-horn array antenna
Including higher-order mode TE_{21}

CHAPTER 7

DISCUSSION AND CONCLUSION

A detailed mathematical formulation has been presented for analyzing the mutual coupling effects in a planar finite array of open-ended circular-waveguides. The approach was to set up an integral equation and to solve it in the approximate sense. The generality of the analysis has been highlighted by the inclusion of higher-order modes, in addition to the dominant mode, into the coupling coefficients. Satisfactory results applied to various antenna configurations have proved the validity of the analysis.

Significant deterioration of the cross polarization performance for a closely-packed horn array was clearly predicted. It is evident that the principal factor contributing the deterioration comes from coupling between the TE_{11} and TE_{21} modes. In a result discussing the dependence of the scattering coefficient S_{21} on the aperture size, it is to be expected that the mutual coupling effects in an array can be minimized by increasing the horn size. Practically, this consideration may be shadowed by the overall array size and the grating lobe effect. Nevertheless, it is worthwhile to be taken as an initial choice in the design. In this event, other effects would certainly dominate over the mutual coupling in determining the cross-polar levels. Studies also reveal that polarization of the excited mode in active elements play an important role in the variation of coupled powers between adjacent members in the array. The mode interaction is more pronounced in the E-plane than in the H-plane, for a given geometry.

Generally, in analyzing a conical horn array account must be taken of higher-order modes that are excited at the aperture but are cut off before reaching the throat. These higher-order modes, on one hand alter the actual aperture field locally, and on the other hand cause further coupling with the dominant mode when they travel back toward the horn throat. The present study permits the inclusion of higher-order modes, but does not include a phase error in the aperture plane caused by the flare angle of the horn and also due to the change in phase at the cut off point. Minimal error would result for conical horns with small flare angle (up to 5 degrees). Treatment of actual horn geometry is considered beyond the scope of this thesis.

Particular attention has been given to the numerical accuracy and efficiency. With regard to numerical integration required for the coupling coefficient, various techniques have been looked at. The Gaussian quadrature is found to converge rather slowly and does not handle singularities effectively. The Simpson Quadrature Used Adaptively – Noise Killed (SQUANK) [28] is not a desirable technique despite its significance in round-off error guard (which guards against the effects of excessive round-off error in function values). The SQUANK algorithm requires a rather large number of calls to the function evaluating subroutine; thus it becomes less economic in this particular problem (where numerical integration is frequently encountered). Among the techniques investigated, adaptive Romberg is found to be a good candidate due to its fast convergence for a required degree of accuracy. This technique was actually implemented in the computer program. As far as solution of the matrix equation is concerned, Gauss elimination with partial pivoting is employed. Small

residuals are obtained with this method. The numerical accuracy poses no critical problem, presumably due the the strong dominance of diagonal elements in the coupling coefficient matrix [C].

The computation of the elements in the coupling matrix [C] and the solution of the matrix equation are the two most time-consuming steps in calculating the mutual coupling in an array, often accounting for over 90% of the CPU time. Although the software is quite general for evaluating the coupling between arbitrary elements, nearest-coupling is found to be dominant. It is, therefore, felt that for elements that are separated by more than three times the normalized diameter (D/λ), the coupling coefficient between them can take on a preset minimum value in order to reduce the computations. A special arrangement of elements, in say an equi-angular lattice fashion, may offer some advantage.

The radiation patterns of an array are easily derived since the aperture field, with mutual coupling effects already taken into consideration, for each waveguide is known. Radiation characteristics are determined with greater accuracy by this approach. The usefulness of this research can be found in the synthesis of direct radiating array patterns or of the secondary patterns of single or dual reflector antennas fed by a multiple–feed array. In the latter case, a possible procedure that can be called for is first to treat the scattering from the subreflector by either Near-field Physical Optics or Geometrical Optics in combination with the Uniform Geometrical Theory of Diffraction (UGTD) [29]. The scattered field from the main reflector is then obtained by means of Physical Optics integration of the surface currents. The option of employing FFT with a sampling technique may be included to enhance the speed. The

investigation of performance of offset reflector antennas with an array feed is a very interesting research topic where further work would be productive.

In conclusion, the main objective of the study has been successfully accomplished. An analytical formulation was derived and a computer program was developed to evaluate the mutual coupling effects in an array feed. From the software that was developed, a first-hand knowledge of the extent to which mutual coupling will degrade overall antenna performance is obtained. Thus corrective solutions to minimize the effects may be incorporated into a design at an earlier stage. The present analysis can be extended to investigate the mutual coupling effects in a finite planar array of rectangular waveguides. Only limited difficulties are envisioned for this application, but in the moment method solution, the basis and weighting functions would be the rectangular waveguide modal fields instead of those of circular waveguides.

REFERENCES

[1] P. J. B. Clarricoats, C. G. Parini, S. M.Tun: "Conical Horn Array Feed Performance," **IEE Conference Publication**, 1983, pp. 195–199.

[2] K. S. Rao: "Mutual Coupling Effects on the Radiation Patterns of Dominant and Dual-Mode Circular Horn Arrays : An Experimental Study," **SPAR Aerospace** Technical Report No. RML–009–85–55.

[3] R. F. Harrington: **Field Computation by Moment Methods,** Mac Millan, New York, 1988.

[4] J. Luzwick and R. F. Harrington: "Mutual Coupling Analysis in a Finite Planar Rectangular Waveguide Antenna Array ," Department of Electrical and Computer Engineering, **Syracuse University,** Technical Report No. 7,June 1978.

[5] A. J. Fenn, G. A. Thiele., B. A. Munk: "Moment Method Analysis of Finite Rectangular Waveguide Phased Array", **IEEE Trans. Antenna and Propagation**, Vol. AP-30, No. 4, July 1982, pp. 554–564.

[6] A. G. Cha, J. K. Hsiao: "A Matrix Formulation of Large-Scale Numerical Computation of the Finite Planar Waveguide Array Problem", **IEEE Trans. Antenna and Propagation**, Vol. AP-22, No. 1, January 1974, pp. 106–108.

[7] H. Steyskal: "Mutual Coupling Analysis of a Finite Planar Waveguide Array," **IEEE Trans. Antenna and Propagation,** Vol AP-22, No. 1, July 1974, pp. 594–599.

[8] Ch. Fernez: "Exact Formulation for Planar arrays: application to rectangular waveguide," **IEE Conference Publication**, 1978, pp. 443-447.

[9] C. P. Wu: "Numerical Solutions for the Coupling Between Waveguides in Finite Arrays," **Radio Science**, Vol. 4, No. 3, March 1969, pp. 245–254.

[10] R. J. Mailloux: "Radiation and Near-Field Coupling Between two Collinear Open-Ended Waveguides," **IEEE Trans. Antenna and Propagation**, Vol. AP-17, No. 1, January 1969, pp. 594–599.

[11] _____: "First–Order Solutions for Mutual Coupling Between Waveguides which Propagate Two Orthogonal Modes," **IEEE Trans. Antenna and Propagation**, Vol. AP-17, No. 6, November 1969, pp. 740-746.

[12] T. S. Bird: "Mode Coupling in a Planar Circular Waveguide Array," **IEE Microwaves, Optics and Antennas**, Vol. 3, No. 5, September 1979, pp. 172–180.

[13] R. Mitra (Ed.): **Computer Techniques for Electromagnetics**, Pergamon Press, 1973.

[14] M. C. Bailey and C. W. Bostian: "Mutual Coupling in a Finite Planar Array of Circular Apertures," **IEEE Trans. Antenna and Propagation**, Vol. AP-22, No. 2, March 1974, pp. 178–184.

[14] M. C. Bailey and C. W. Bostian: "Mutual Coupling in a Finite Planar Array of Circular Apertures," **IEEE Trans. Antenna and Propagation**, Vol. AP-22, No. 2, March 1974, pp. 178–184.

[15] M. C. Bailey and C. T. Swift: "Input Admittance of a Circular Waveguide Aperture Covered by a Dielectric Slab," **IEEE Trans. Antenna and Propagation**, Vol. AP-16, No. 4, July 1968, pp. 386–391.

[16] B. A. Mishustin: "Radiation From the Aperture of a Circular Waveguide with an infinite flange," **Soviet Radiophysics**, Vol. 8, No. 6, 1965, pp. 852–858.

[17] R. F. Harrington: **Time-Harmonic Electromagnetic Fields**, McGraw-Hill, New York, 1961.

[18] R. E. Collin and R. Zucker: **Antenna Theory, Part 1**, McGraw-Hill, New York, 1968.

[19] J. A. Stratton: **Electromagnetic Theory**, McGraw-Hill, New York, 1941.

[20] M. Abramovitz and I. A. Stegun: **Handbook of Mathematical Functions**, Dover, New York,1965.

[21] N. W. McLachlan: **Complex Variable Theory and Transform Calculus with Technical Applications**, Cambridge University Press, 1963.

[22] A. C. Ludwig: "The definition of Cross-Polarization," **IEEE Trans. Antenna and Propagation**, Vol. AP-21, January 1973, pp. 116–119.

[23] R. E. Collin: **Antennas and Radiowave Propagation**, McGraw-Hill, 1985.

[24] M. C. Bailey: "Mutual Coupling Between Circular Waveguide-fed Apertures in a Rectangular Ground Plane," **IEEE Trans. Antennas and Propagation**, Vol. AP-22, July 1974, pp. 597-599.

[25] M. C. Bailey: "Mutual Coupling in a Finite size Phased Array of Circular Waveguide Elements," **Digest of the IEEE G-AP International Symposium**, Williamsburg, Va., USA, December 1972, pp. 161–164.

[26] P. J. B. Clarricoats *et al.* : "Effects of Mutual Coupling in Conical Horn Arrays," **IEE Proceedings**, Vol. 131, Part H, No. 3, June 1984, pp. 165–170.

[27] N. A. Adatia, B. Claydon and D. Brain: "Primary-feed Elements for Multiple and Contoured Beam Satellite Antenna," **IEE Conference Publication**, 1981, pp. 98–103.

[28] J. N. Lyness: Algorithm 379, Comm. ACM, vol. 13, No. 1, April 1970, pp. 260-262.

[29] R. G. Koujoumjian and P. H. Pathak: "A Uniform Geometrical Theory of Diffraction for an Edge in a Perfectly Conducting Surface," **IEEE Proceedings**, vol. 62, No. 11, Nov. 1974, pp. 1448-1461.

APPENDIX A

MODE FUNCTIONS OF A CIRCULAR WAVEGUIDE

The fields in a hollow guide of circular cross section of radius "a" are solutions to the scalar Helmholtz equation. The general solution is of the form

$$\Psi = A J_p(\lambda_{pq}\rho)\cos(p\phi - \psi)$$

with A is an arbitrary constant and ψ is the polarization angle.

It is well understood that there is no TEM wave in a hollow waveguide. There exists only the transverse electric (TE) and transverse magnetic (TM) waves.

A. TE modes

In this particular mode, the longitudinal component E_z equals to zero. A solution of

$$\nabla_t^2 h_z + k_c^2 h_z = 0$$

is required such that $(\partial h_z/\partial z) = 0$ at $\rho=a$ for all value of ϕ. This leads to characteristic values of λ_{pq} that statisfiy the relation

$$J_p'(\lambda_{pq} a) = 0$$

For each p there are a denumerably infinite number of zeros. These are ordered and designated by x'_{pq}. The eigenvalue (or wavenumber) λ_{pq} is then given by

$$\lambda_{pq} = \frac{x'_{pq}}{a}$$

The lower order zeros x'_{pq} are listed in Table A-1.

Table A-1

Ordered zeros of $J'_p(x')$

p	x'_{p1}	x'_{p2}	x'_{p3}	x'_{p4}
0	3.832	7.016	10.173	13.324
1	1.841	5.331	8.536	11.706
2	3.054	6.706	9.969	13.170
3	4.201	8.015	11.346	
4	5.317	9.282	12.682	

The Cartesian components of the magnetic field h are

$$h_{mx} = \frac{j\gamma_{pq}}{2\lambda_{pq}} [-J_{p-1}(\lambda_{pq}\rho) \cos((p-1)\phi - \psi) + J_{p+1}(\lambda_{pq}\rho) \cos((p+1)\phi - \psi)] \quad \text{(A-1)}$$

$$h_{my} = \frac{j\gamma_{pq}}{2\lambda_{pq}} [J_{p-1}(\lambda_{pq}\rho) \sin((p-1)\phi - \psi) + J_{p+1}(\lambda_{pq}\rho) \sin((p+1)\phi - \psi)] \quad \text{(A-2)}$$

$$h_{mz} = J_p(\lambda_{pq}\rho) \cos(p\phi - \psi) \quad \text{(A-3)}$$

The polarization angle ψ is relative to the y axis, as noted in Figure A-1.

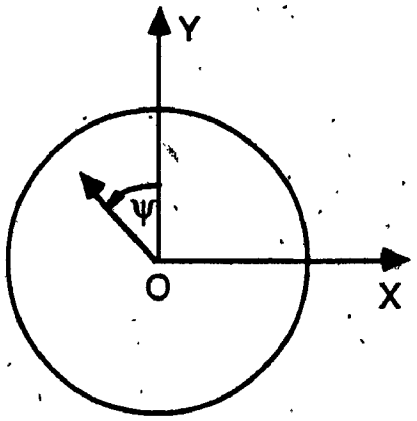

Figure A-1

The propagation constant γ_{pq} of mode pq is given by

$$\gamma_{pq}^2 = k^2 \varepsilon_r - \lambda_{pq}^2$$

ε_r is the dielectric constant of the waveguide filling.

The TE mode impedance Z_{pq} is

$$Z_{pq} = \frac{k Z_0}{\gamma_{pq}}$$

Z_0 is the free-space impedance.

The normalization factor N_m of TE waves is derived as follows:

$$N_m = \iint_A \bar{h}_m \cdot \bar{h}_m \, dS$$

h_m denotes the transverse components of vector h.

Substitution of h_m to get

$$N_m = -\frac{\gamma_{pq}^2}{4\lambda_{pq}^2}\left[\iint_S J_{p-1}^2(\lambda_{pq}\rho)\,\rho d\rho d\phi + \iint_S J_{p+1}^2(\lambda_{pq}\rho)\,\rho d\rho d\phi - 2\iint_S J_{p-1}(\lambda_{pq}\rho)\,J_{p+1}(\lambda_{pq}\rho)\cos 2(p\phi-\psi)\,\rho d\rho d\phi\right]$$

Two separate cases are to be considered, that is when p=0 and when $p\neq 0$,

i. <u>p = 0</u>

$$N_m = -2\pi\frac{\gamma_{pq}^2}{\lambda_{pq}^2}\int_0^a J_1^2(\lambda_{pq}\rho)\,\rho d\rho$$

By means of TE boundary condition, $J'_p(\lambda_{pq}a) = 0$, N_m is reduced to

$$N_m = -\frac{\pi}{(\lambda_{pq}a)^2}(\gamma_{pq}a^2 J_0(\lambda_{pq}a))^2 \qquad \text{(A-6)}$$

ii. <u>$p \neq 0$</u>

The third integral in the expression of N_m will vanish due to the presence of a cosine term. The remaining integrals are simplified and combined to give

$$N_m = -\frac{\pi}{2(\lambda_{pq}a)^2}(\gamma_{pq}a^2 J_p(\lambda_{pq}a))^2\left(1-\left(\frac{p}{\lambda_{pq}a}\right)^2\right) \qquad \text{(A-7)}$$

B. <u>TM modes</u>

The solution for TM modes parallels to that for the TE modes with the exception that the boundary conditions require that $e_z=0$ at $\rho=a$ for all ϕ. The characteristics values of λ_{pq} satisfy the relation

$$J_p(\lambda_{pq} a) = 0$$

The Bessel functions $J_p(x)$ have a denumerably infinite number of zeros, which are designated by x_{pq}. The lower-order are tabulated in Table A-2.

Table A-2

Ordered zeros of $J_p(x)$

p	x_{p1}	x_{p2}	x_{p3}	x_{p4}
0	2.405	5.520	8.654	11.792
1	3.832	7.106	10.173	13.324
2	5.136	8.417	11.620	14.796
3	6.380	9.761	13.015	
4	7.588	11.065	14.372	

The transverse magnetic field components are readily derived from those of TE modes. They are

$$\bar{h}_{pq} = \frac{1}{Z_{pq}}(\bar{z} \times \bar{h}_{pq}^{TE}) \qquad \text{(A-8)}$$

where the components of h_{pq}^{TE} are listed in (A-1) and (A-2).

It is noted that for TM modes, the polarization angle ψ is relative to the x axis.

The TM mode impedance Z_{pq} is

$$Z_{pq} = \frac{\gamma_{pq}}{k\varepsilon_r} Z_0 \qquad \text{(A-9)}$$

The procedure of evaluation the normalization factor N_m for TM modes is identical to that of TE modes. The final expression is, thus, presented below:

$$N_m = -\frac{\pi a^4}{\varepsilon_{op} (\lambda_{pq} a)^2} \frac{k^2 \varepsilon_r^2}{Z_0^2} J'^2_p (\lambda_{pq} a) \qquad \text{(A-10)}$$

APPENDIX B

ELIMINATION OF ∇_t IN EQUATION (2.19)

From equation (2.19)

$$C_{mn}^{(ij)} = \frac{j}{2\pi\omega\mu_0}\frac{Z_n}{N_m}\left[k^2 \iint_{D_i} \bar{h}_m \cdot \left(\iint_{D_j} \bar{h}_n' G(|\bar{r} - \bar{r}'|)\, dS' \right) dS + \right.$$

$$\left. \iint_{D_i} \bar{h}_m \cdot \nabla_t \nabla_t \cdot \left(\iint_{D_j} \bar{h}_n' G(|\bar{r} - \bar{r}'|)\, dS' \right) dS \right]$$

Consider the second term and identify it as

$$I = \iint_{D_i} dS\, \bar{h}_m \cdot \nabla_t \nabla_t \cdot \iint_{D_j} \bar{h}_n' G(|\bar{r} - \bar{r}'|)\, dS'$$

In explicit form,

$$I = \iint_{D_i} dS\, (h_{mx}\bar{i}_x + h_{my}\bar{i}_y) \cdot \left(\frac{\partial}{\partial x}\bar{i}_x + \frac{\partial}{\partial y}\bar{i}_y\right) \iint_{D_j} \left(\frac{\partial}{\partial x}\bar{i}_x + \frac{\partial}{\partial y}\bar{i}_y\right) \cdot \bar{h}_n' G\, dS'$$

Let the inner integral be

$$J = \iint_{D_j} \left(\frac{\partial}{\partial x}\bar{i}_x + \frac{\partial}{\partial y}\bar{i}_y\right) \cdot \bar{h}_n' G\, dS'$$

$$= \iint_{D_j} \left(\frac{\partial}{\partial x} G\bar{i}_x + \frac{\partial}{\partial y} G\bar{i}_y\right) \cdot \bar{h}_n'\, dS'$$

From the definition of Green's function, it can be shown that

$$\frac{\partial}{\partial x} G = -\frac{\partial}{\partial x'} G \quad \text{and} \quad \frac{\partial}{\partial y} G = -\frac{\partial}{\partial y'} G$$

Thus,

$$J = -\iint_{D_j} \left(\frac{\partial}{\partial x'} G \bar{i}_x + \frac{\partial}{\partial y'} G \bar{i}_y \right) . \bar{h}'_n \, dS'$$

By Green's theorem:

$$\oint \bar{B} . \bar{n} \, dl = \iint_S \nabla . \bar{B} \, dS$$

J is re-arranged as

$$J = -\int_C h'_{nx} n'_x G \, dl + \iint_{D_j} \frac{\partial}{\partial x'} h'_{nx} G \, dS'$$

$$-\int_C h'_{ny} n'_y G \, dl + \iint_{D_j} \frac{\partial}{\partial y'} h'_{ny} G \, dS'$$

where C is the boundary of D_j and n is the outward normal vector of contour C. Since the mode function satisfy the condition $\bar{h}.\bar{n} = 0$, therefore

$$J = -\iint_{D_j} \left(\frac{\partial}{\partial x'} h'_{nx} + \frac{\partial}{\partial y'} h'_{ny} \right) G \, dS'$$

The integral I is now become

$$I = \iint_{D_i} dS \left(h_{mx} \bar{i}_x + h_{my} \bar{i}_y \right) . \left(\frac{\partial}{\partial x} \bar{i}_x + \frac{\partial}{\partial y} \bar{i}_y \right) \iint_{D_j} \left(\frac{\partial}{\partial x'} h'_{nx} + \frac{\partial}{\partial y'} h'_{ny} \right) G \, dS'$$

By the same way, the differential operator can be reduced to give

$$I = -\iint_{D_i} dS \left(\frac{\partial}{\partial x} h_{mx} + \frac{\partial}{\partial y} h_{my} \right) \iint_{D_j} dS' \left(\frac{\partial}{\partial x'} h'_{nx} + \frac{\partial}{\partial y'} h'_{ny} \right) G$$

In vector notation,

$$I = -\iint_{D_i} dS \, \nabla_t . \bar{h}_m \iint_{D_j} dS' \, \nabla'_t . \bar{h}'_n \, G$$

From Maxwell's equation, the transverse magnetic field components are related to the longitudinal field component by

$$\bar{\nabla}_t . \bar{h}_m = j\gamma_m h_{mz}$$

Hence,

$$I = \gamma_m \gamma_n \iint_{D_i} dS \, h_{nz} \iint_{D_j} dS' \, h'_{nz} G$$